NASA TECHNICAL NOTE

NASA TN D-4153

c. 1

NASA TN D-4153

DETERMINATION OF
BOUNDARY-REFLECTED-DISTURBANCE LENGTHS
IN THE LANGLEY 16-FOOT TRANSONIC TUNNEL

by Francis J. Capone and Edward M. Coates, Jr.

Langley Research Center
Langley Station, Hampton, Va.

NASA TN D-4153

DETERMINATION OF BOUNDARY-REFLECTED-DISTURBANCE LENGTHS

IN THE LANGLEY 16-FOOT TRANSONIC TUNNEL

By Francis J. Capone and Edward M. Coates, Jr.

Langley Research Center
Langley Station, Hampton, Va.

NATIONAL AERONAUTICS AND SPACE ADMINISTRATION

DETERMINATION OF BOUNDARY-REFLECTED-DISTURBANCE LENGTHS

IN THE LANGLEY 16-FOOT TRANSONIC TUNNEL

By Francis J. Capone and Edward M. Coates, Jr.
Langley Research Center

SUMMARY

An investigation has been conducted to determine boundary-reflected-disturbance lengths in the Langley 16-foot transonic tunnel. Cone-cylinder and ogive-cylinder bodies were tested at Mach numbers from 0.70 to 1.30 and at angles of attack from -3.8° to 4.0°. Geometric variables included nose-cone half-angle, body diameter, and body length. The test Reynolds number per meter varied from 10.66×10^6 to 13.25×10^6 (test Reynolds number per foot varied from 3.25×10^6 to 4.04×10^6).

Results showed that the stronger the bow shock wave, the shorter the maximum interference-free model length as a result of the boundary-reflected disturbance. Some wind-tunnel-wall interference associated with the reflected expansion field emanating at the cone-cylinder juncture was experienced for the bodies with 0.1980-percent blockage at Mach numbers from 1.00 to 1.06 and for the body with 0.0980-percent blockage at a Mach number of 1.00. No interference was found for a 0.0062-percent-blockage body. Base pressure was influenced by the proximity of the boundary-reflected disturbance at the base of the model.

INTRODUCTION

The maximum permissible length of a model for interference-free testing at transonic and supersonic speeds is usually determined by the requirement of avoiding impingement of boundary-reflected disturbances from the tunnel walls on the model. The maximum model length for a given tunnel size and Mach number is approximately equal to the shock-reflection length. However, models are usually made shorter than the shock-reflection length in order to avoid any undesirable interactions of the reflected disturbance on the base of the model. A review of the problems encountered when too large a model is tested is given in reference 1. Some early measurements of shock-reflection lengths are given in reference 2.

The present investigation was undertaken to determine boundary-reflected-disturbance lengths in the Langley 16-foot transonic tunnel. Although this 16-foot transonic tunnel has been in operation since December 1950 (ref. 3), the need for

shock-reflection data became apparent when the maximum tunnel Mach number was increased from about 1.08 to 1.30 in 1961. This increase in speed was brought about by the use of test-section plenum suction. The present report summarizes existing shock-reflection data measured in the 16-foot transonic tunnel. Tests were conducted with both existing and new cone-cylinder and ogive-cylinder models. Geometric variables included nose-cone half-angle, body diameter, and body length. The models were tested at Mach numbers from 0.70 to 1.30 and at angles of attack from -3.8° to 4.0°. The test Reynolds number per meter varied from 10.66×10^6 to 13.25×10^6 (test Reynolds number per foot varied from 3.25×10^6 to 4.04×10^6).

SYMBOLS

The units used for the quantities defined in this paper are given both in the International System of Units (SI) and in the U.S. Customary Units.

$C_{p,b}$ base pressure coefficient, $\dfrac{p_b - p_\infty}{q}$

d_m model maximum diameter

d_s sting diameter

l model overall length

l/d_m model fineness ratio

L boundary-reflected-disturbance length as defined in figure 1(a)

M free-stream Mach number

p_b base pressure

p_l local static pressure

$p_{t,\infty}$ free-stream total pressure

p_∞ free-stream static pressure

q free-stream dynamic pressure

r   radius

x   longitudinal distance, measured from model nose, positive rearward

x_s length of cylindrical portion of sting

α nominal angle of attack of body center line (does not include change in angle of attack due to deflection under load), deg

θ nose-cone half-angle, deg

ϕ meridian angle, measured from top of model in clockwise direction when looking upstream, deg

APPARATUS AND PROCEDURE

Models

A sketch showing model installation is given in figure 1(a). Geometric characteristics of the six configurations are shown in figure 1(b). Figure 2 presents photographs of configuration 3 mounted in the wind-tunnel test section. Each of the configurations had a single row of pressure orifices at $\phi = 0^O$ (top of model) extending the length of the model.

Configurations 1, 2, 3, and 4 (d_m = 21.59 cm (8.50 in.)).- Configurations 1, 2, 3, and 4 were constructed in three sections: interchangeable nose, main cylindrical body, and cylindrical body extension. The important geometric characteristics of configurations 1, 2, 3, and 4 are summarized in the table of figure 1(b). The interchangeable nose pieces were constructed of plastic with 10.16-cm-long (4.00-in.) aluminum tips. Two of the noses were cones with half-angles of 10° (configurations 1 and 4) and 20° (configuration 2). The third nose was an ogive that faired smoothly into an aluminum tip with a half-angle of 20°. (See configuration 3 in fig. 1(b).) The cylindrical body and the extension were fabricated from aluminum. The extension increased the fineness ratio from 10.00 (configuration 4) to 11.29 (configurations 1, 2, and 3). The sting supporting this model had a 7.95-cm (3.13-in.) diameter at the base of the model.

Configuration 5 (d_m = 15.24 cm 6.00 in.)).- Configuration 5 was constructed of mahogany covered with a thin layer of clear plastic and had a brass nose tip. The nose-cone half-angle was 10° and the model was 152.40 cm (60.00 in.) long with a fineness ratio of 10.00. The sting diameter was 3.81 cm (1.50 in.).

3

Configuration 6 (d_m = 3.81 cm (1.50 in.)).- Configuration 6 was also constructed of mahogany with a plastic overlay but with no metal nose tip. The nose-cone half-angle was 10° and the model was 38.10 cm (15.00 in.) long with a fineness ratio 10.00. The sting diameter and model diameter were 3.81 cm (1.50 in.) and, as a result, the model had no base area.

Wind Tunnel and Instrumentation

This investigation was conducted in the Langley 16-foot transonic tunnel, which is a single-return, atmospheric wind tunnel with a slotted octagonal test section. (See fig. 1(a).) The average distance from center line to wall is 2.36 m (7.75 ft). Test-section plenum suction is used for speeds above a Mach number of 1.10. The models were sting supported, and the support system was pivoted so that the models rotated about the 40.84-m (134.00-ft) tunnel station.

The static surface and base pressures were measured with three pressure-scanning units, each capable of measuring 48 pressures. Each scanning unit contained a pressure transducer. For configurations 1, 2, and 4, the outputs of the transducers were recorded on punch cards. For configurations 3, 5, and 6, the outputs were recorded on magnetic tape.

Tests

All configurations were tested at Mach numbers from 0.70 to 1.30 and at angles of attack from -3.8^o to 4.0^o. The spacing of test Mach numbers between M = 1.0 and 1.25 for each configuration was chosen in order to establish boundary-reflected-disturbance lengths for that particular configuration. Since configuration 3 was tested after a pre-liminary analysis of data from configurations 1, 2, and 4, there is a closer spacing of test Mach numbers. The test Reynolds number per meter varied from 10.66×10^6 to 13.25×10^6 (test Reynolds number per foot varied from 3.25×10^6 to 4.04×10^6). Boundary-layer transition was not fixed for these tests.

CORRECTIONS AND ACCURACIES

The angle of attack has been corrected for wind-tunnel-flow angularity but not for model deflection under load at angle of attack. Hence, model angle of attack should be considered to be nominal. No estimate of model deflection has been made. A small correction was applied to tunnel stagnation pressure to account for the effects of water condensation in the test-section flow. This correction, which decreases the stagnation pressure, varies from 0 N/m^2 (0 psf) at M = 1.04 to about 1675.8 N/m^2 (35 psf) at M = 1.30.

4

The accuracies of the data have been estimated to be:

$p_l/p_{t,\infty}$ . . . . ±0.010

$C_{p,b}$ . . . . ±0.010

M . . . . ±0.005

RESULTS AND DISCUSSION

Pressure Distributions

Pressure distributions for configurations 1, 2, and 3 are presented in figures 3, 4, and 5, respectively. At subsonic speeds the pressure distributions show expected trends: an expansion about the cone shoulder or the ogive nose and recovery to essentially free-stream conditions. At supersonic speeds greater than M = 1.04, impingement of a boundary-reflected disturbance originating at the model nose is characterized by a sharp increase in pressure ratio. Otherwise, the pressure distributions are similar to those at subsonic speeds. The small effects of angle of attack were mainly due to the fact that the orifices were located on top of the models ($\phi = 0^O$). Pressure distributions at $\phi = 0^O$ at negative angles of attack are equivalent to pressure distributions at $\phi = 180^O$ at positive angles of attack.

In figures 3(l) and 3(o), a comparison is made of the data for configuration 1 ($\theta = 10^O$) at M = 1.20 and 1.30 and the theoretical results of reference 4. The results of reference 4 are for no interference and show good agreement with the experimental results obtained in the present investigation.

For M = 1.00 to 1.06, interference on the bodies is not caused by boundary-reflected disturbances originating at the model nose. Consider, for example, configuration 1 at M = 1.00 (fig. 3(e)). At $x/d_m \approx 6.75$, there is an increase in pressure ratio with an expansion of the flow to just above free-stream conditions. Since any shock wave originating at the model nose at M = 1.00 will be normal, this interference is not caused by a boundary-reflected disturbance originating at the model nose. This interference is probably due to the reflected expansion field emanating at the cone-cylinder juncture. This flow condition exists for configuration 1 at M = 1.00 and 1.025 (figs. 3(e) and 3(f)); for configuration 2 at M = 1.00, 1.025, and 1.04 (figs. 4(e), 4(f), and 4(g)); and for configuration 3 at M = 1.00, 1.025, 1.04, and 1.06 (figs. 5(e), 5(f), 5(g), and 5(h)). An examination of these figures shows that the disturbance moves downstream on the model as Mach number is increased. At M = 1.06 for configuration 3, there is also a reflected bow disturbance at approximately $x/d_m = 4.0$.

Further examples of this interference are illustrated in figure 6 where a comparison of pressure distributions is made for the cone-cylinder bodies with a fineness ratio of 10.00. For configurations 4 and 5 at M = 1.00 and 1.04, the interference is similar to

that for configuration 1 whereas configuration 6 is interference free. (See figs. 6(c) and 6(d).) Since these three configurations are of different lengths, it might be concluded that the reflected expansion field of configuration 6, would impinge on the sting portion (noninstrumented portion) of this model (sting and model diameters are equal). However, pressures measured along one wall in the wind tunnel show no evidence of the expansion field of configuration 6 striking the wall. Pressure distributions along the wall do show the expansion fields of configurations 4 and 5 impinging on the wall. These results indicate some wind-tunnel-wall interference for the bodies having larger diameters. The following table lists the percent of blockage (ratio of model maximum cross-sectional area to tunnel test-section cross-sectional area) for the various configurations tested:

Configuration	Percent blockage
1, 2, 3, 4	0.1980
5	.0980
6	.0062

A similar interference effect in the same Mach number range is illustrated with a series of schlieren photographs in reference 5. The model of reference 5 was tested in the Ames 2- by 2-foot transonic wind tunnel and the Ames 14-foot transonic wind tunnel. The percentages of blockage for the model in these two wind tunnels were 0.250 and 0.005, respectively. At M = 1.00, 1.02, and 1.06, the 0.25-percent-blockage model shows a terminal shock pattern impinging on the model, whereas for the model with 0.005-percent blockage, the terminal shock pattern impinges downstream of the model at all Mach numbers. As stated in reference 5, the location of this shock pattern is probably determined primarily by the impingement of the expansion field from the cone shoulder on the walls of the wind-tunnel test section. Reference 4 also presents some experimental data showing similar results for three large wind tunnels.

At the other Mach numbers of figure 6 (M = 0.70 to 0.95 and M = 1.075 to 1.30), there is excellent agreement with the exception of the pressures over the conical portion of configuration 6. This lack of agreement may be due to the nose-cone half-angle not being exactly 10°. In addition, the nose of this model (the only model with no metal nose tip) was not as sharp as the noses of the other configurations.

<center>Boundary-Reflected-Disturbance Length</center>

A summary of the boundary-reflected-disturbance lengths for the various configurations is presented in figure 7. Also included are data for a Mach angle reflection (ref. 6) and data of reference 2 scaled up for the Langley 16-foot transonic tunnel with 2.36 m (7.75 ft) as the distance from center line to wall. The data of reference 2 are for a

12-sided tunnel and were not adjusted for the difference in the boundary layers of the two wind tunnels. The data of reference 6 do not include the boundary-layer effects of the 16-foot transonic tunnel. These two curves have been included as a basis of comparison.

Increasing the nose-cone half-angle from 10° to 20° caused a large reduction in maximum interference-free model length. This reduction is primarily due to the higher strength shock and steeper shock-incident and reflection angles generated by the larger nose angle. The bow shock was weakened with the ogive nose. It should be noted that the ogive and the $\theta = 20^O$ noses used the same nose tip.

Base Pressure Comparison

The variation of base pressure coefficient with Mach number for configurations 1, 2, 3, and 4 is presented in figure 8. The effect of the proximity of the sting flare to the model base can be seen at subsonic speeds and at the higher supersonic speeds. The base pressure coefficient is more negative for configuration 4 than for the configurations with the longer bodies. This difference is due to a positive pressure field of the sting flare feeding forward and affecting the base pressure.

The effect of the location of the boundary-reflected disturbances on the base pressure coefficients is illustrated in the Mach number range from about 1.05 to 1.25. The base pressure coefficient for all the configurations is most negative at $M = 1.10$. A sharp decrease in the magnitude of the negative base pressure coefficient at Mach numbers from 1.10 to 1.20 is probably due to the location of the reflected bow shock just downstream of the model base and its interaction with the base flow. The Mach number at which the negative base pressure is a minimum is dependent upon the shock-reflection length. The effects of the boundary-reflected disturbances have apparently dissipated by $M = 1.25$, as the data for configurations 1, 2, and 3 are nearly the same.

CONCLUDING REMARKS

An investigation has been conducted to determine boundary-reflected-disturbance lengths in the Langley 16-foot transonic tunnel. Cone-cylinder and ogive-cylinder bodies were tested at Mach numbers from 0.70 to 1.30. Geometric variables included nose-cone half-angle, body diameter, and body length.

Results showed that the stronger the bow shock wave, the shorter the maximum interference-free model length as a result of the boundary-reflected disturbance. Some wind-tunnel-wall interference associated with the reflected expansion field emanating at the cone-cylinder juncture was experienced for the bodies with 0.1980-percent blockage at Mach numbers from 1.00 to 1.06 and for a body with 0.0980-percent blockage at a Mach number of 1.00. No interference was found for a 0.0062-percent-blockage body. Base

pressure was influenced by the proximity of the boundary-reflected disturbance to the base of the model.

Langley Research Center,
    National Aeronautics and Space Administration,
        Langley Station, Hampton, Va., March 24, 1967,
            126-13-01-08-23.

REFERENCES

1. Bielat, Ralph P.; Luoma, Arvo A.; and Daugherty, James C.: Drag Measurements From Different Wind Tunnels. NASA TM X-1271, 1966.

2. Wright, Ray H.; Ritchie, Virgil S.; and Pearson, Albin O.: Characteristics of the Langley 8-Foot Transonic Tunnel With Slotted Test Section. NACA Rept. 1389, 1958. (Supersedes NACA RM L51H10 by Wright and Ritchie and RM L51K14 by Ritchie and Pearson.)

3. Ward, Vernon G.; Whitcomb, Charles F.; and Pearson, Merwin D.: Air-Flow and Power Characteristics of the Langley 16-Foot Transonic Tunnel With Slotted Test Section. NACA RM L52E01, 1952.

4. Estabrooks, Bruce B.: Wall-Interference Effects on Axisymmetric Bodies in Transonic Wind Tunnels With Perforated Wall Test Sections. AEDC-TR-59-12, ASTIA Doc. No: AD-216698, U.S. Air Force, June 1959.

5. Page, William A.: Experimental Study of the Equivalence of Transonic Flow About Slender Cone-Cylinders of Circular and Elliptic Cross Section. NACA TN 4233, 1958.

6. Anon.: Equations, Tables, and Charts for Compressible Flow. NACA Rept. 1135, 1953.

2.63 m (7.75 ft)

L

Sting

Sting support strut

Center of rotation

| | | | | | | | | | |
120 124 128 132 136 140 144 148 152 156

Tunnel station, ft

36 37 38 39 40 41 42 43 44 45 46 47 48

Tunnel station, m
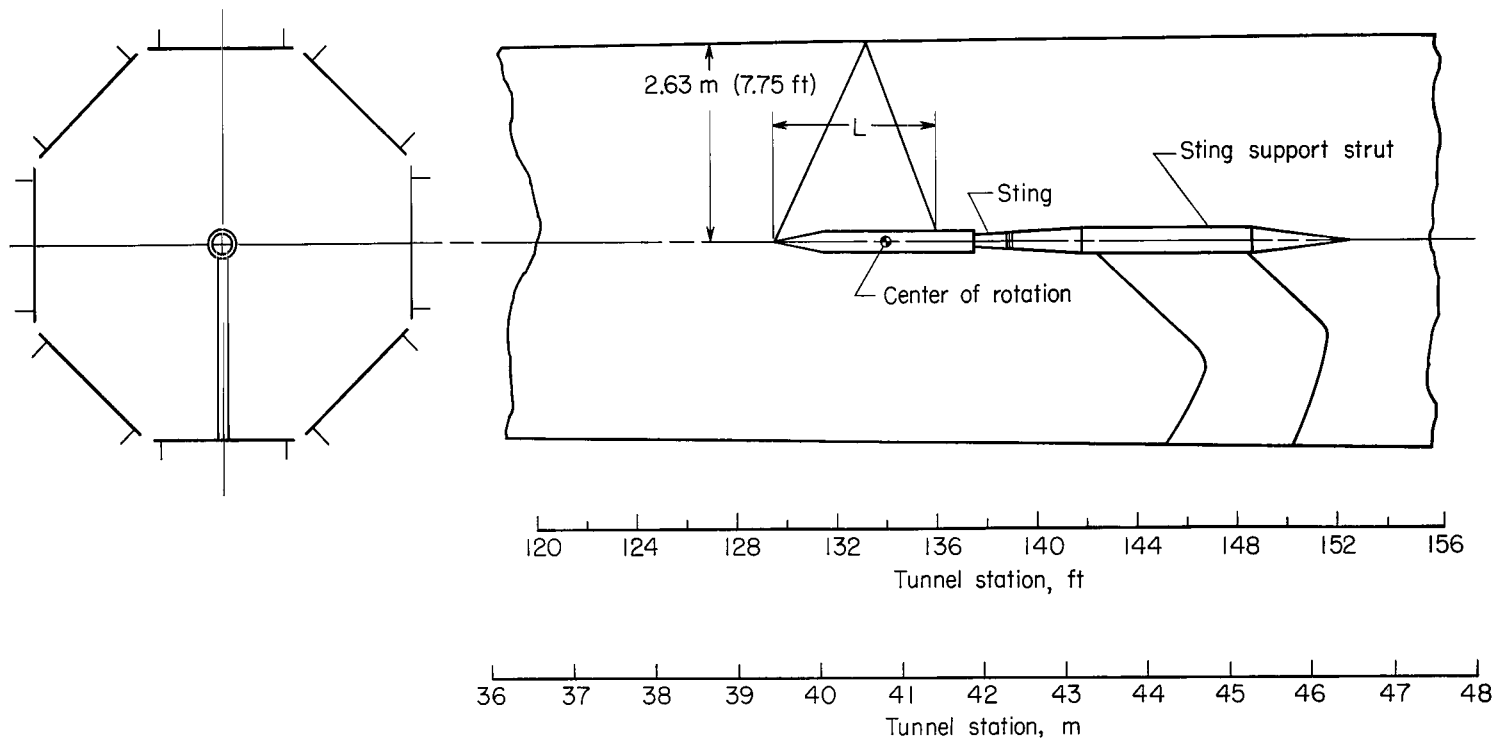
(a) Model installation.

Figure 1.- Sketch of model installation and models tested.

Tunnel station 39.50 m (129.58 ft)

Configuration 1

Configuration 2

Configuration 3

Configuration 4

Tunnel station 39.92 m (130.97 ft)

Configuration 5

Tunnel station 40.47 m (132.77 ft)

Configuration 6

Configuration	d_m	θ	l	l/d_m
1	21.59 (8.50)	10°	243.84 (96.00)	11.29
2	21.59 (8.50)	20°	243.84 (96.00)	11.29
3	21.59 (8.50)	Ogive	243.84 (96.00)	11.29
4	21.59 (8.50)	10°	215.90 (85.00)	10.00
5	15.24 (6.00)	10°	152.40 (60.00)	10.00
6	3.81 (1.50)	10°	38.10 (15.00)	10.00

(b) Configurations tested. All dimensions are in centimeters (inches) unless otherwise indicated.

Figure 1.- Concluded.
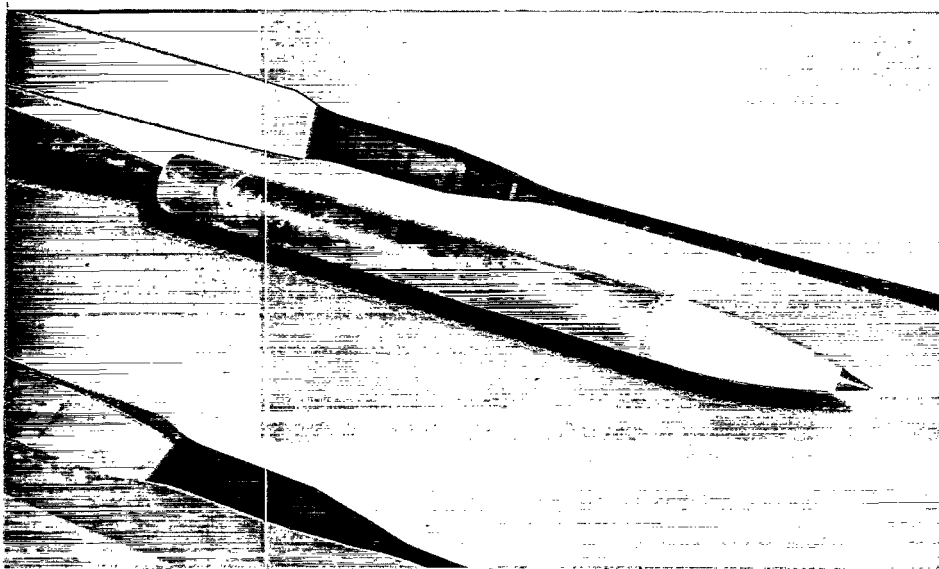
(a) Three-quarter front view.   L-65-7458
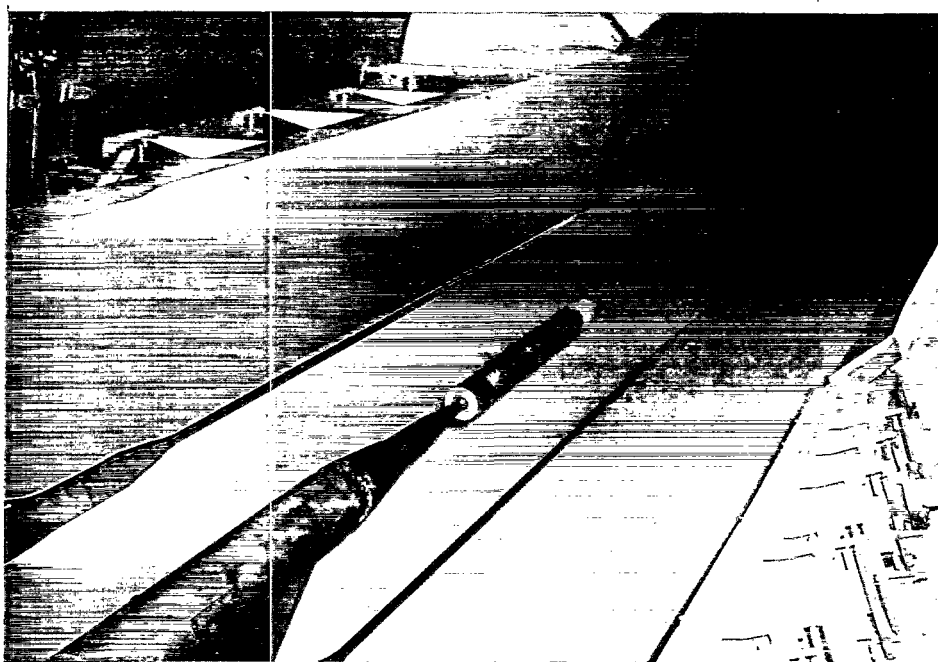
(b) Three-quarter rear view.   L-65-7457

Figure 2.- Photograph of configuration 3 sting mounted in the Langley 16-foot transonic tunnel.
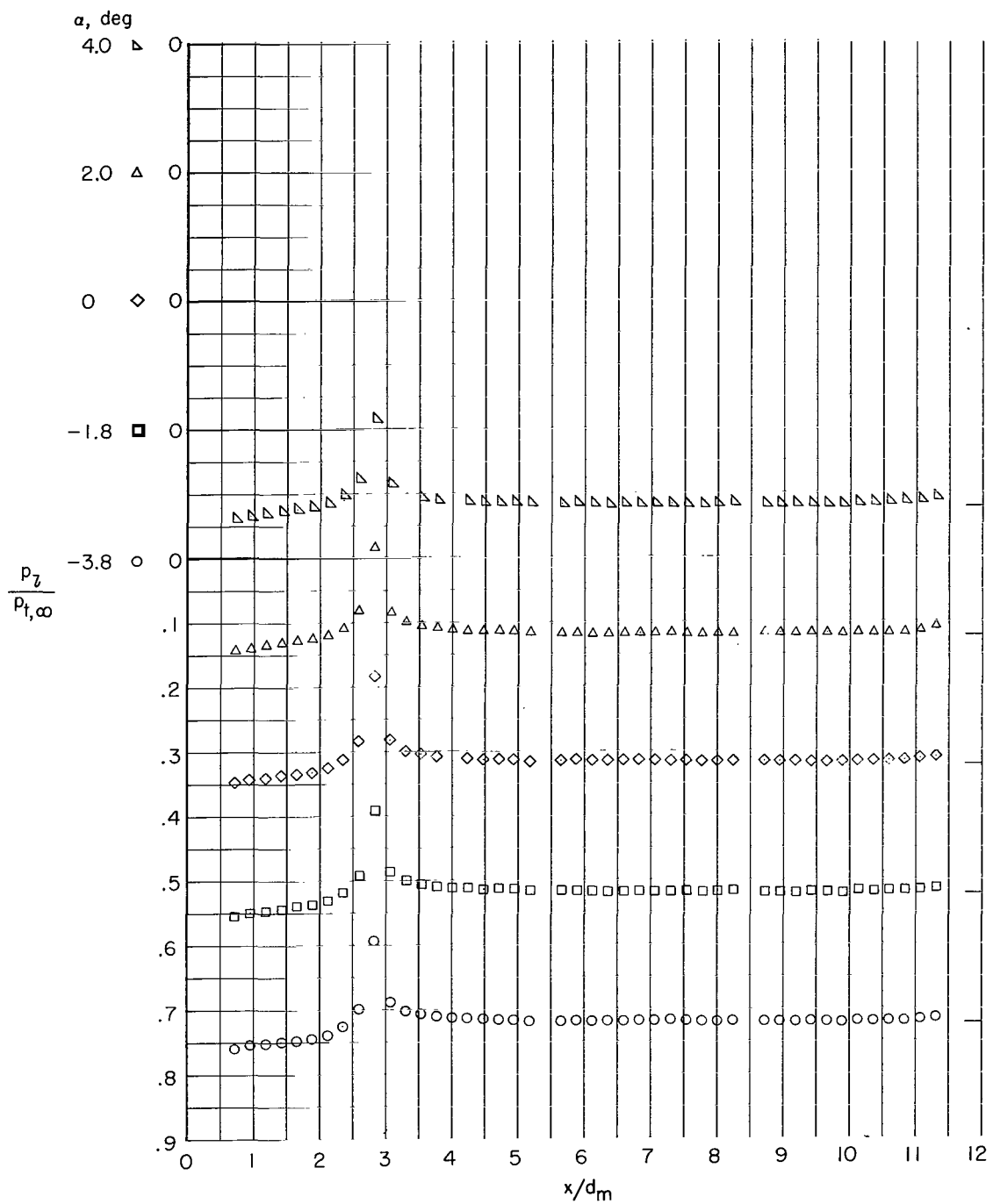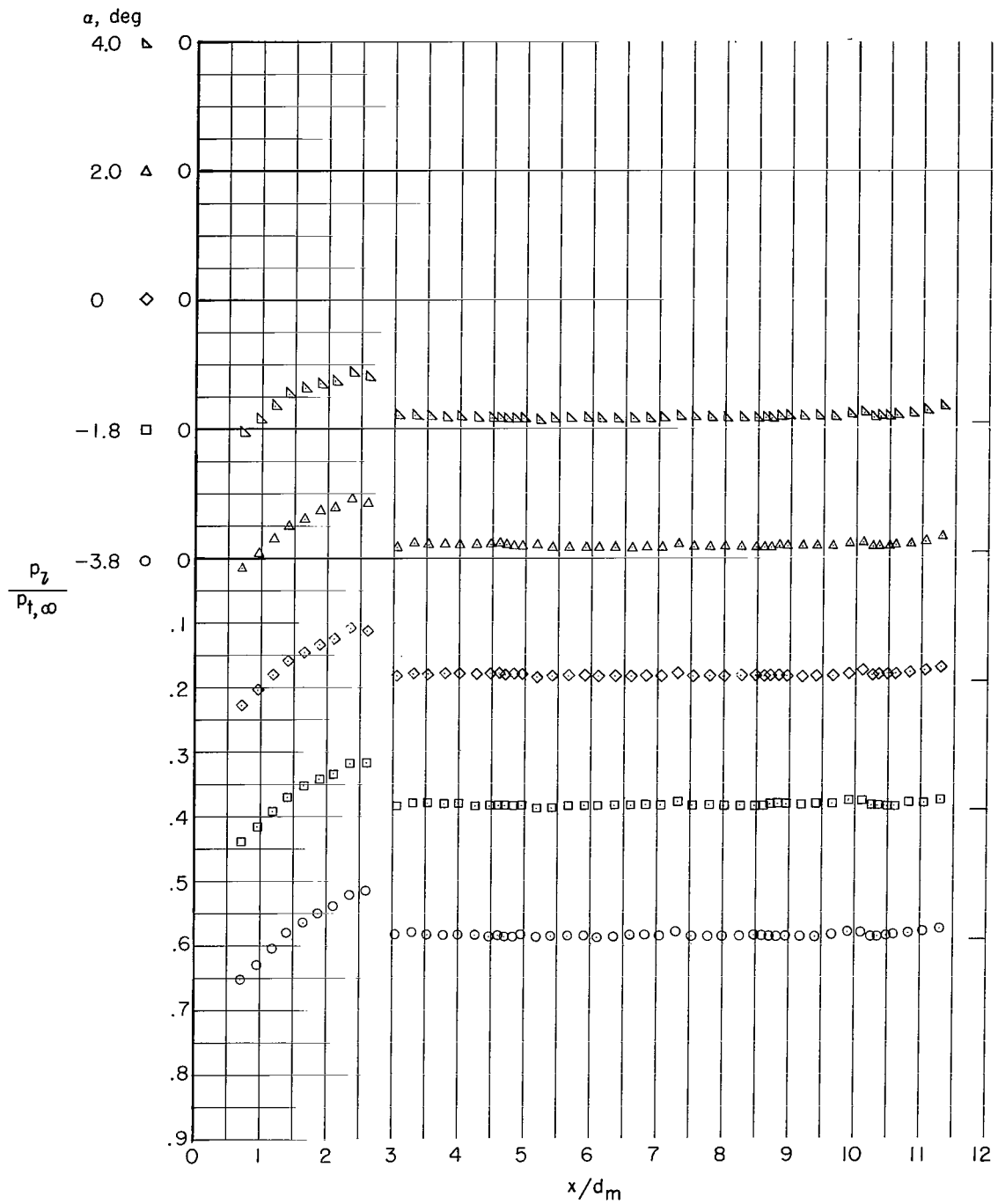
(a) M = 0.70.

Figure 3.- Pressure distributions for configuration 1. $\theta = 10^0$; $l = 243.84$ cm (96.00 in.); fineness ratio of 11.29.
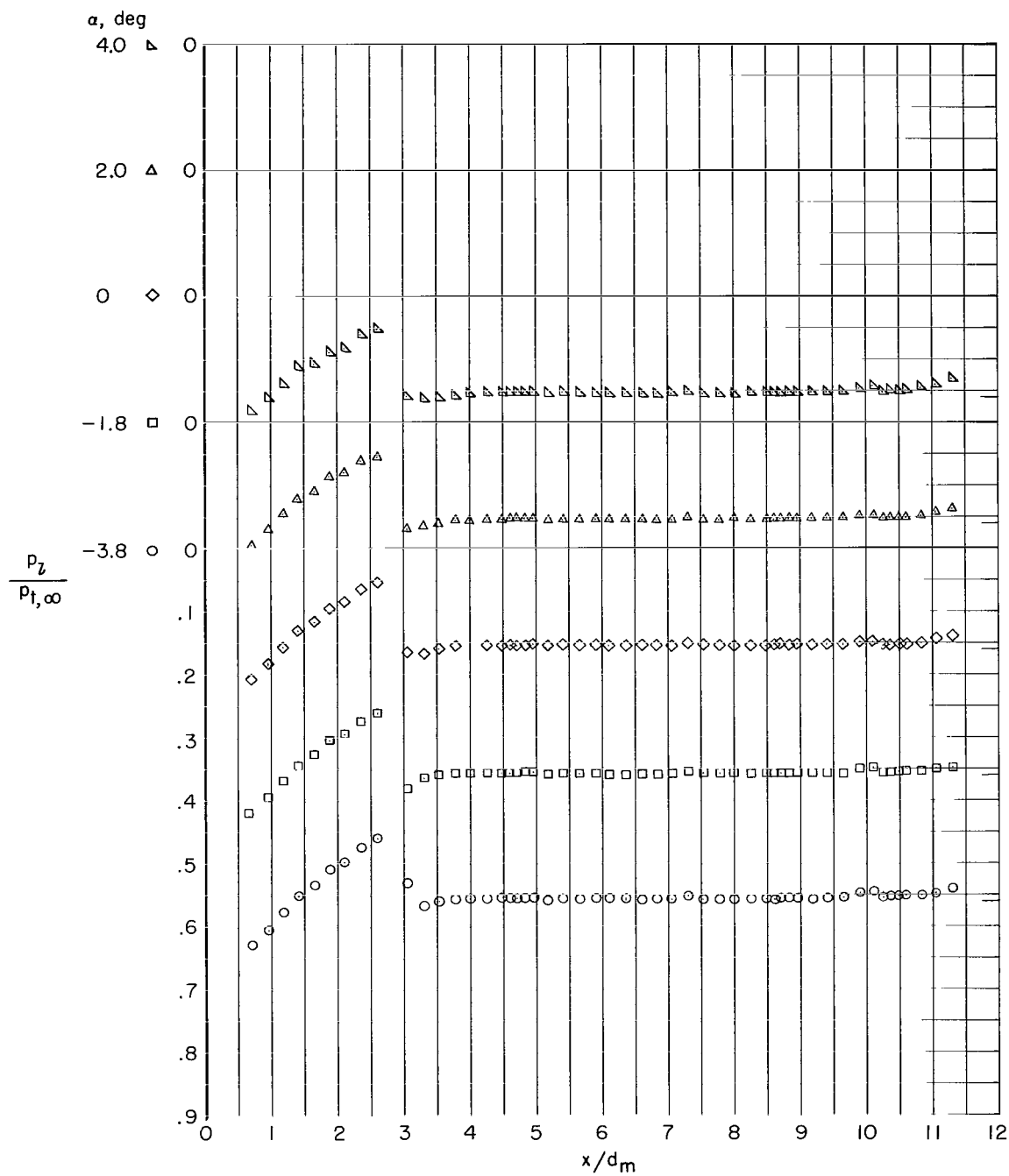Ticks indicate free-stream pressure ratio.
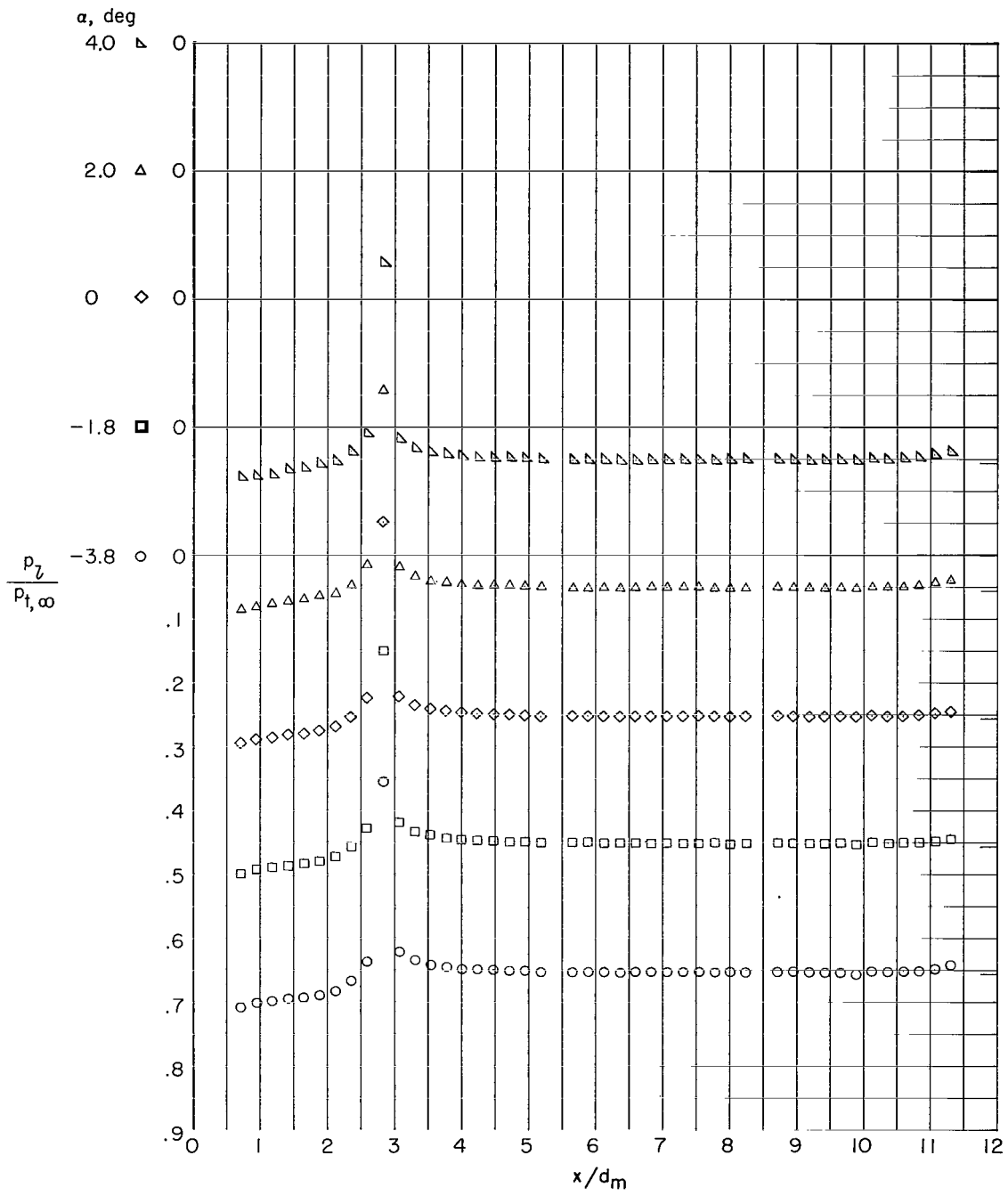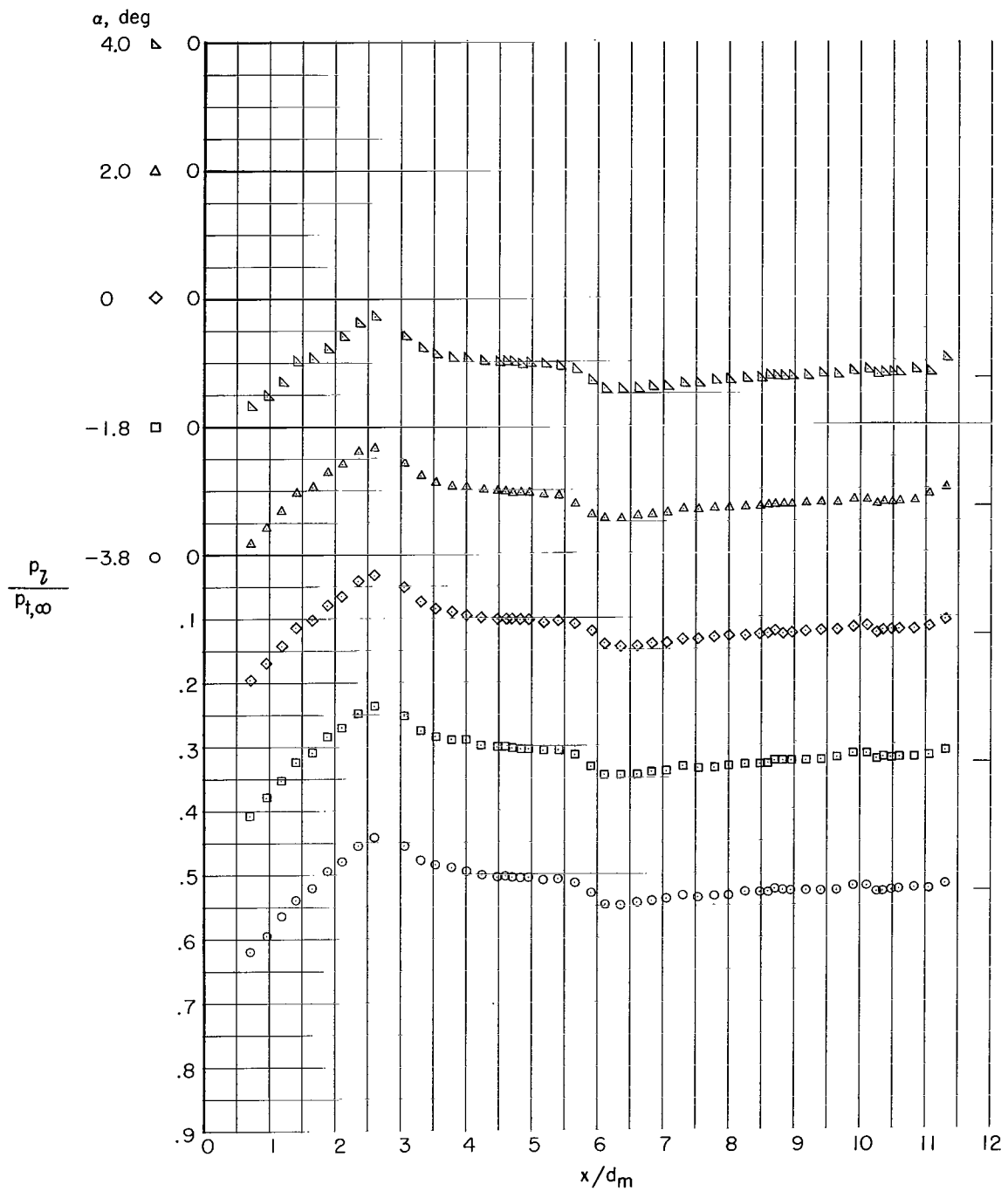
(b) M = 0.80.

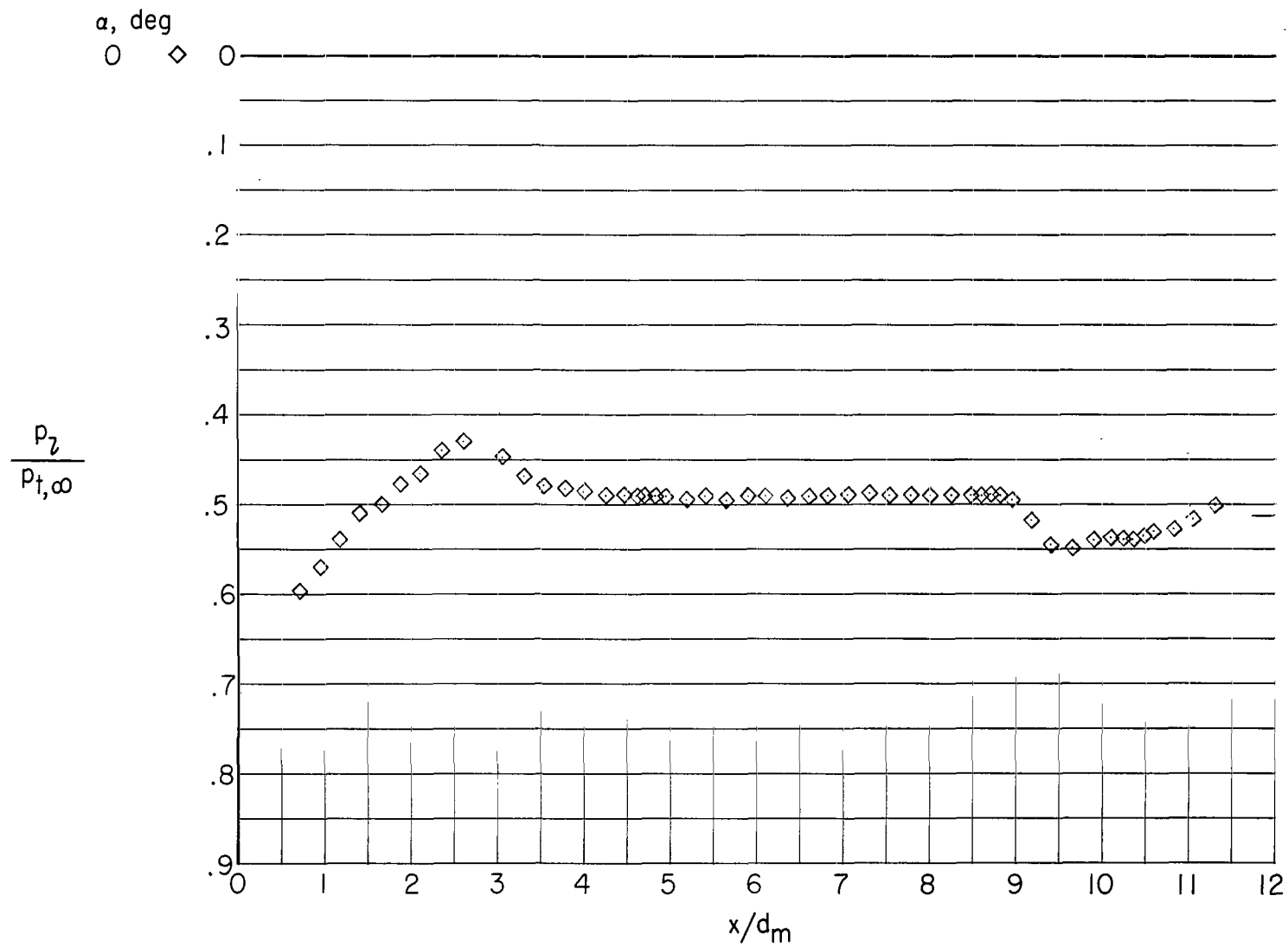Figure 3.- Continued.
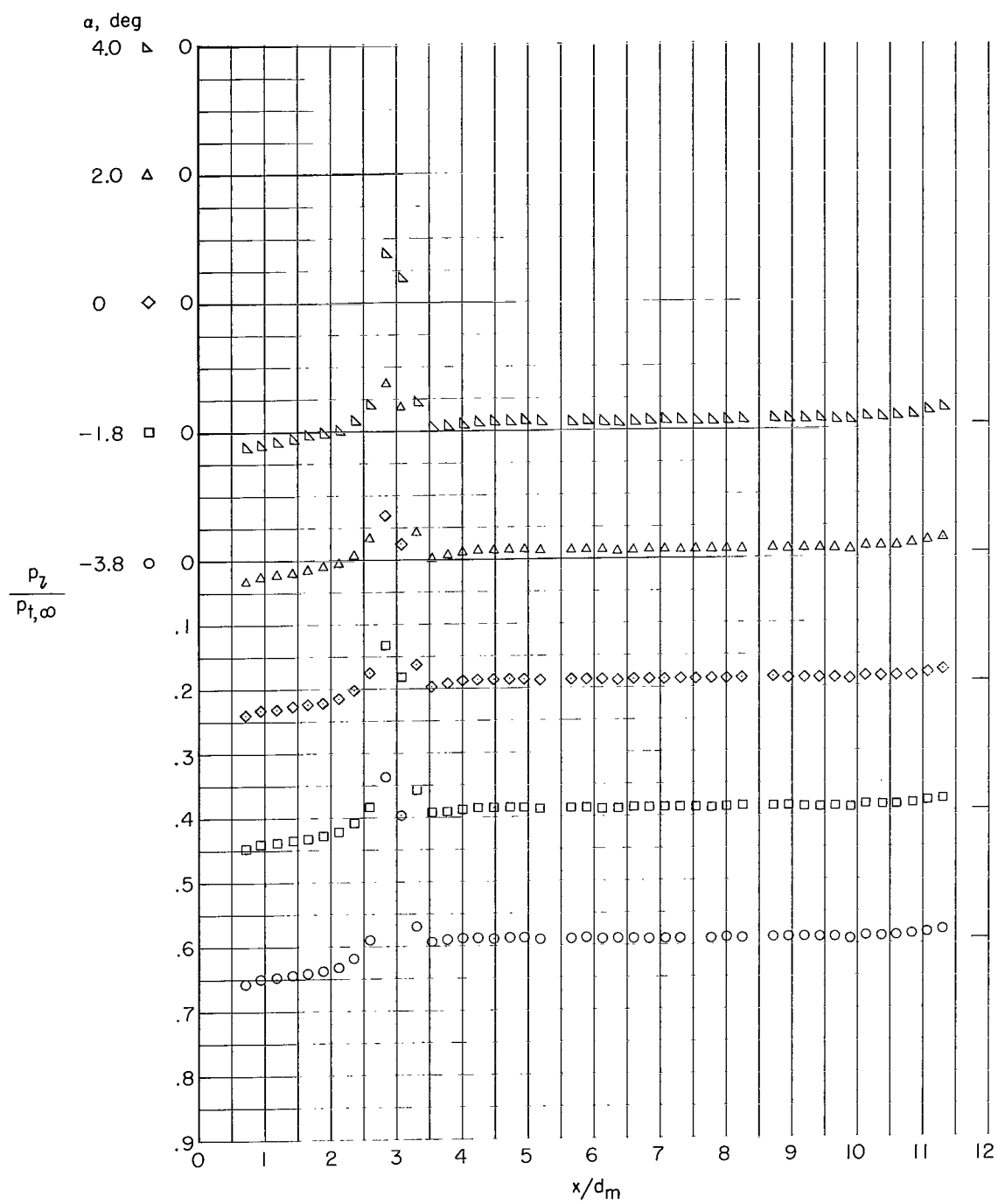
(c) M = 0.90.

Figure 3.- Continued.
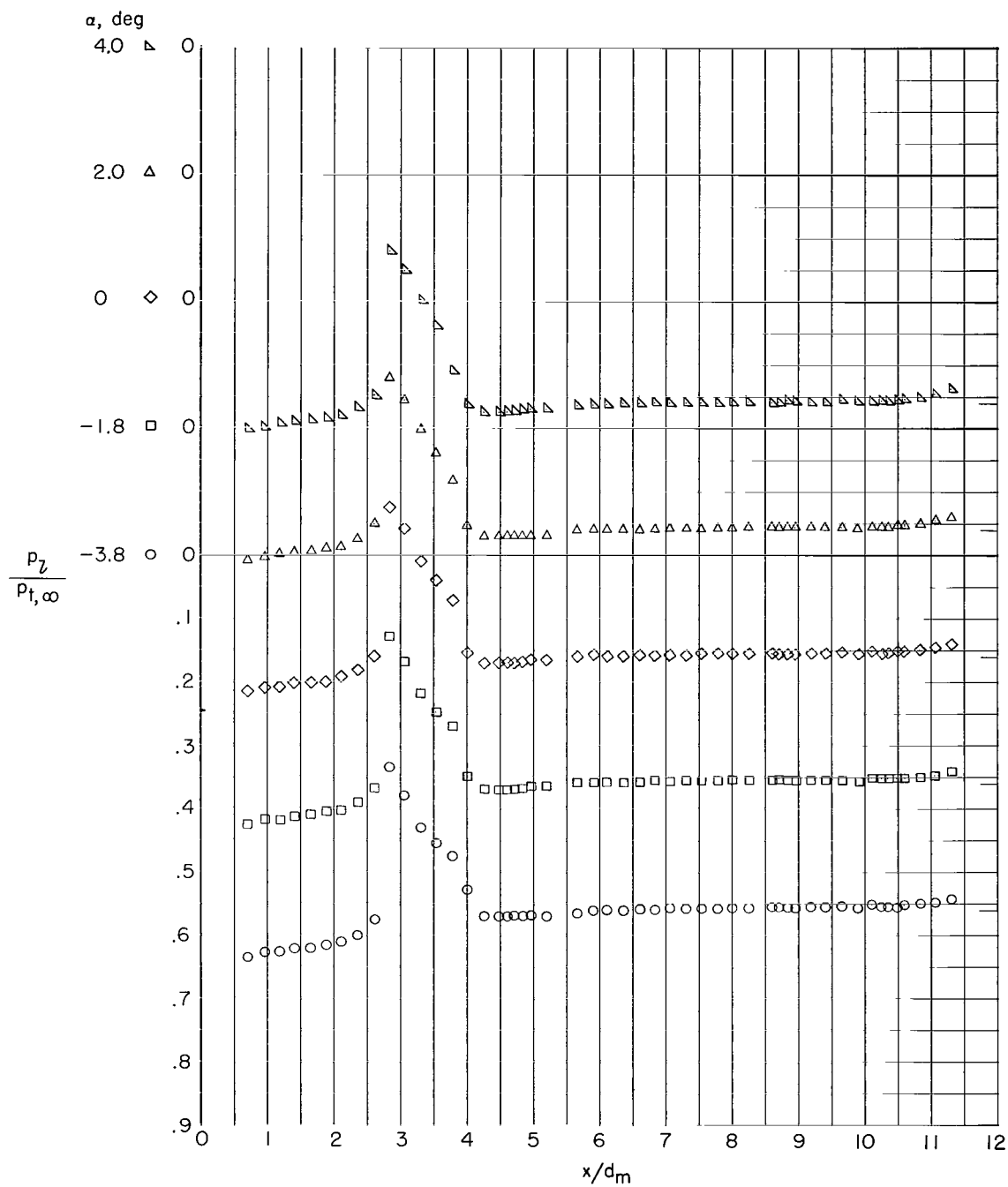
(d) M = 0.95.

Figure 3.- Continued.

15
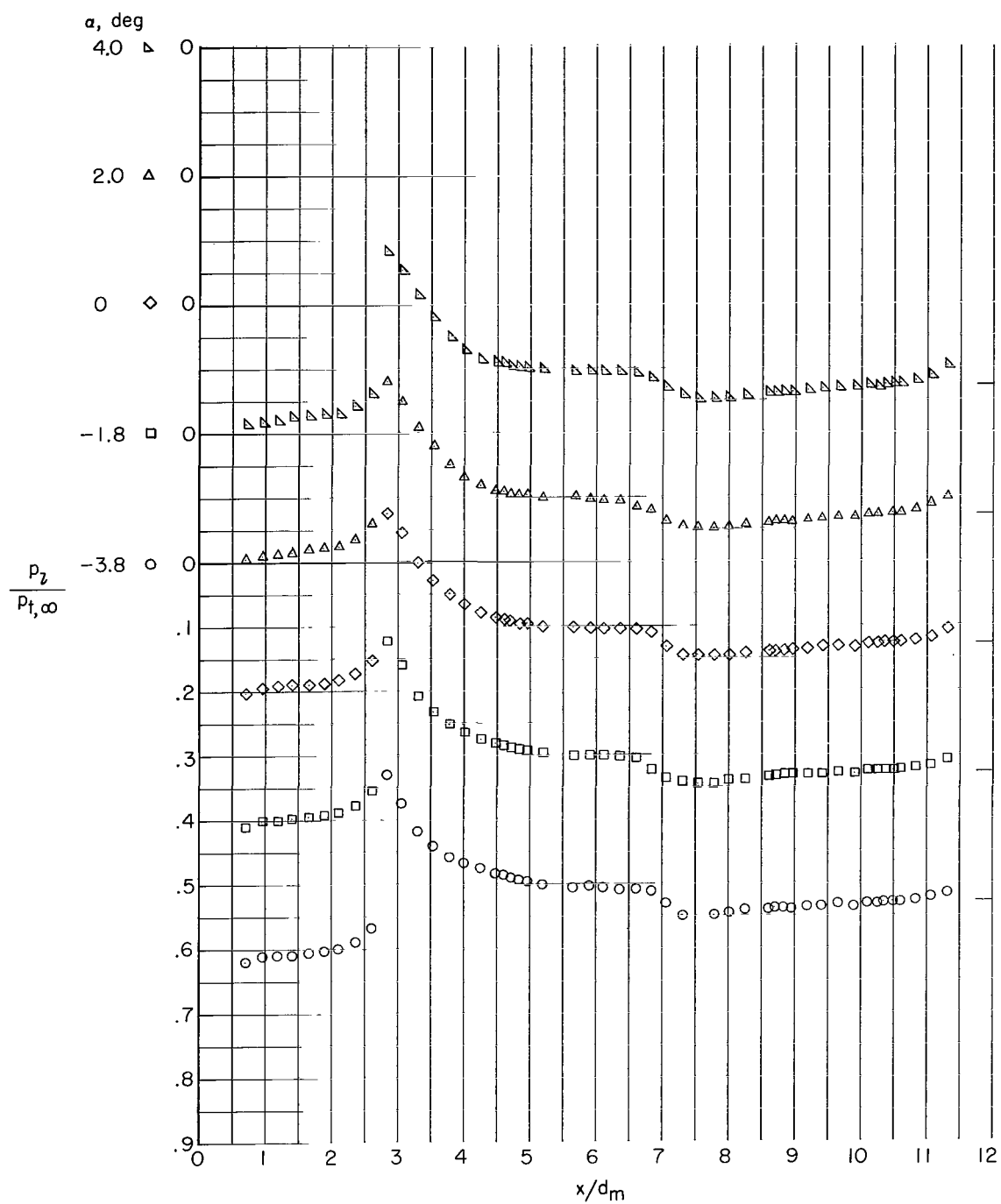
(e) M = 1.00.

Figure 3.- Continued.

16
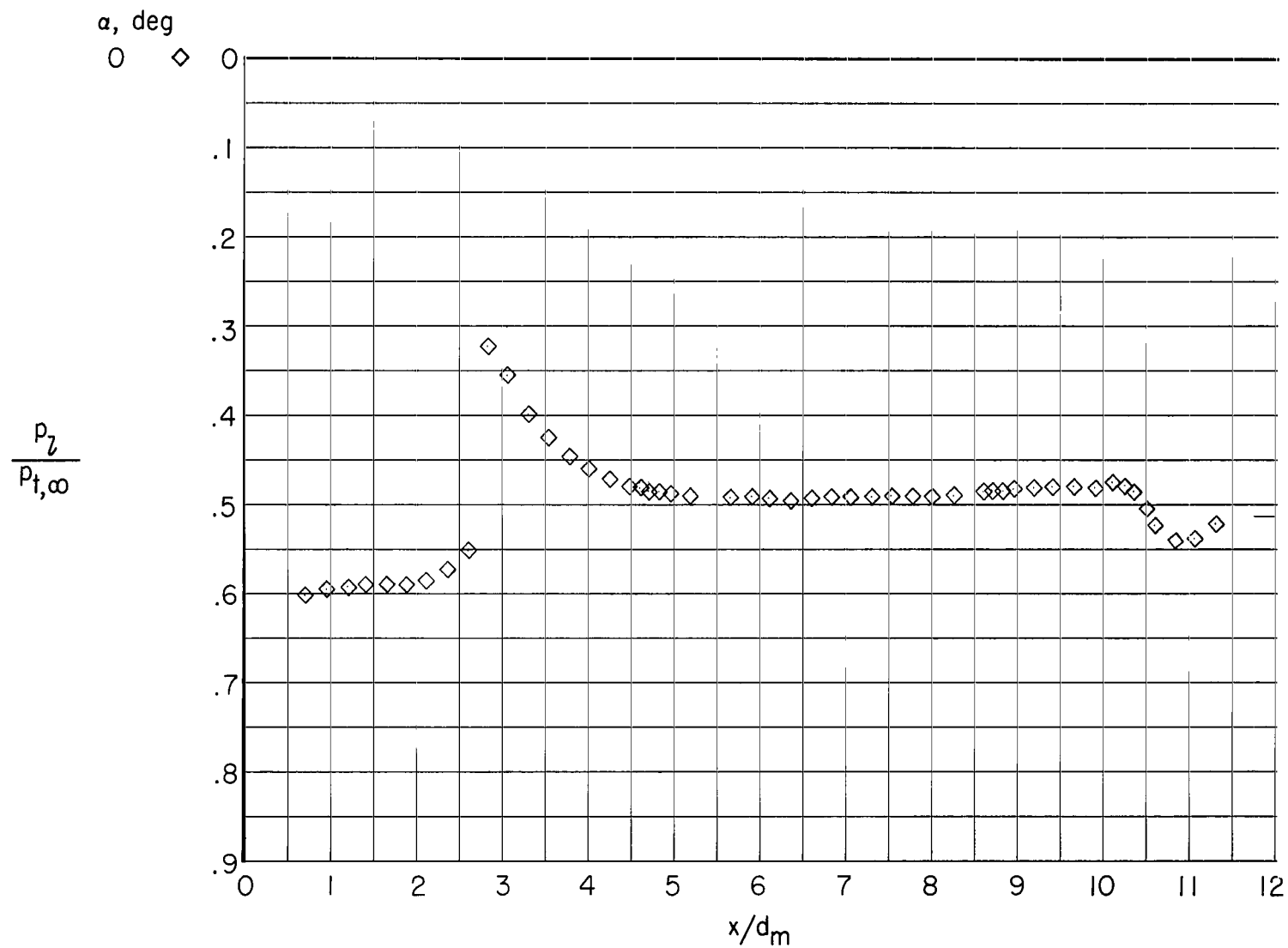
(f) M = 1.025.

Figure 3.- Continued.

(g) M = 1.04.

Figure 3.- Continued.

α, deg

4.0 ◭ 0

2.0 △ 0

0 ◇ 0

$\dfrac{p_l}{p_{t,\infty}}$

−1.8 □ 0

−3.8 ○ 0

.1
.2
.3
.4
.5
.6
.7
.8
.9

0   1   2   3   4   5   6   7   8   9   10   11   12

x/d_m
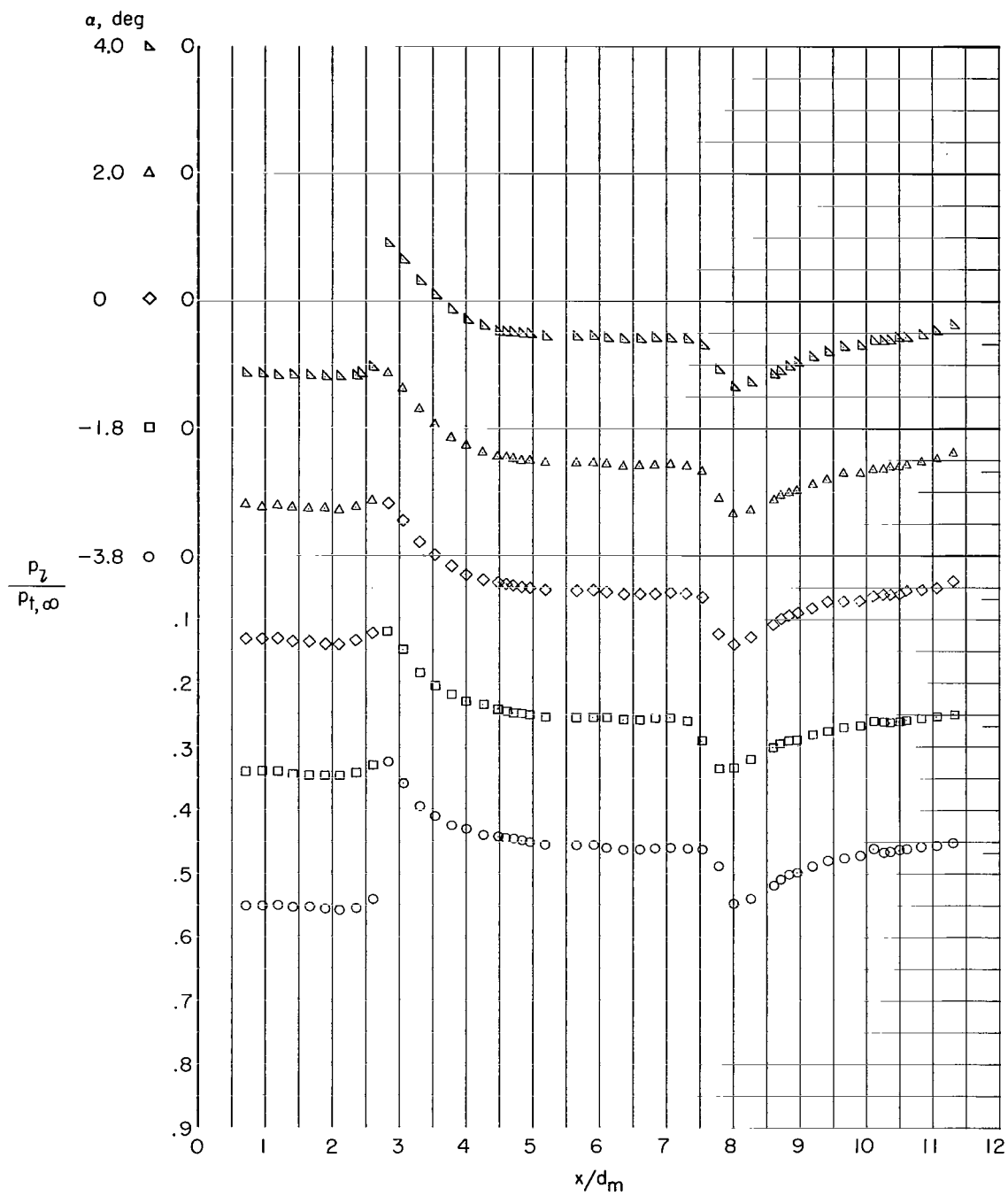
(h) M = 1.10.

Figure 3.- Continued.

19
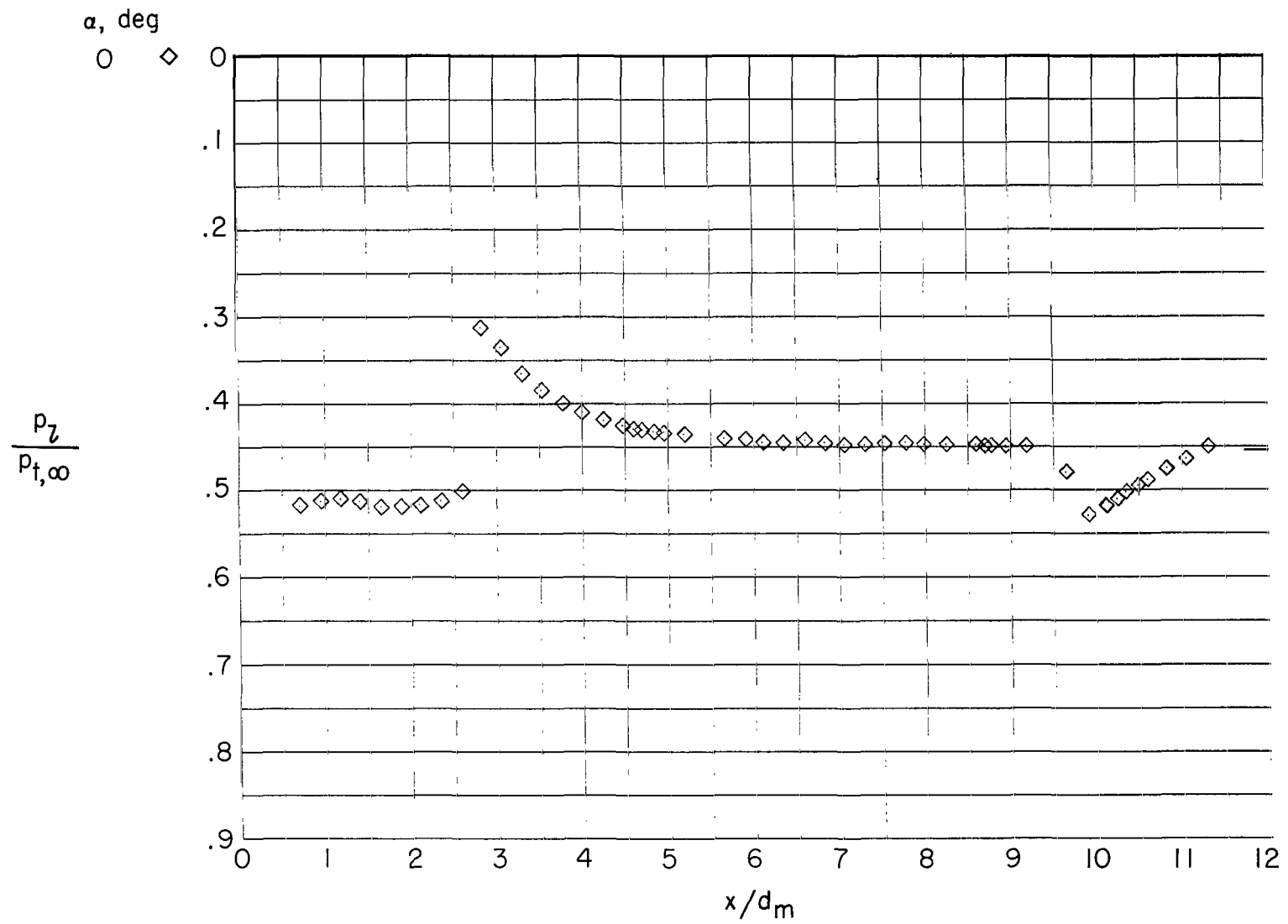
(i) M = 1.125.

Figure 3.- Continued.
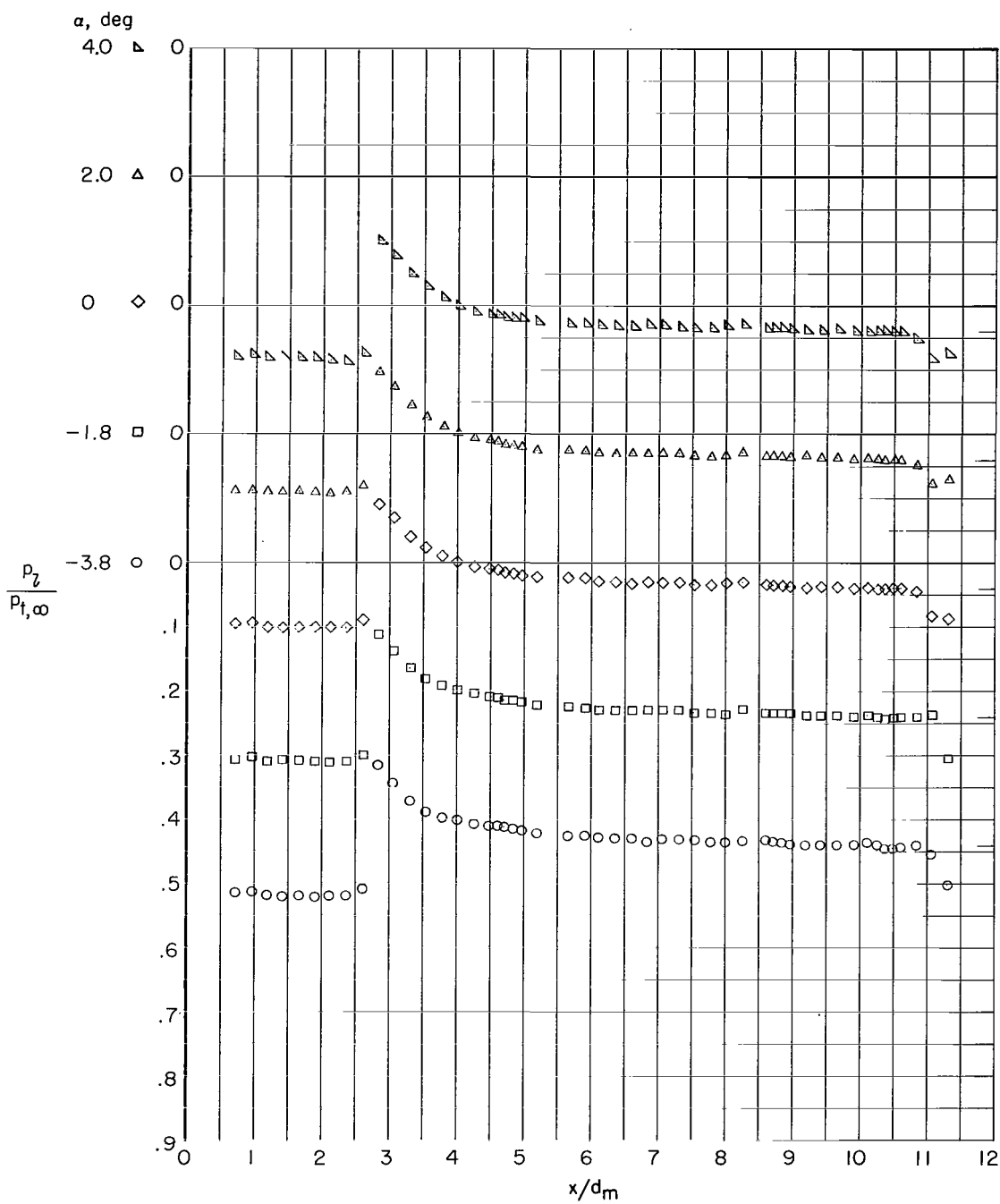
(j) M = 1.15.

Figure 3.- Continued.

α, deg

0   ◇

$$\frac{p_l}{p_{t,\infty}}$$

x/d$_m$
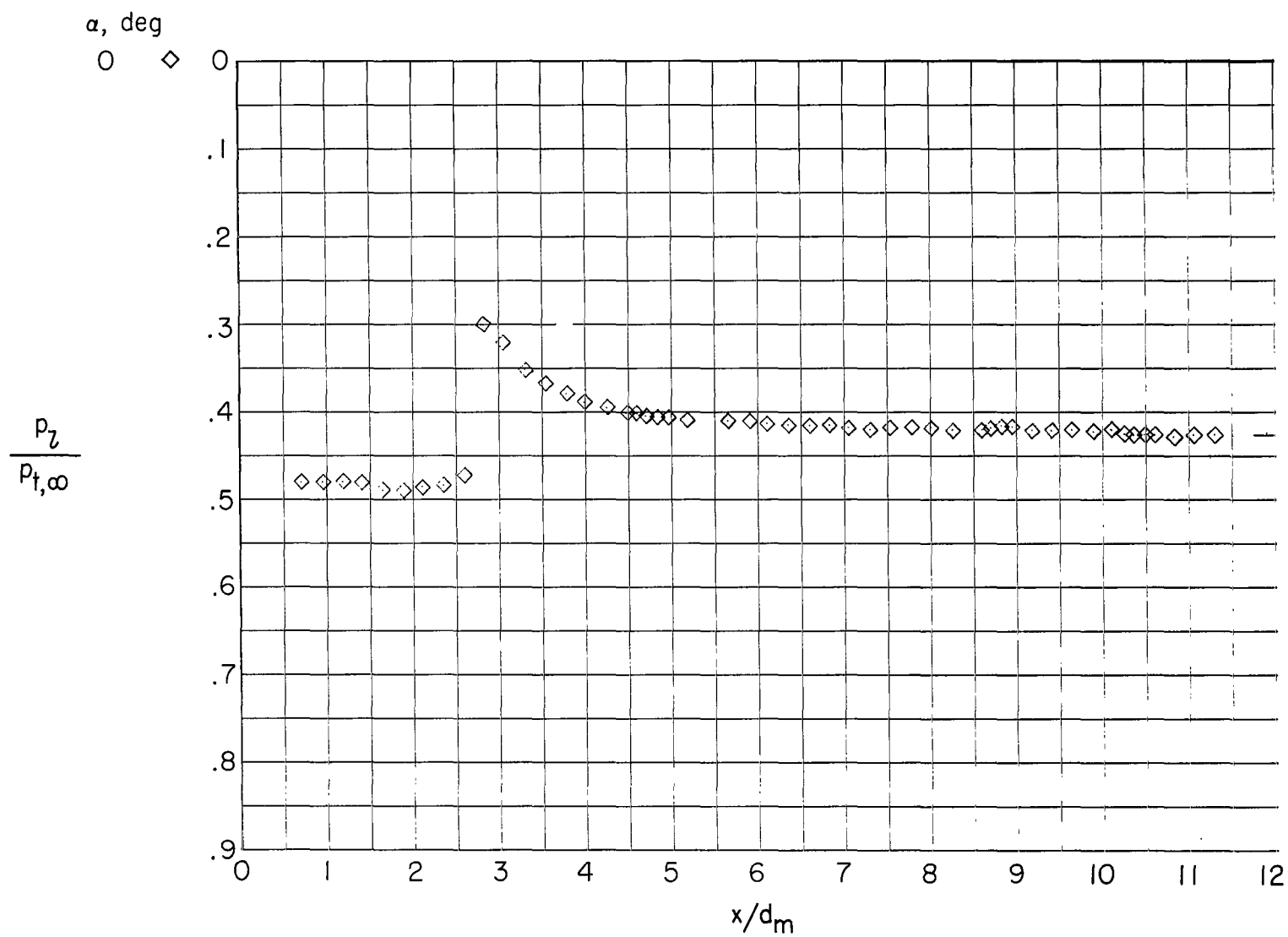
(k) M = 1.175.

Figure 3.- Continued.
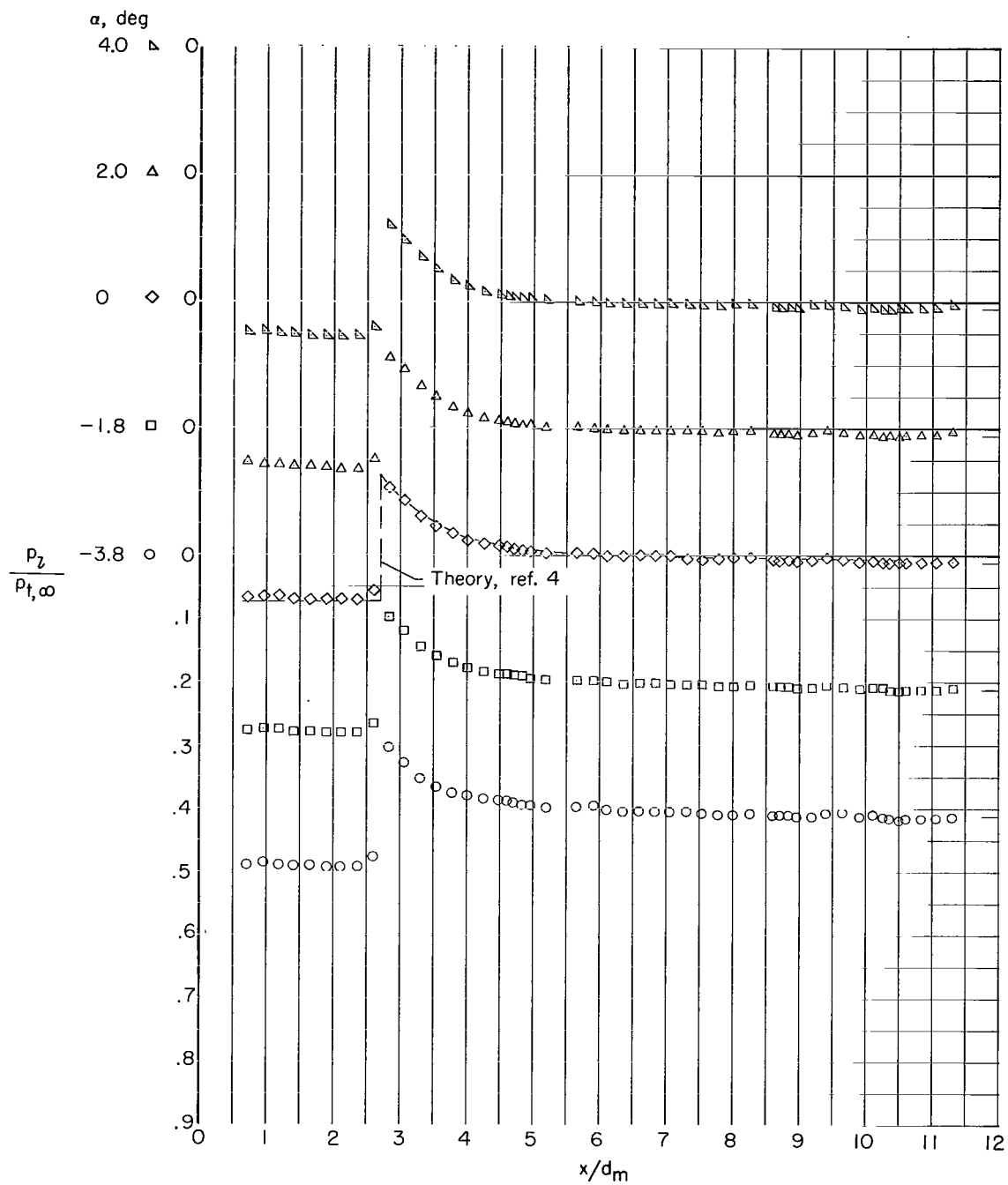
(l) M = 1.20.

Figure 3.- Continued.

23
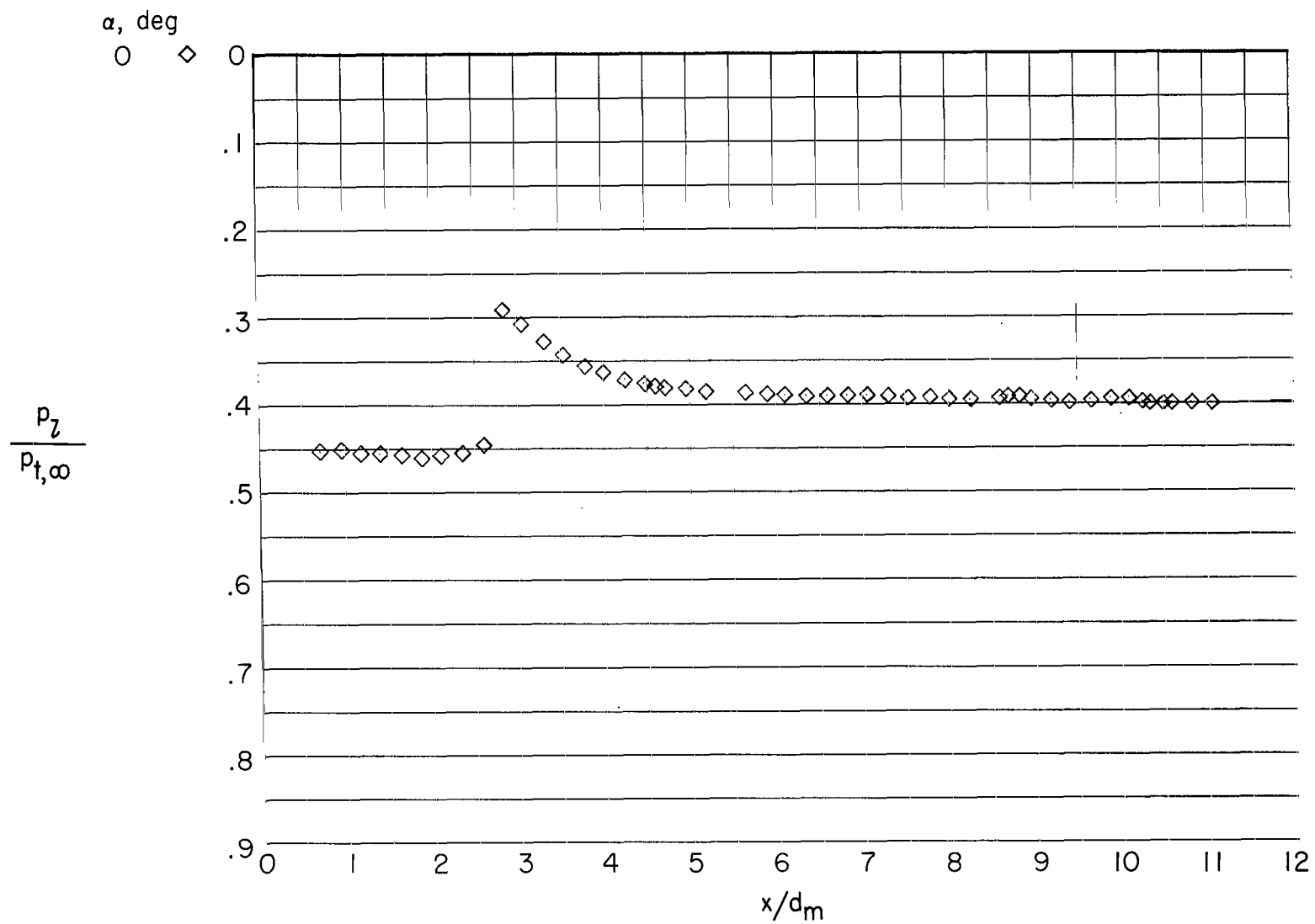
(m) M = 1.225.

Figure 3.- Continued.
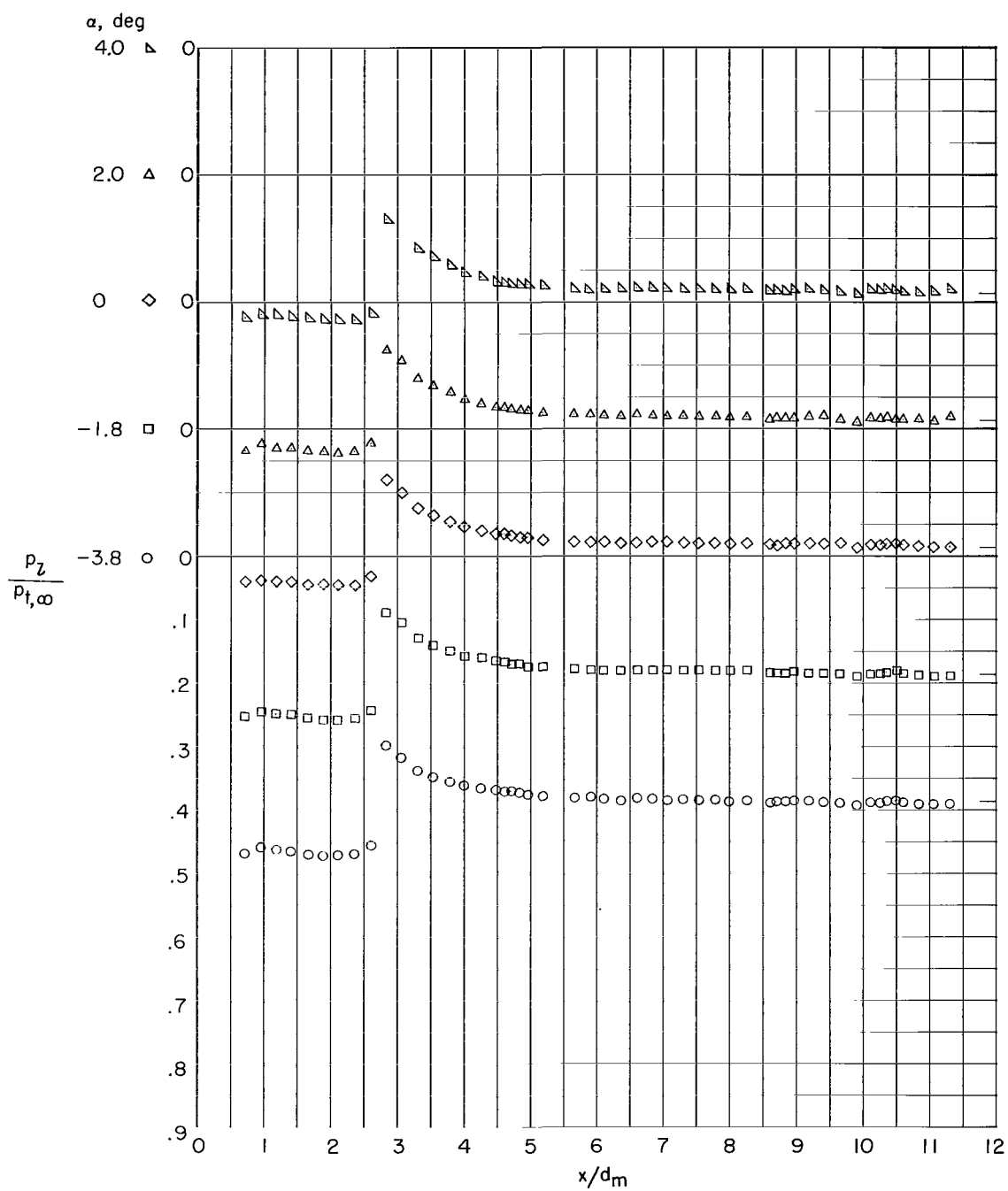
(n) M = 1.25.

Figure 3.- Continued.
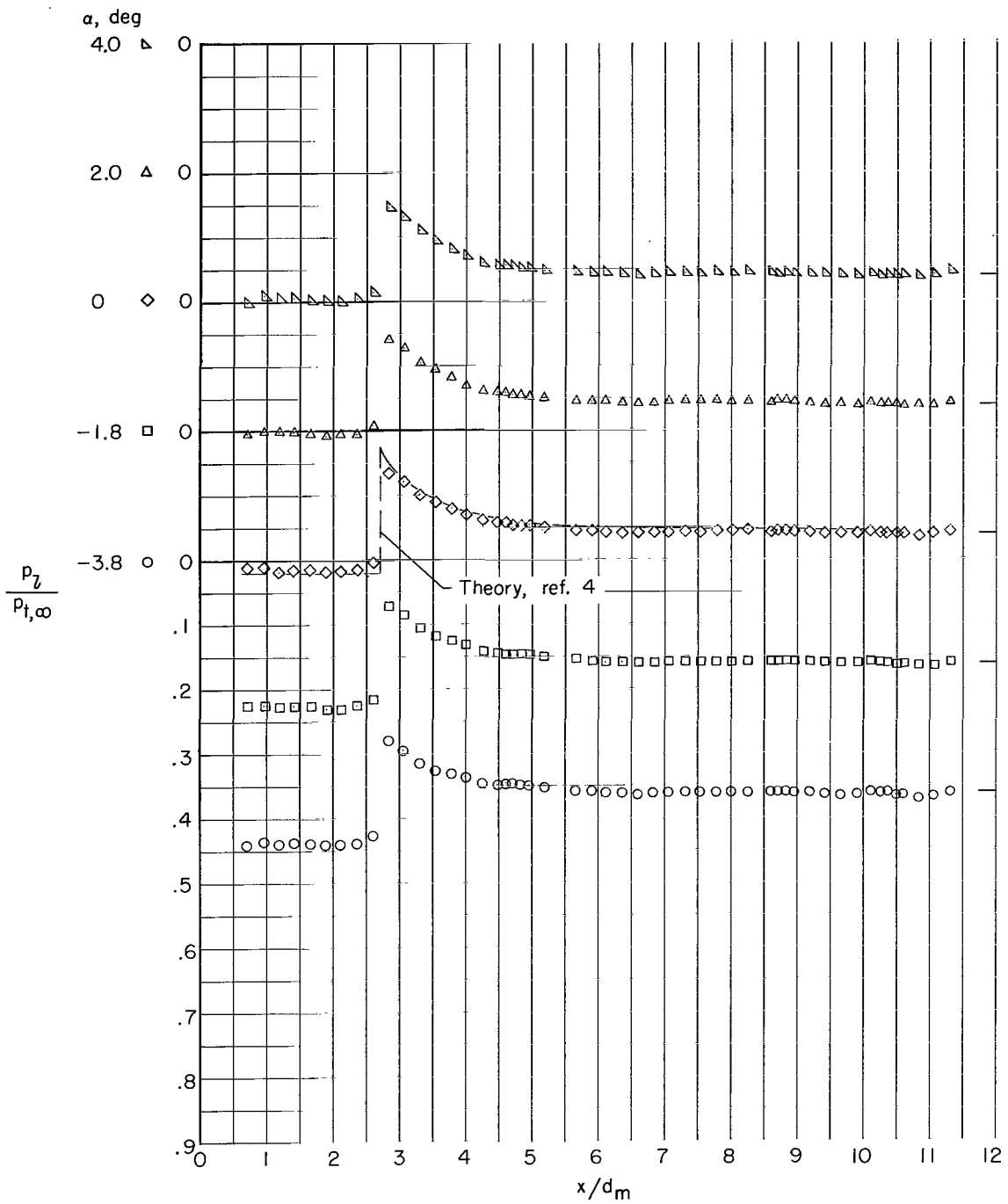
(o) M = 1.30.

Figure 3.- Concluded.
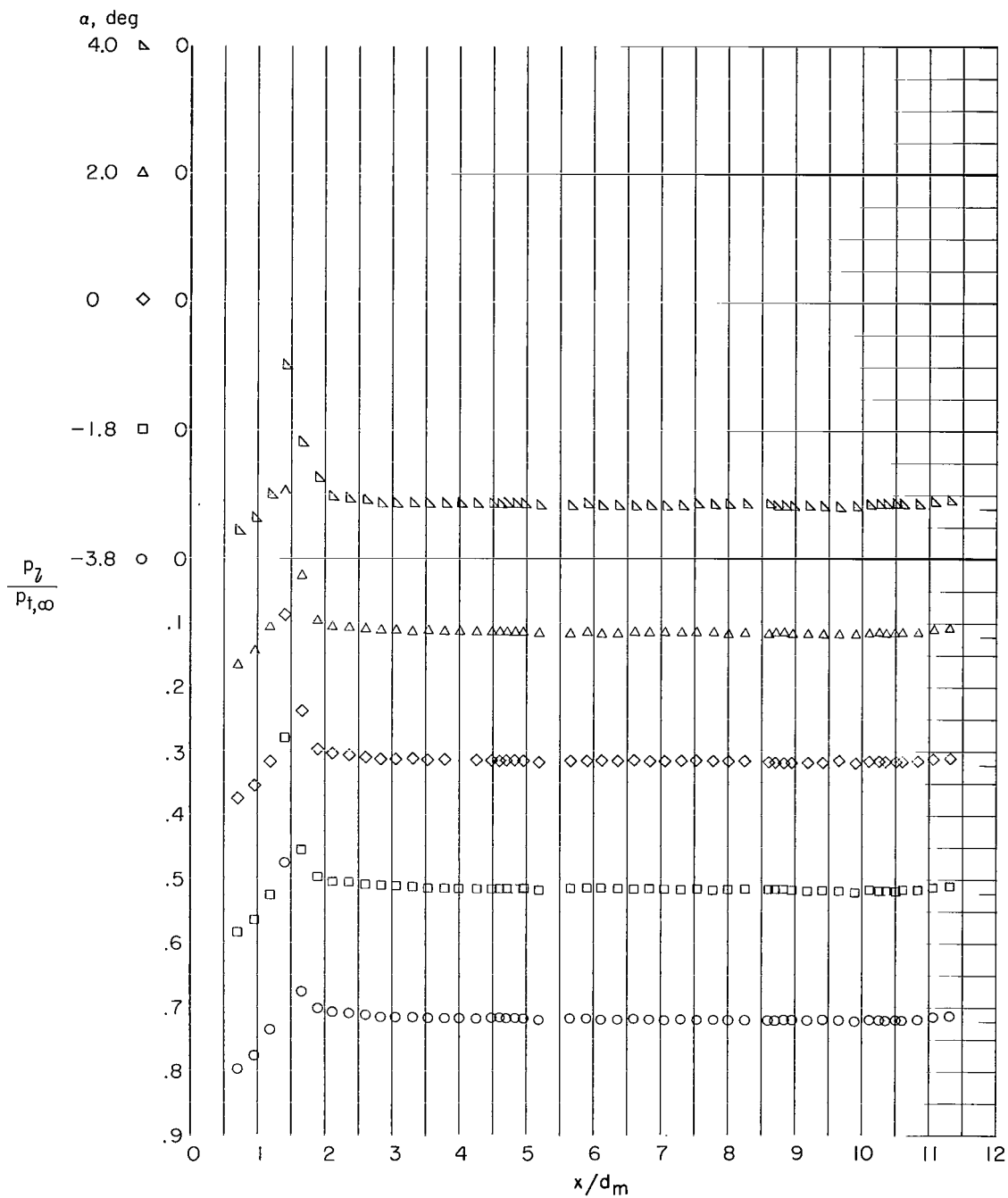
(a) M = 0.70.

Figure 4.- Pressure distributions for configuration 2. $\theta = 20^0$; $l = 243.84$ cm (96.00 in.); fineness ratio of 11.29. Ticks indicate free-stream pressure ratio.
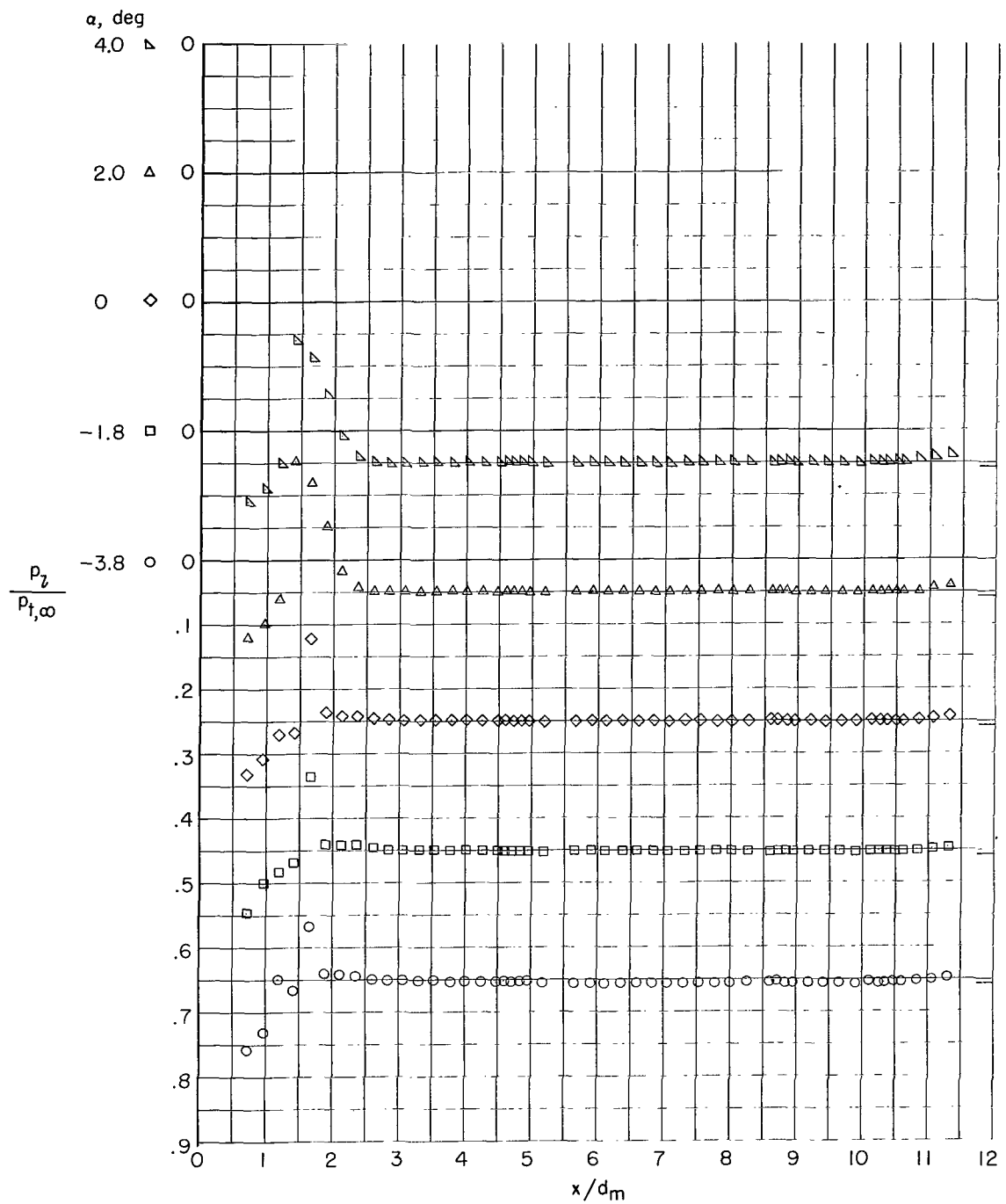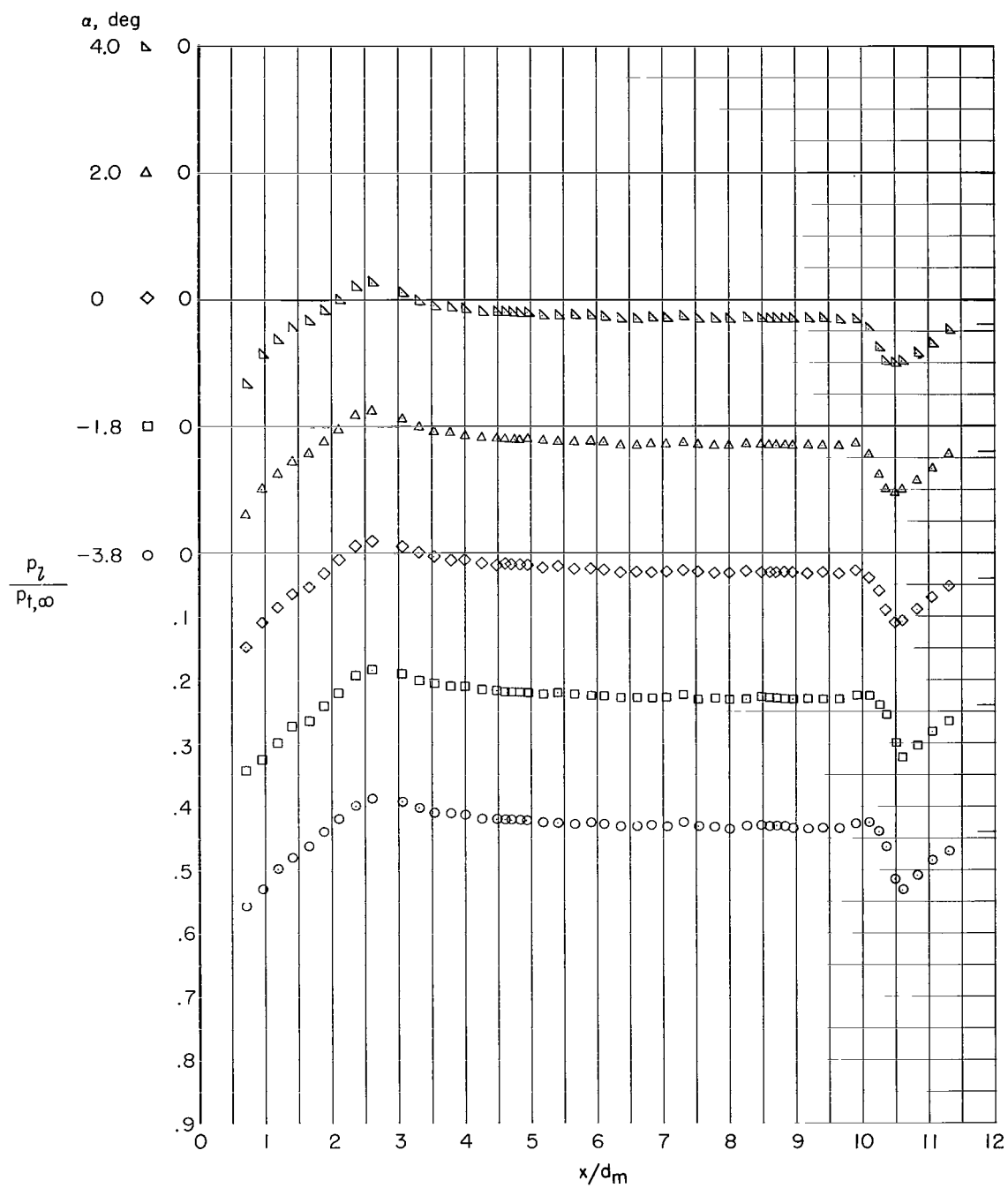
(b) M = 0.80.

Figure 4.- Continued.
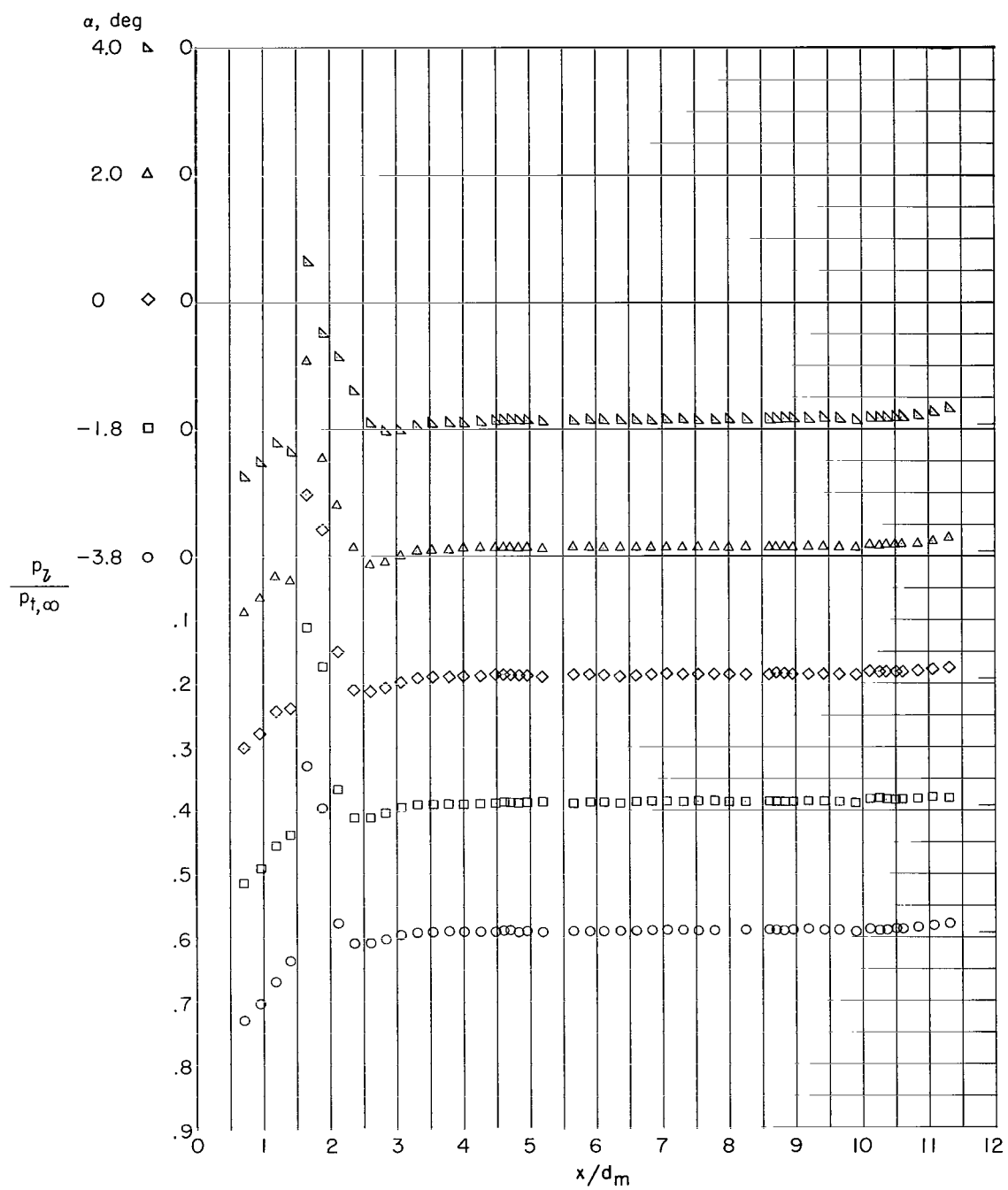
(c) M = 0.90.

Figure 4.- Continued.
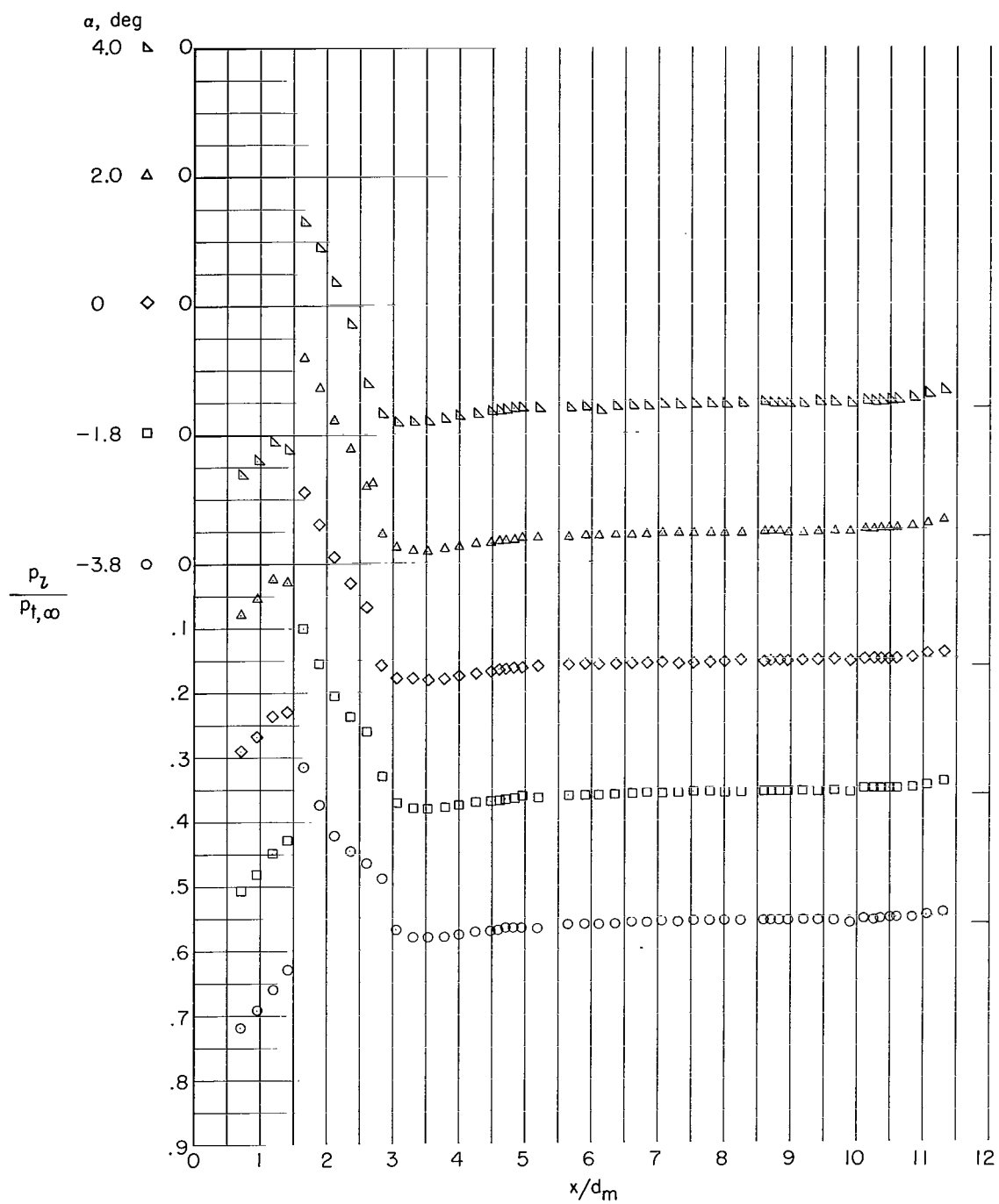
(d) M = 0.95.

Figure 4.- Continued.

30
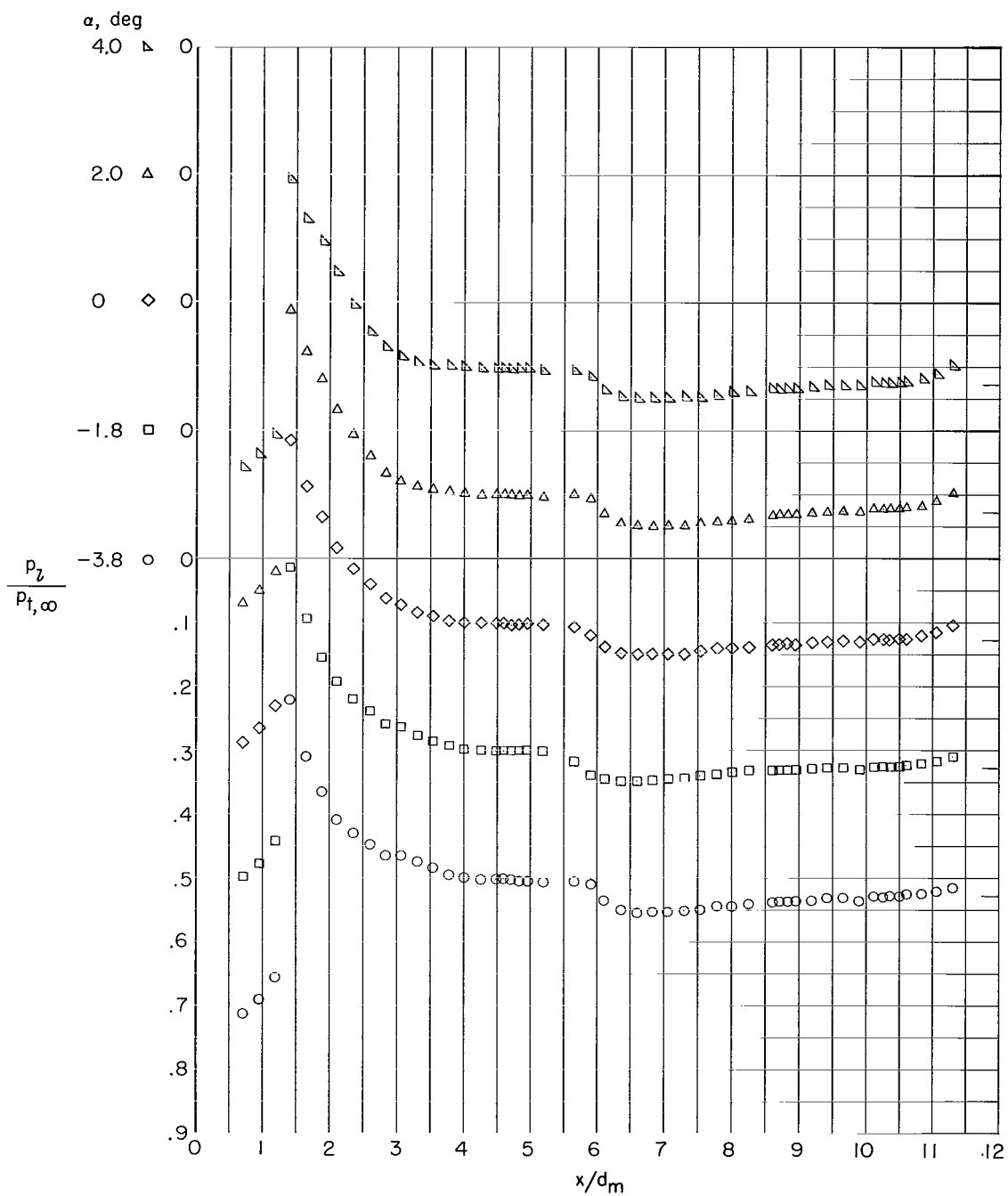
(e) M = 1.00.

Figure 4.- Continued.

31
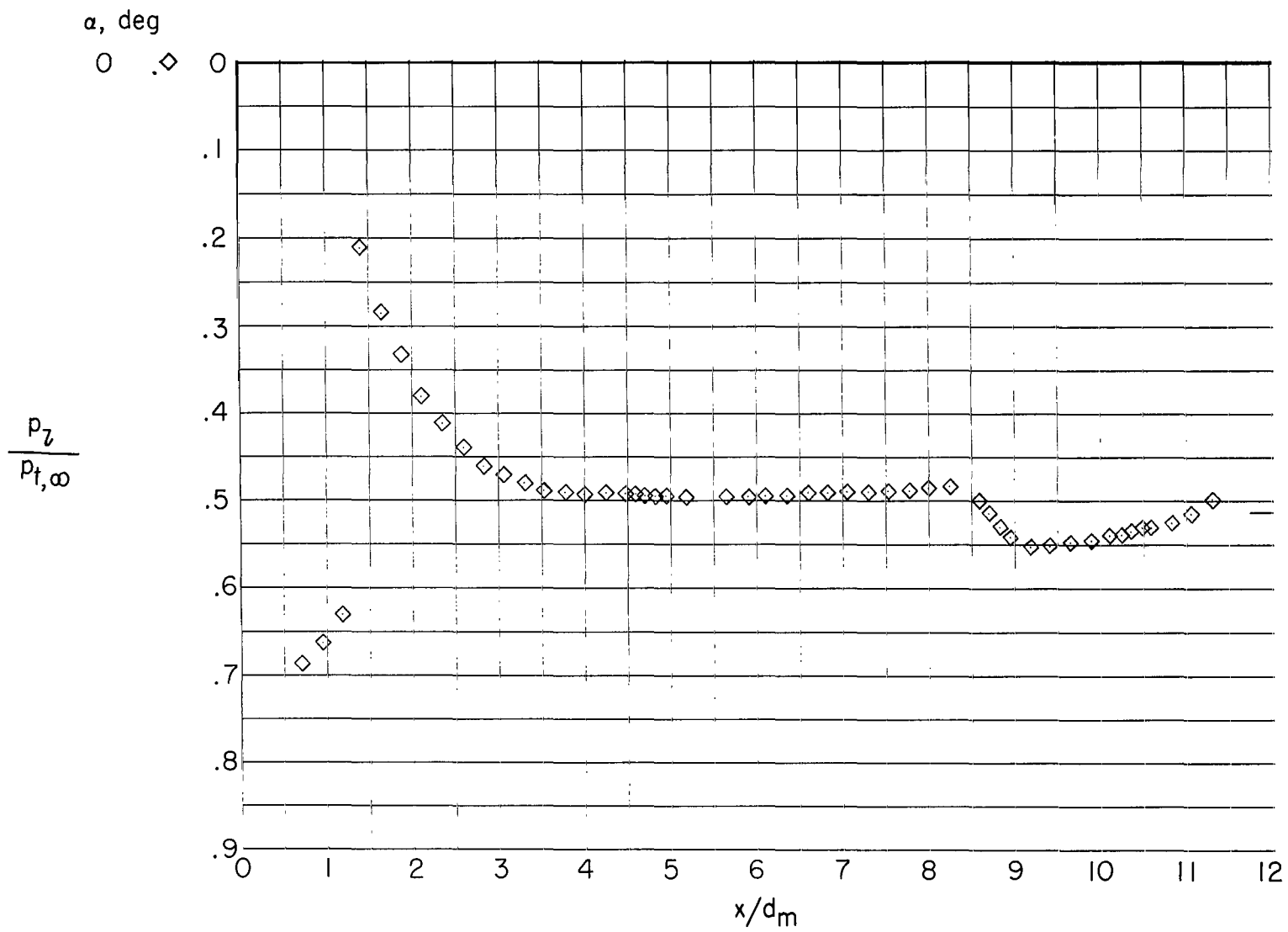
(f) M = 1.025.

Figure 4.- Continued.
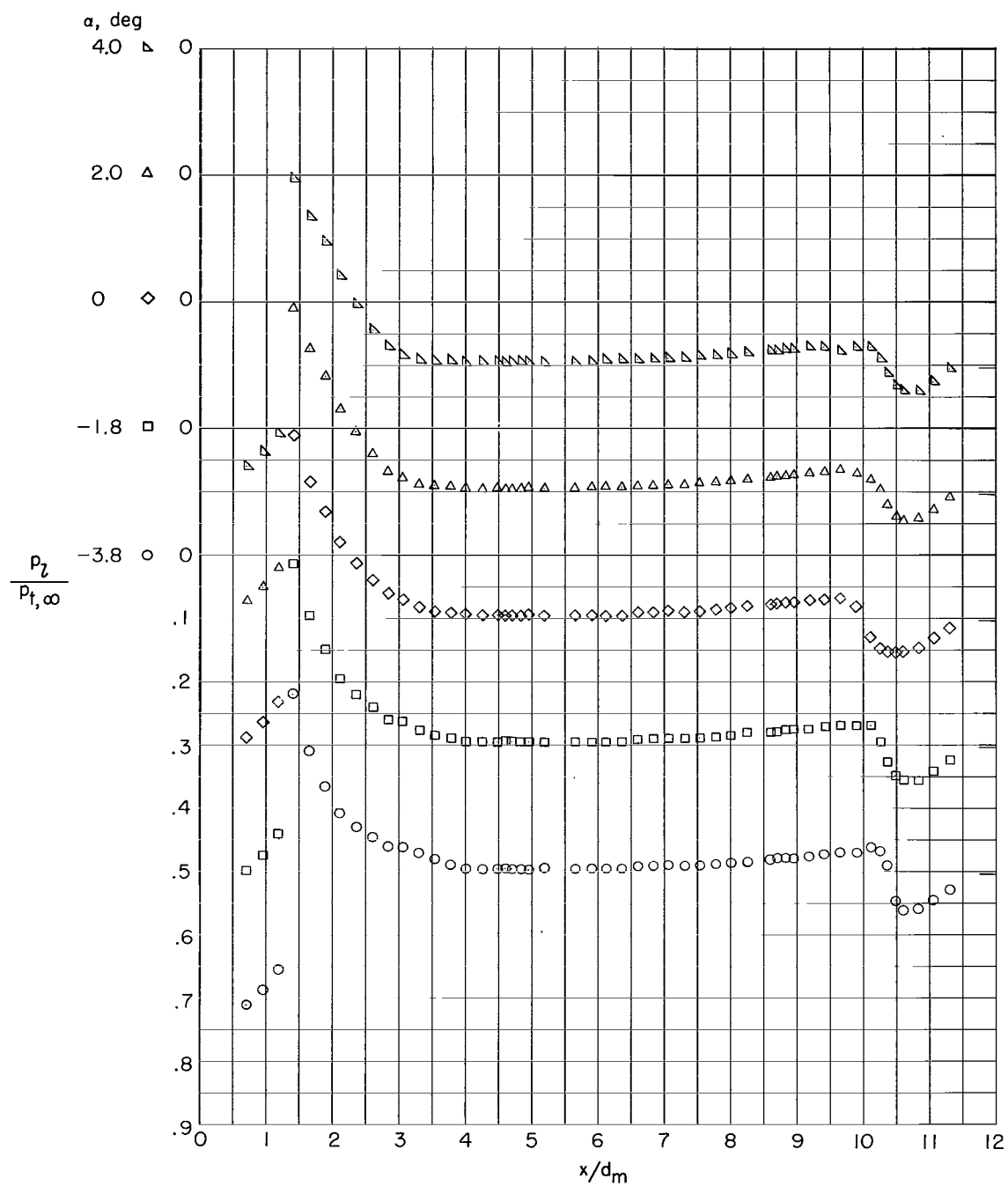
(g) M = 1.04.

Figure 4.- Continued.
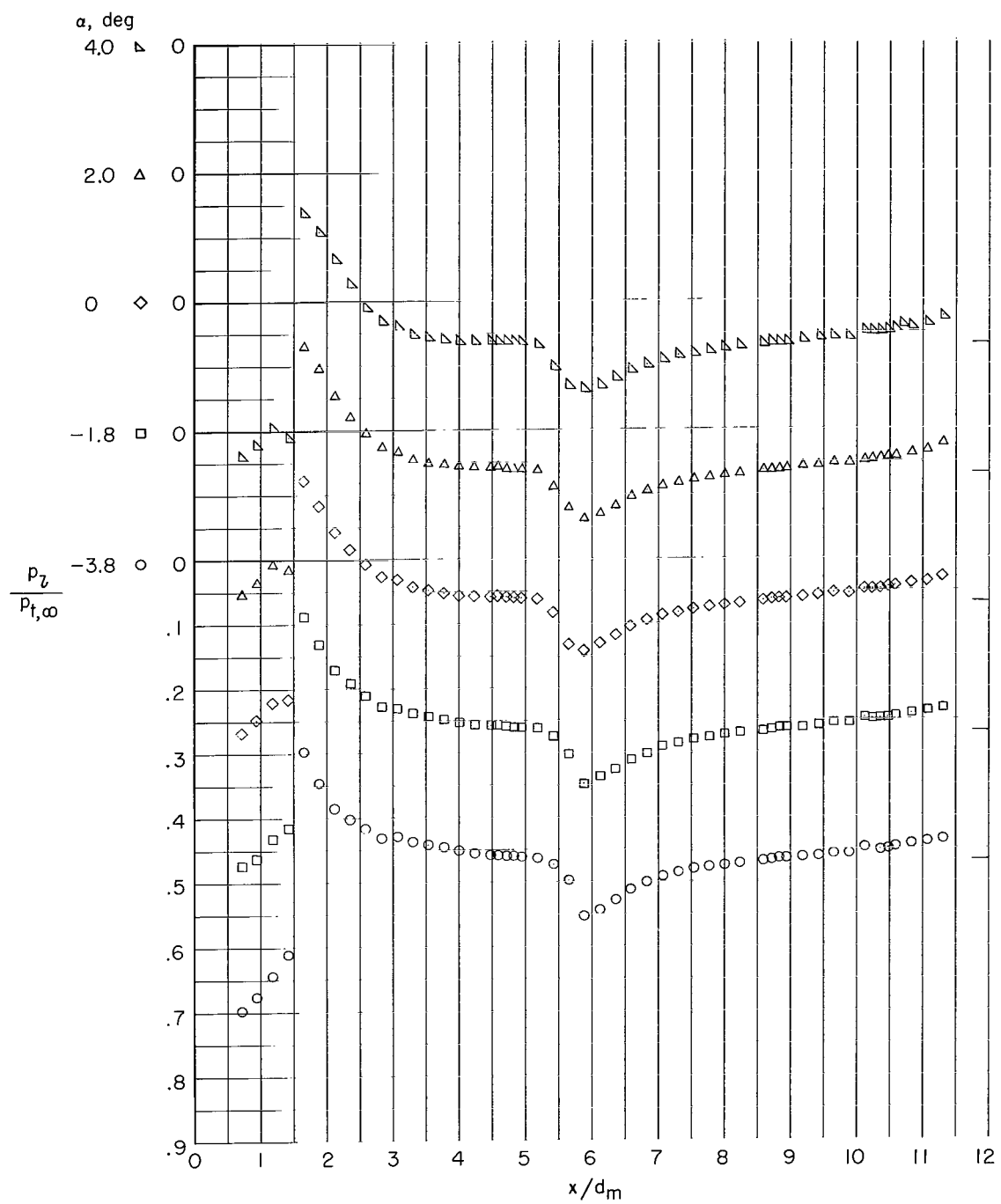
(h) M = 1.10.

Figure 4.- Continued.
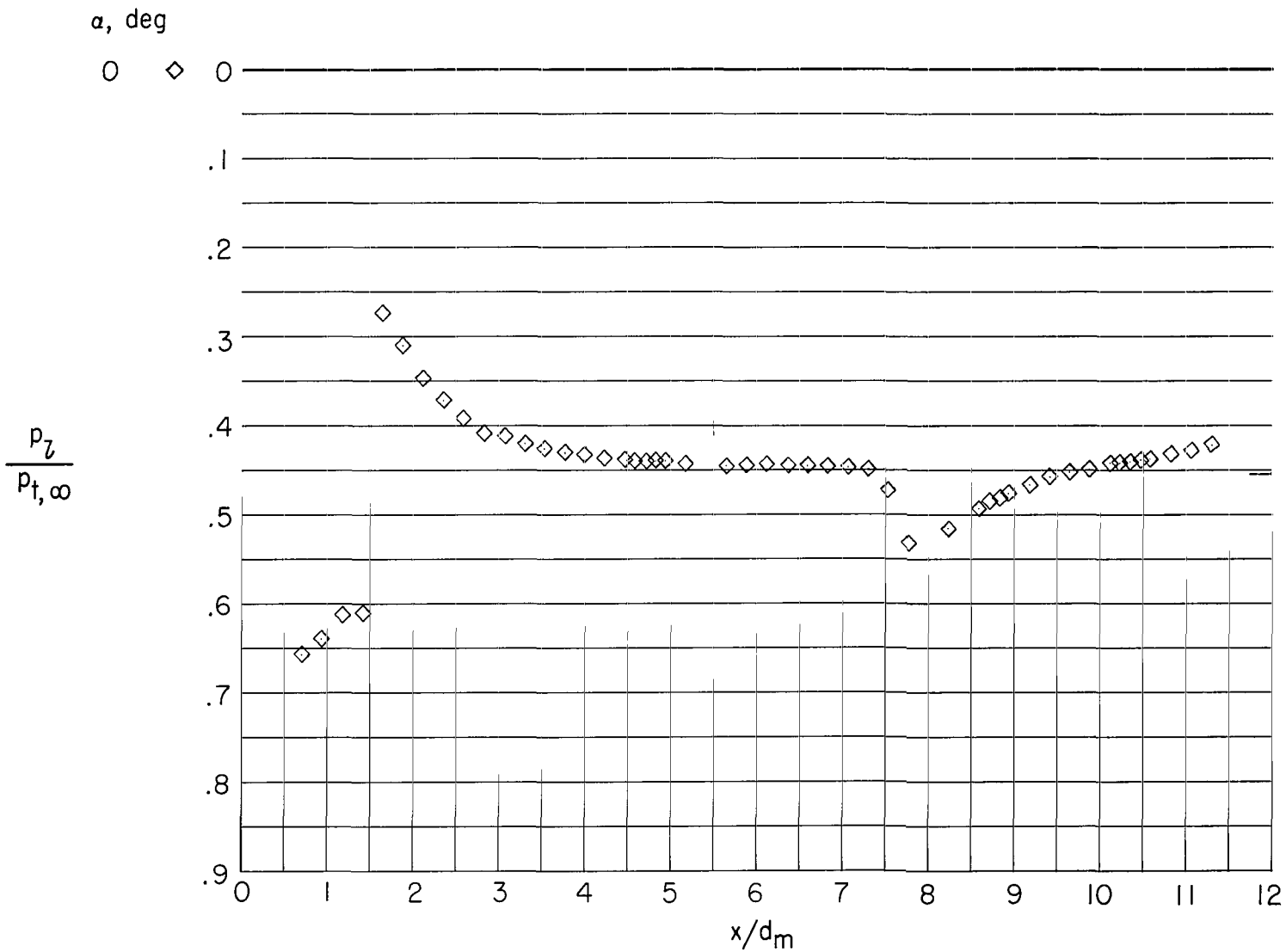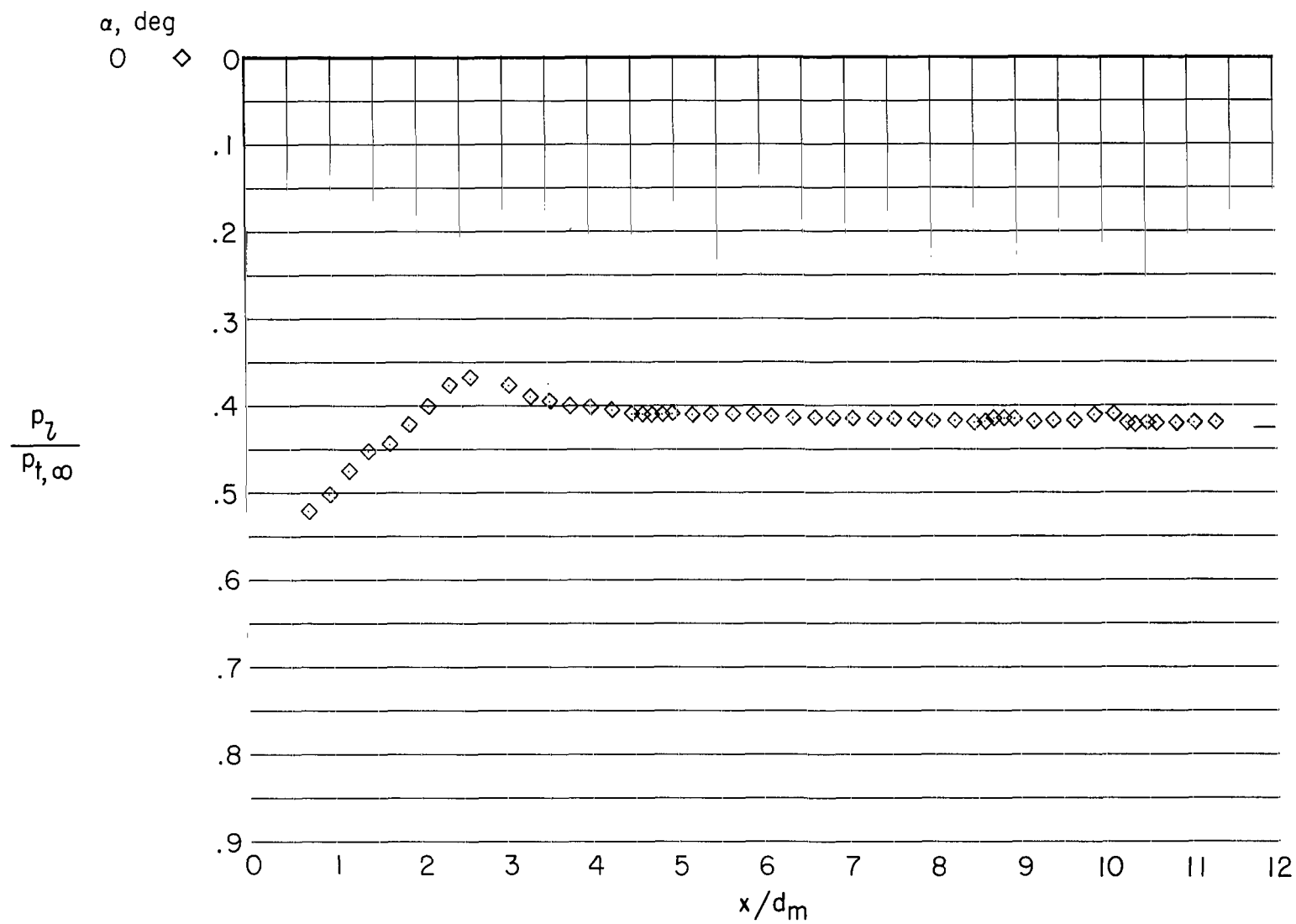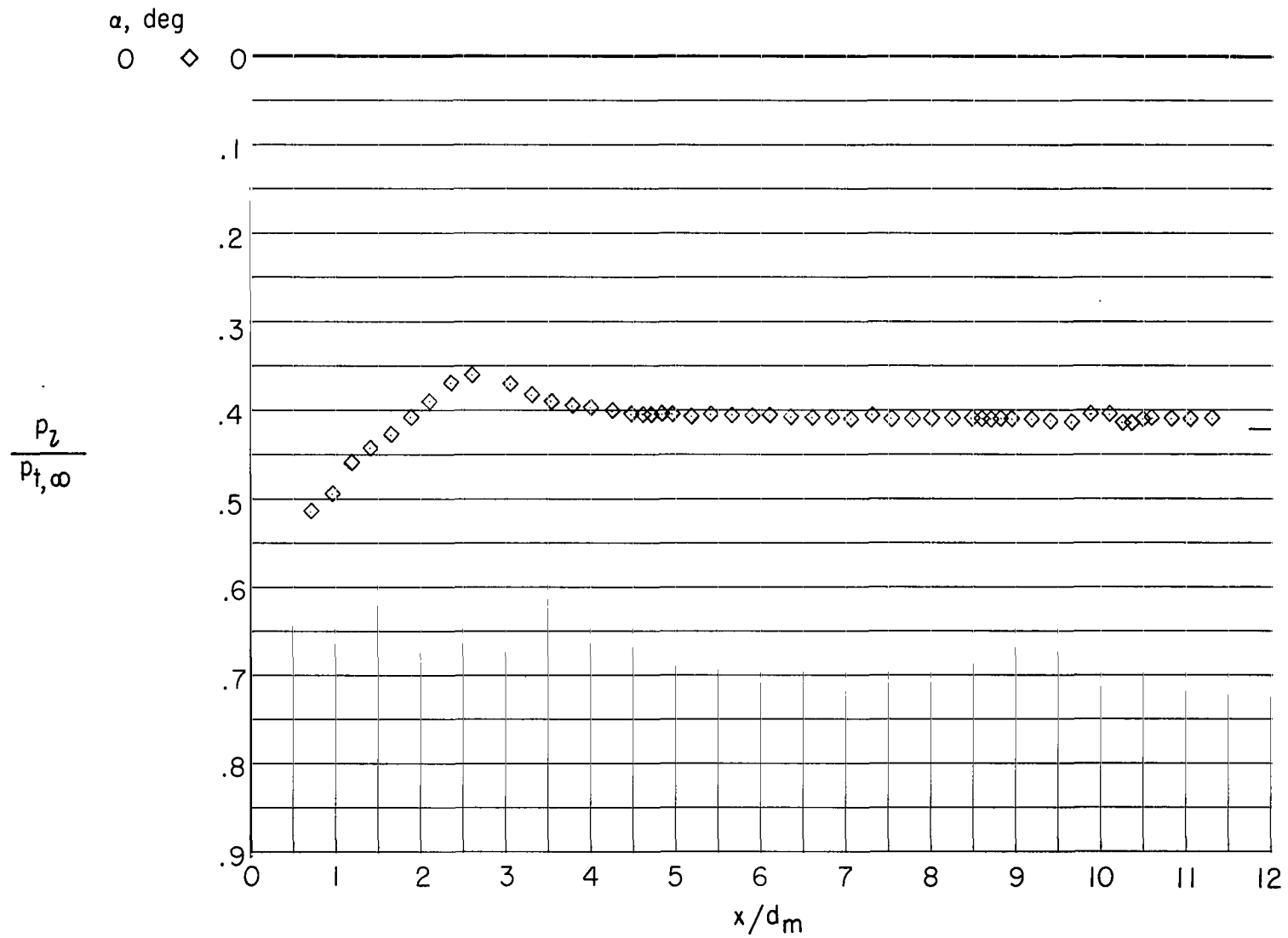
(i) M = 1.125.

Figure 4.- Continued.
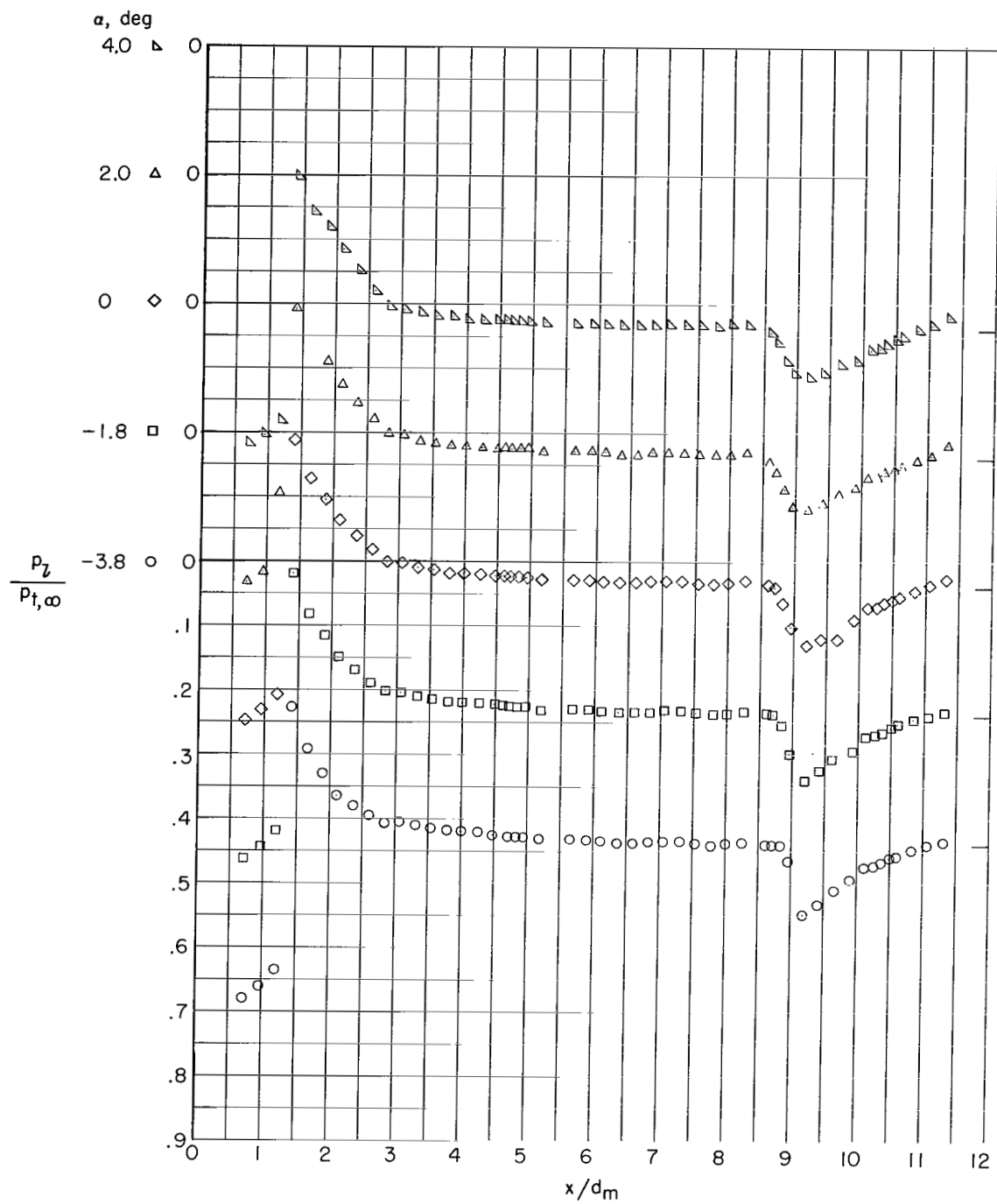
(j) M = 1.15.

Figure 4.- Continued.
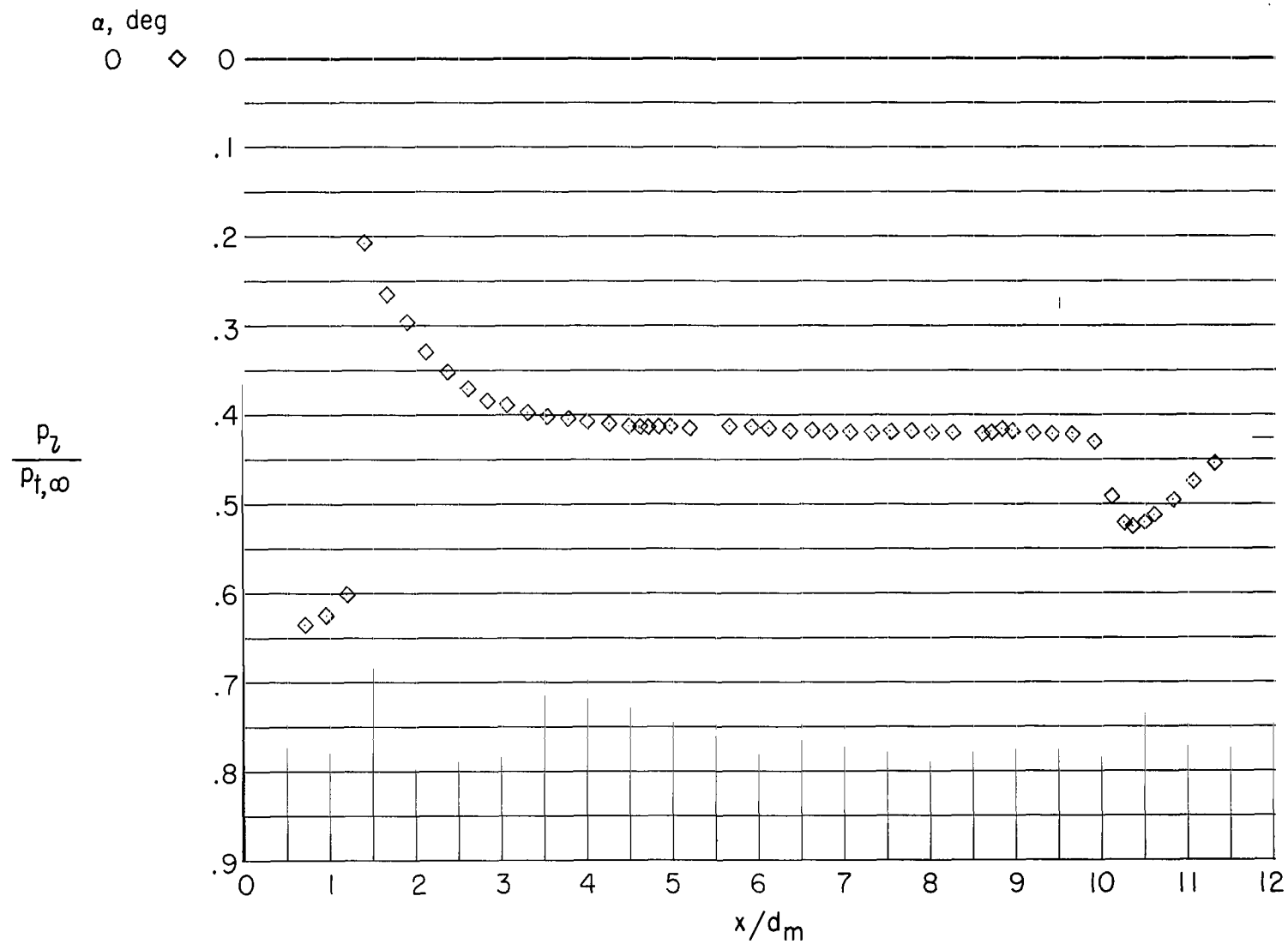
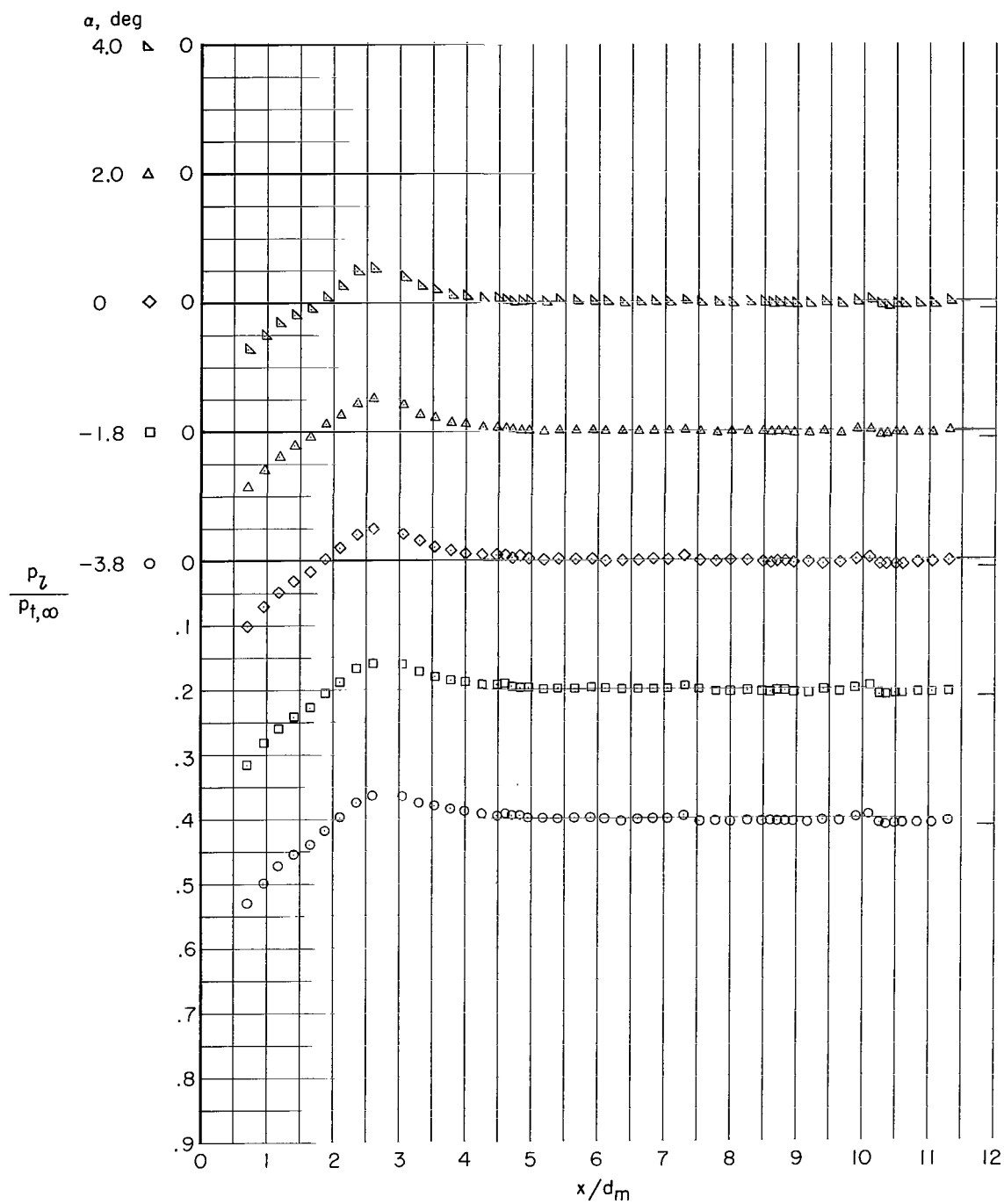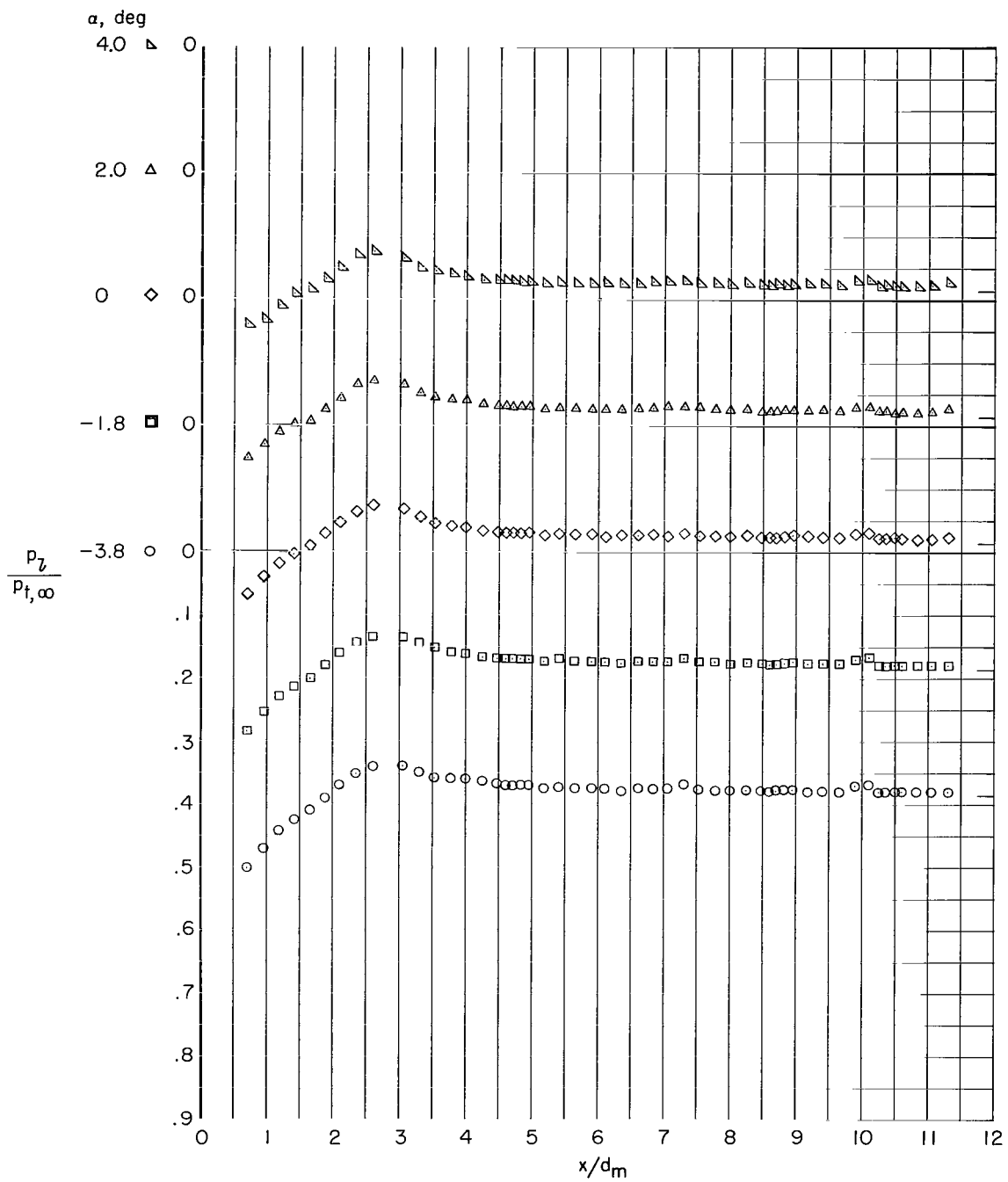(k) M = 1.175.

Figure 4.- Continued.
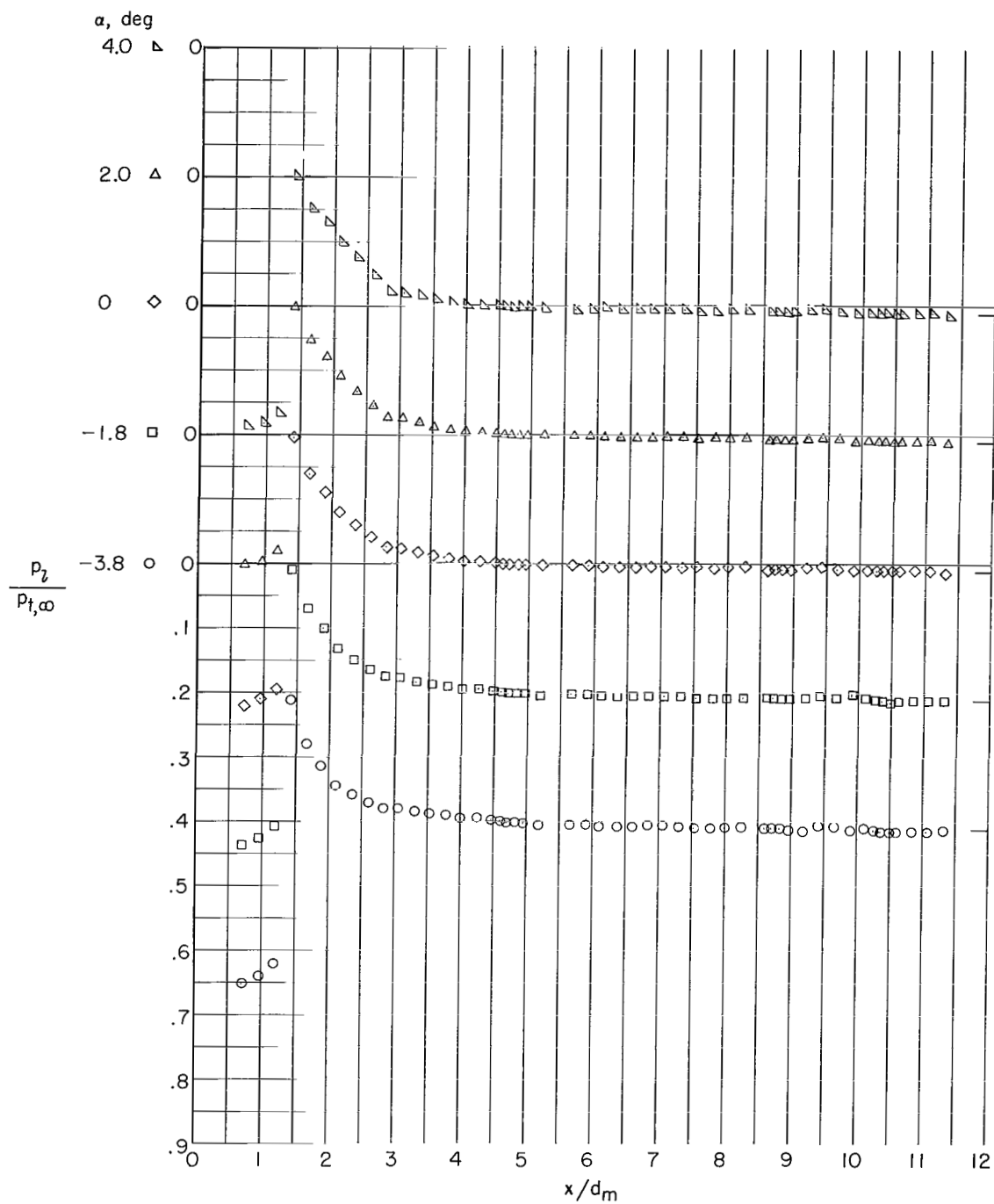
(l) M = 1.20.

Figure 4.- Continued.
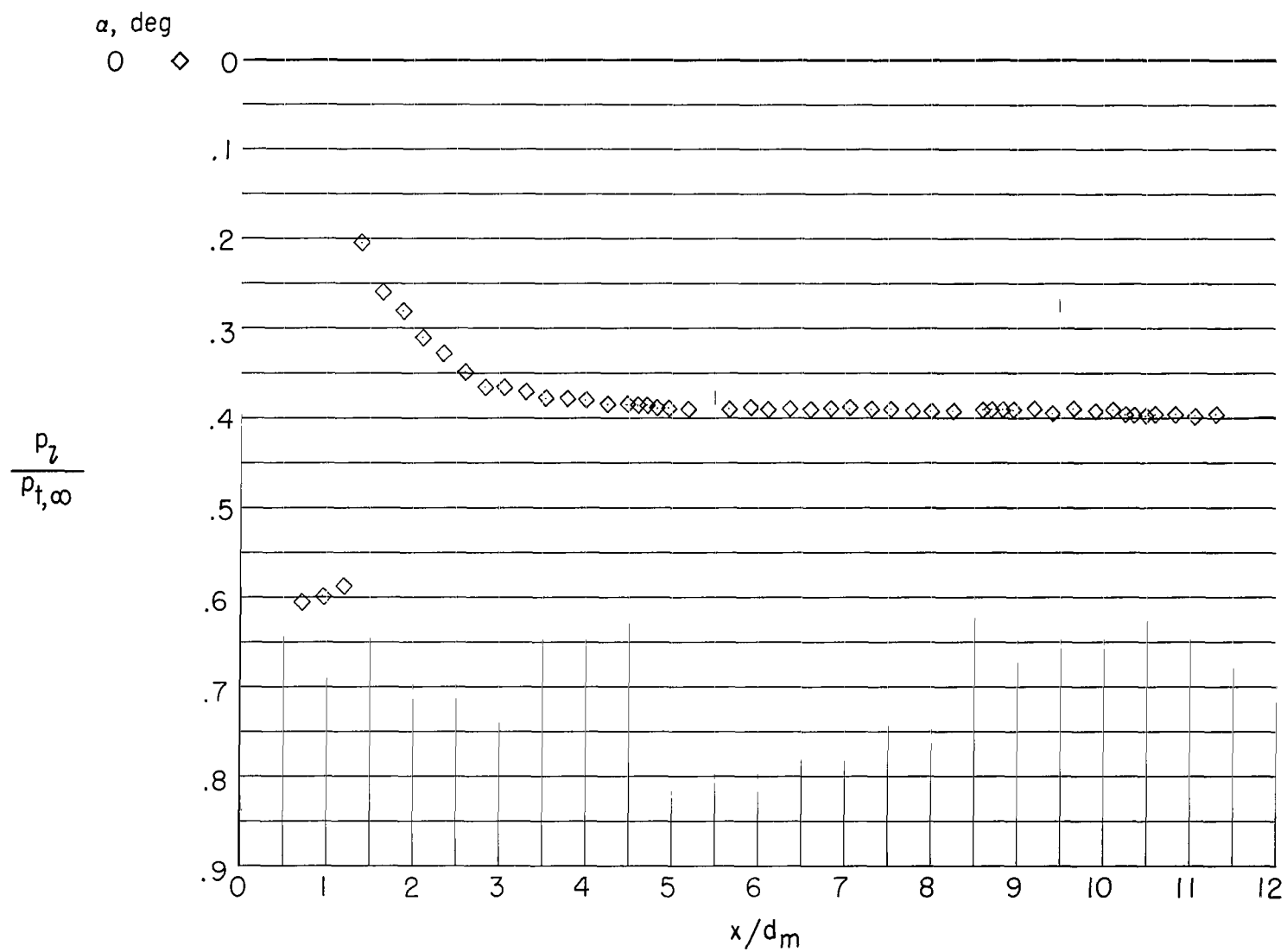
(m) M = 1.225.

Figure 4.- Continued.
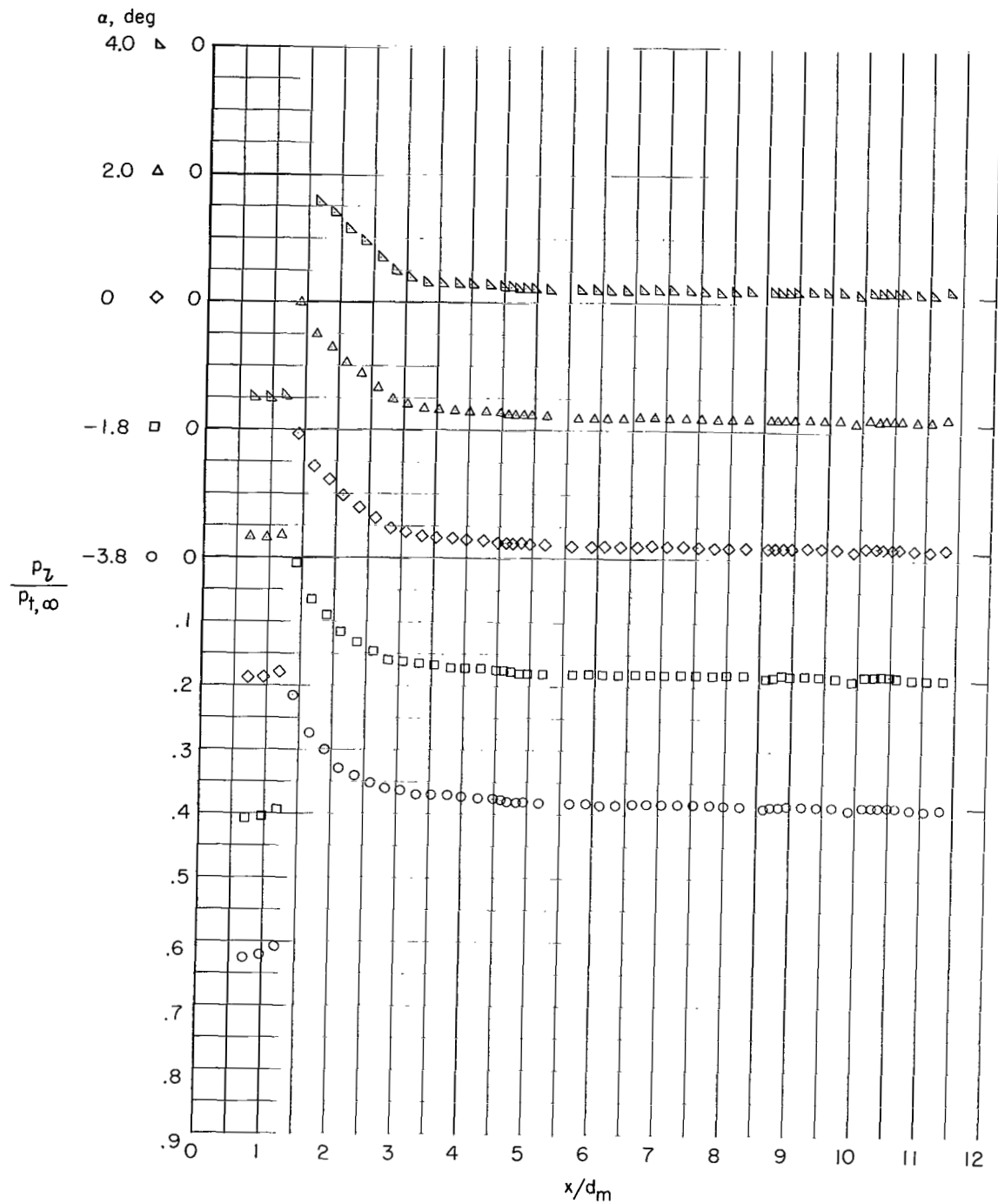
(n) M = 1.25.

Figure 4.- Continued.

40

(o) M = 1.30.

Figure 4.- Concluded.

α, deg

4.0

2.0

0

−1.8

−3.8

$\dfrac{p_l}{p_{t,\infty}}$

0

.1

.2

.3

.4

.5

.6

.7

.8

.9

0 1 2 3 4 5 6 7 8 9 10 11 12

x/d_m
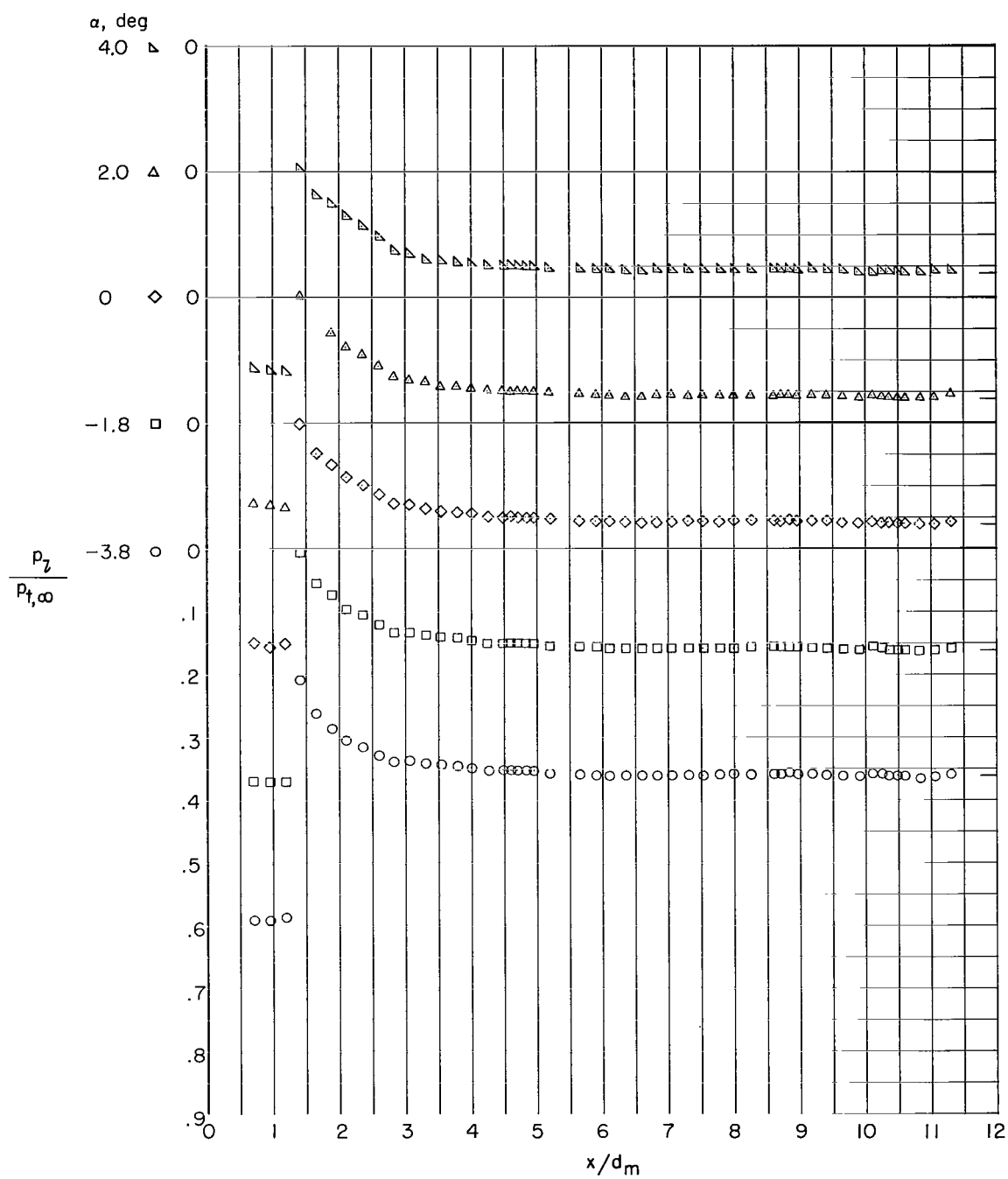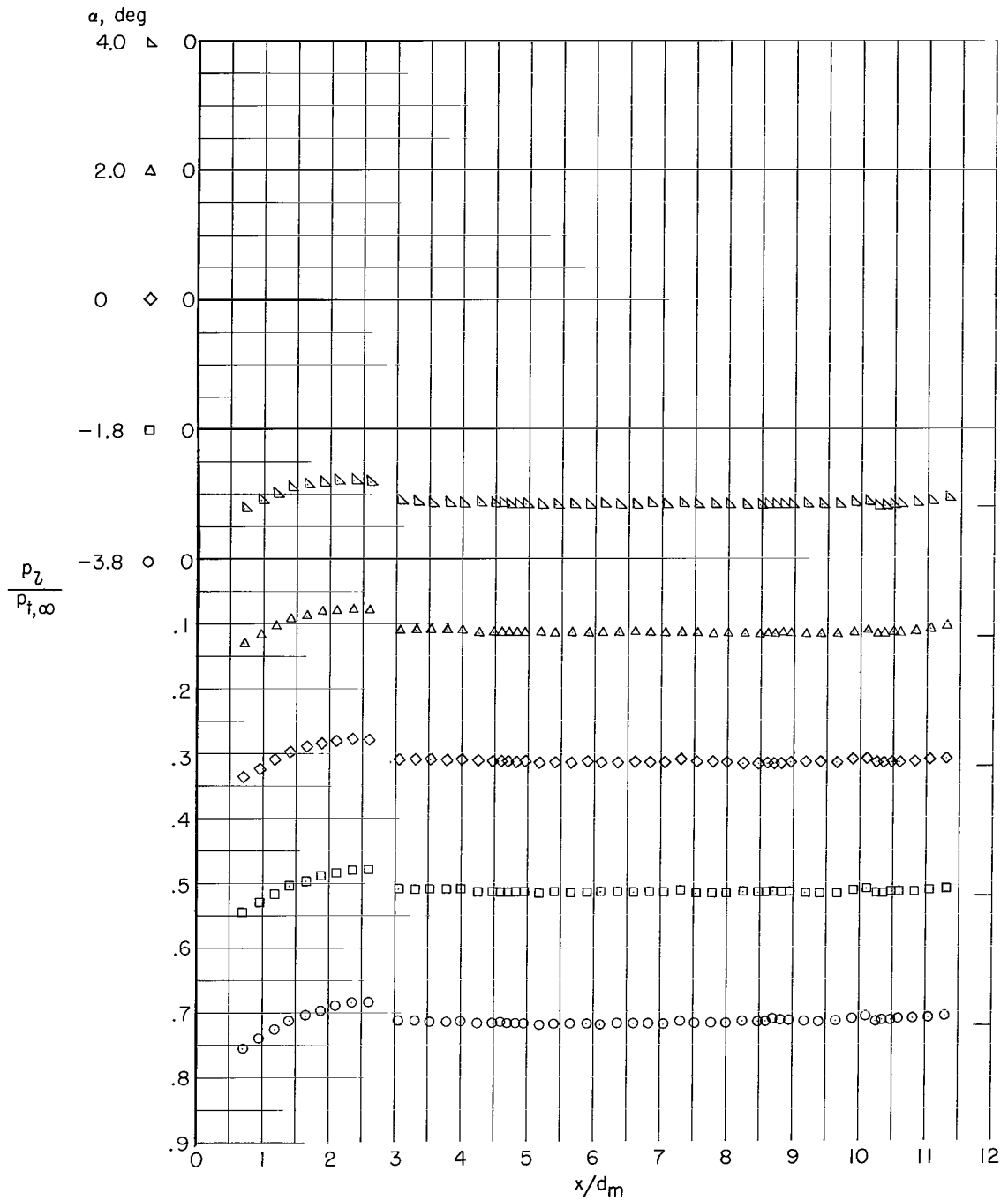
(a) M = 0.70.

Figure 5.- Pressure distributions for configuration 3. Ogive nose; l = 243.84 cm (96.00 in.); fineness ratio of 11.29.
Ticks indicate free-stream pressure ratio.

42
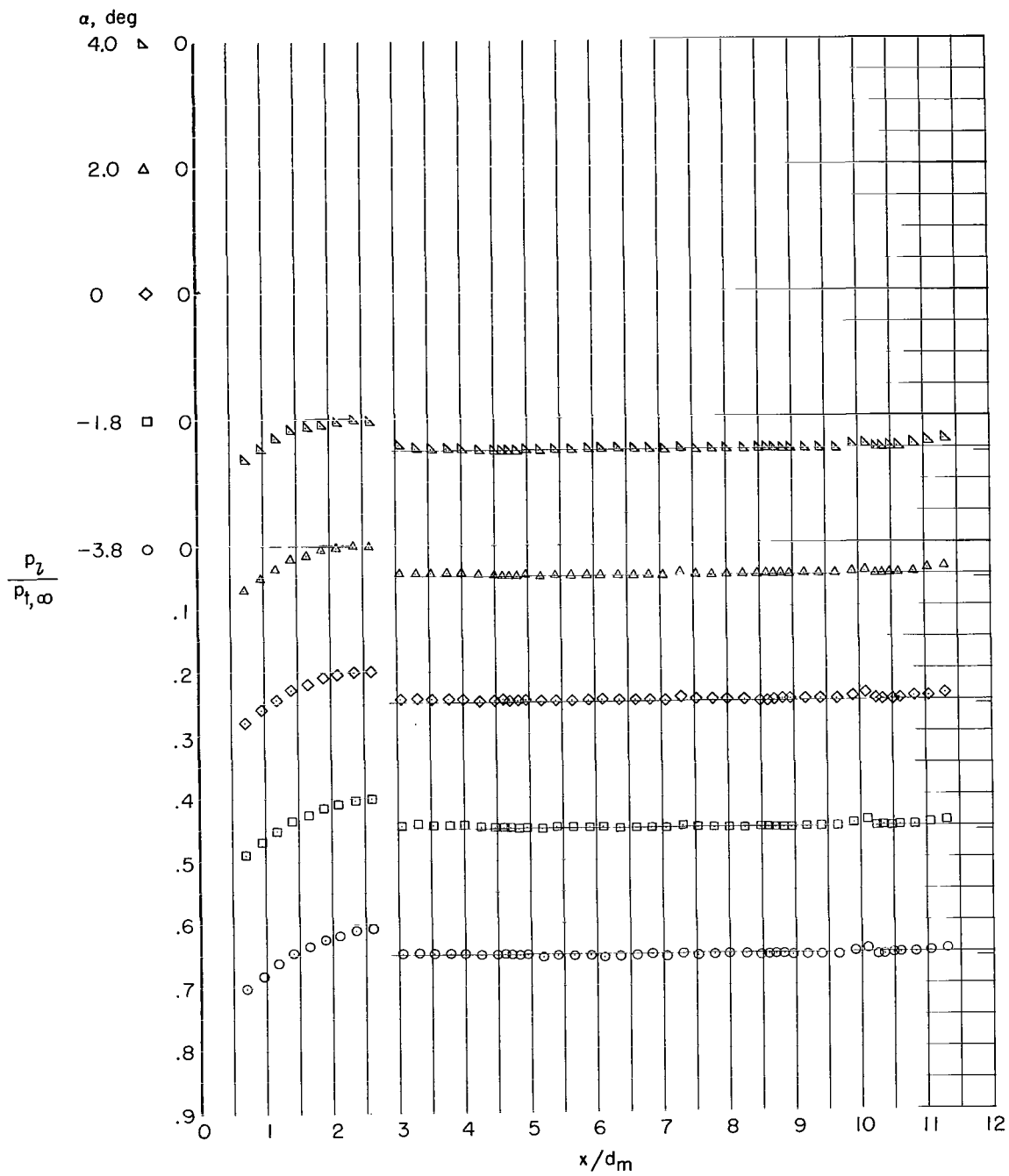
(b) M = 0.80.

Figure 5.- Continued.

43

(c) M = 0.90.

Figure 5.- Continued.

α, deg

4.0

2.0

0

−1.8

−3.8

$\frac{p_l}{p_{t,\infty}}$

.1
.2
.3
.4
.5
.6
.7
.8
.9

0   1   2   3   4   5   6   7   8   9   10   11   12

x/d_m

(d) M = 0.95.

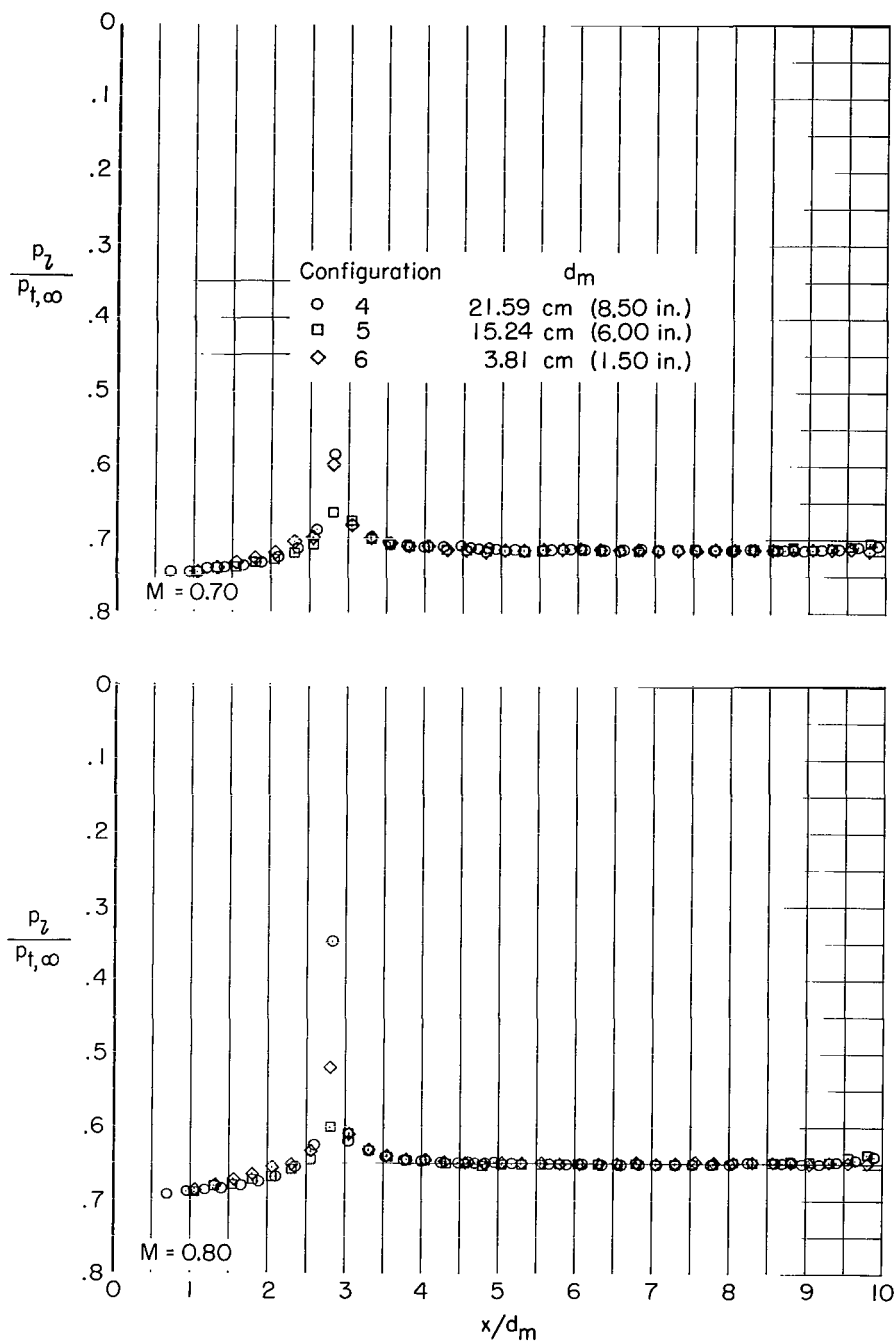Figure 5.- Continued.

45

(e) M = 1.00.

Figure 5.- Continued.

(f) M = 1.025.

Figure 5.- Continued.
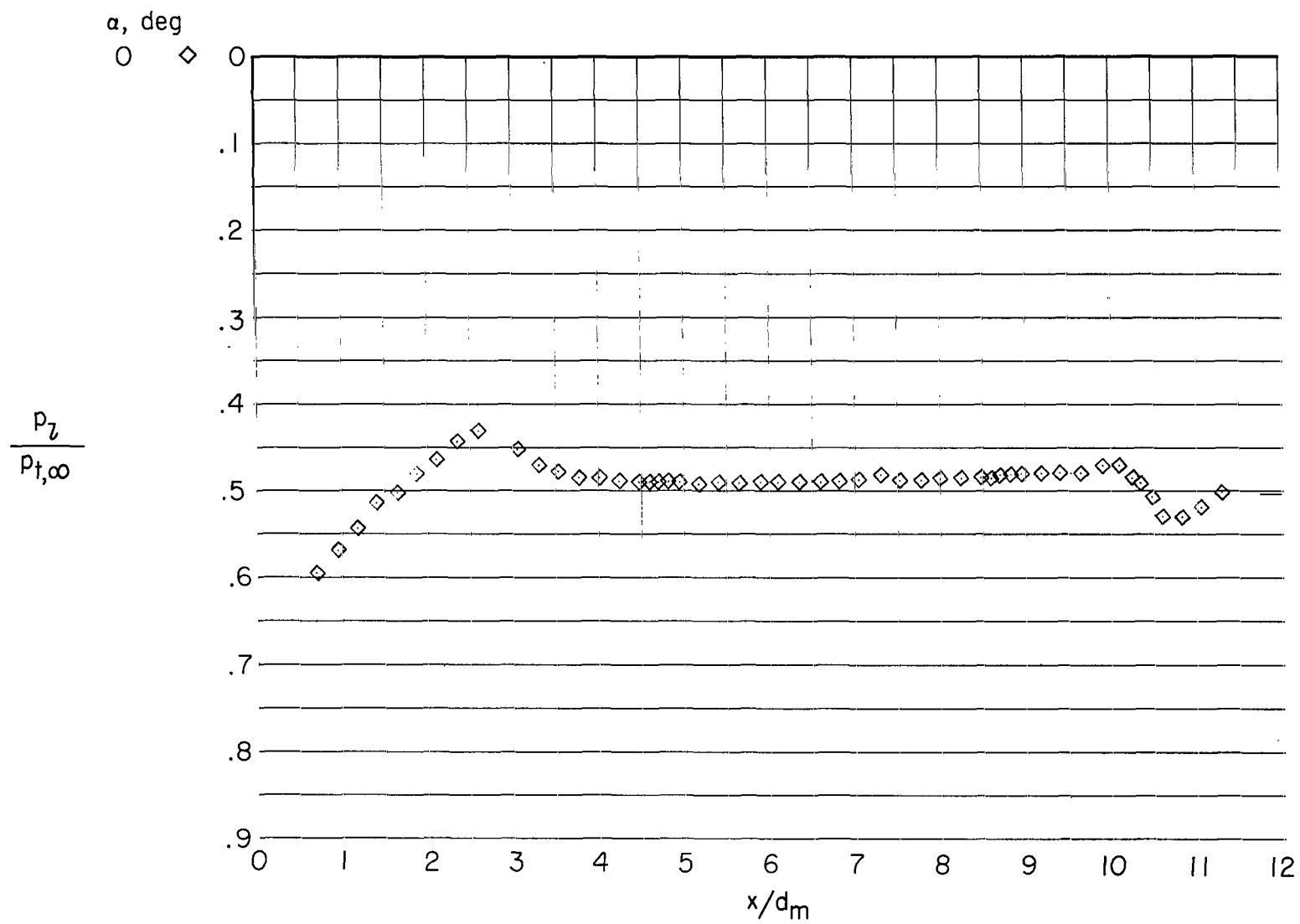
(g) M = 1.04.

Figure 5.- Continued.
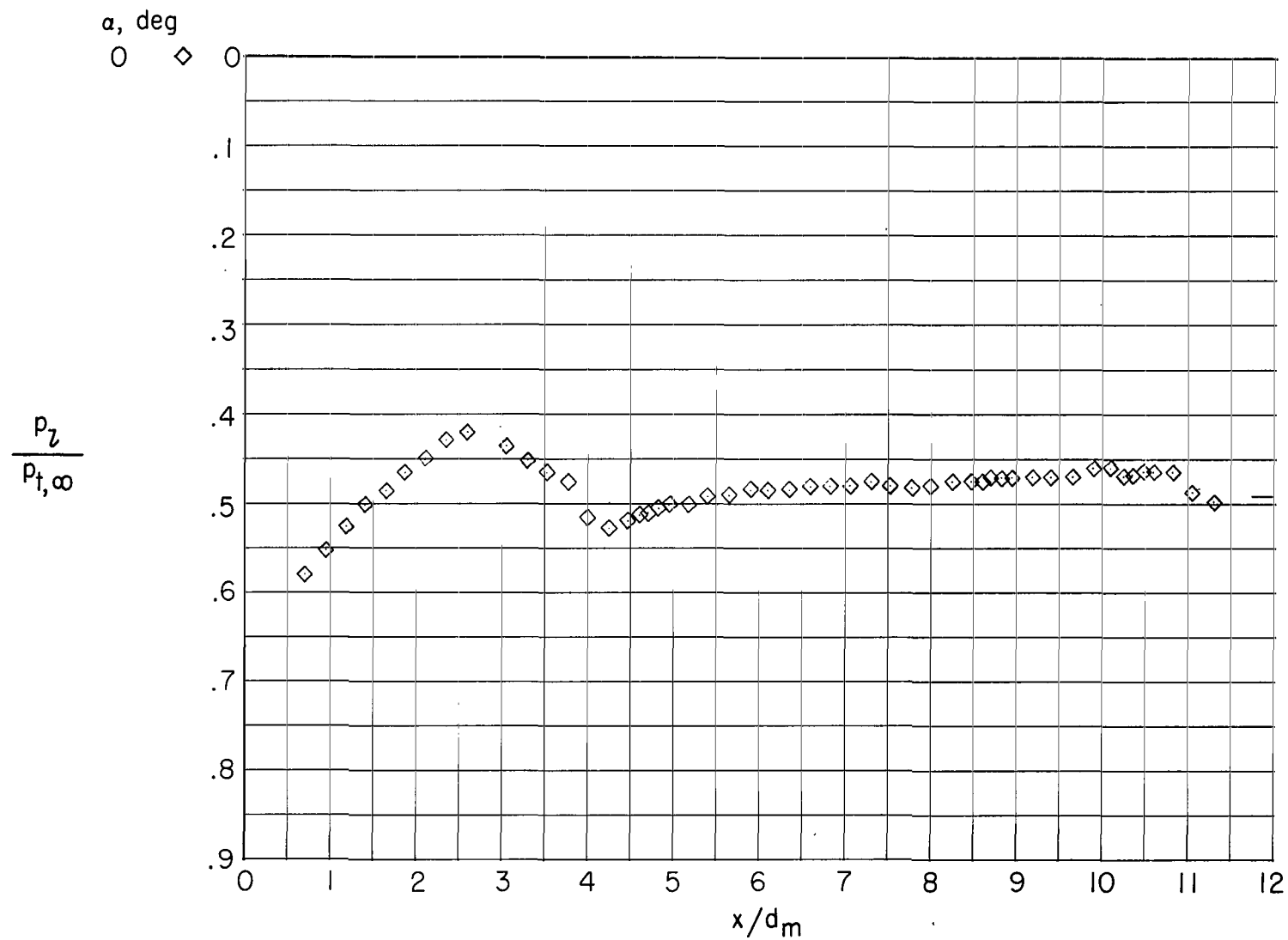
(h) M = 1.06.

Figure 5.- Continued.

50

α, deg

0   ◇   0

$\dfrac{p_l}{p_{t,\infty}}$

x/d$_m$
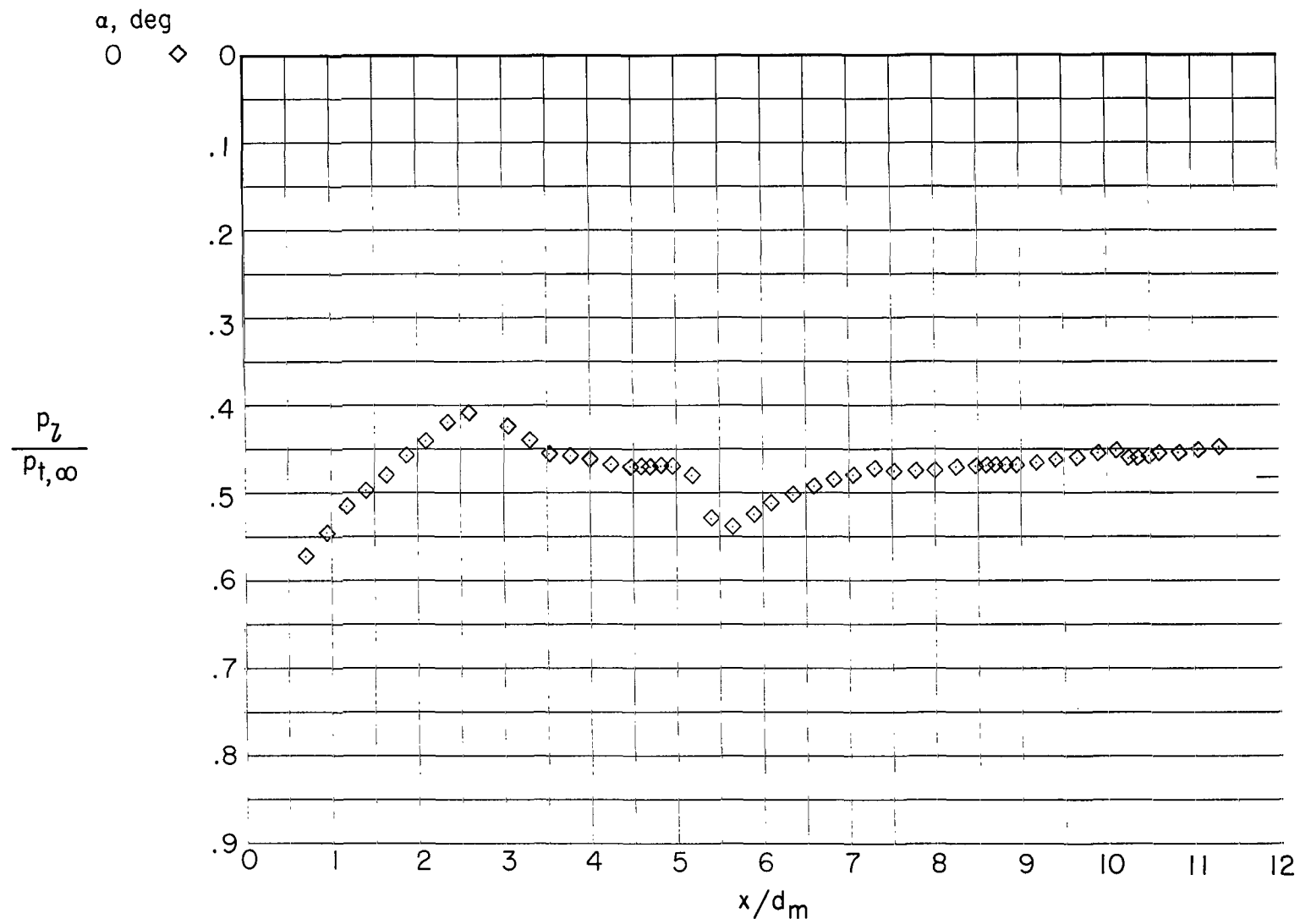
(i) M = 1.075.

Figure 5.- Continued.
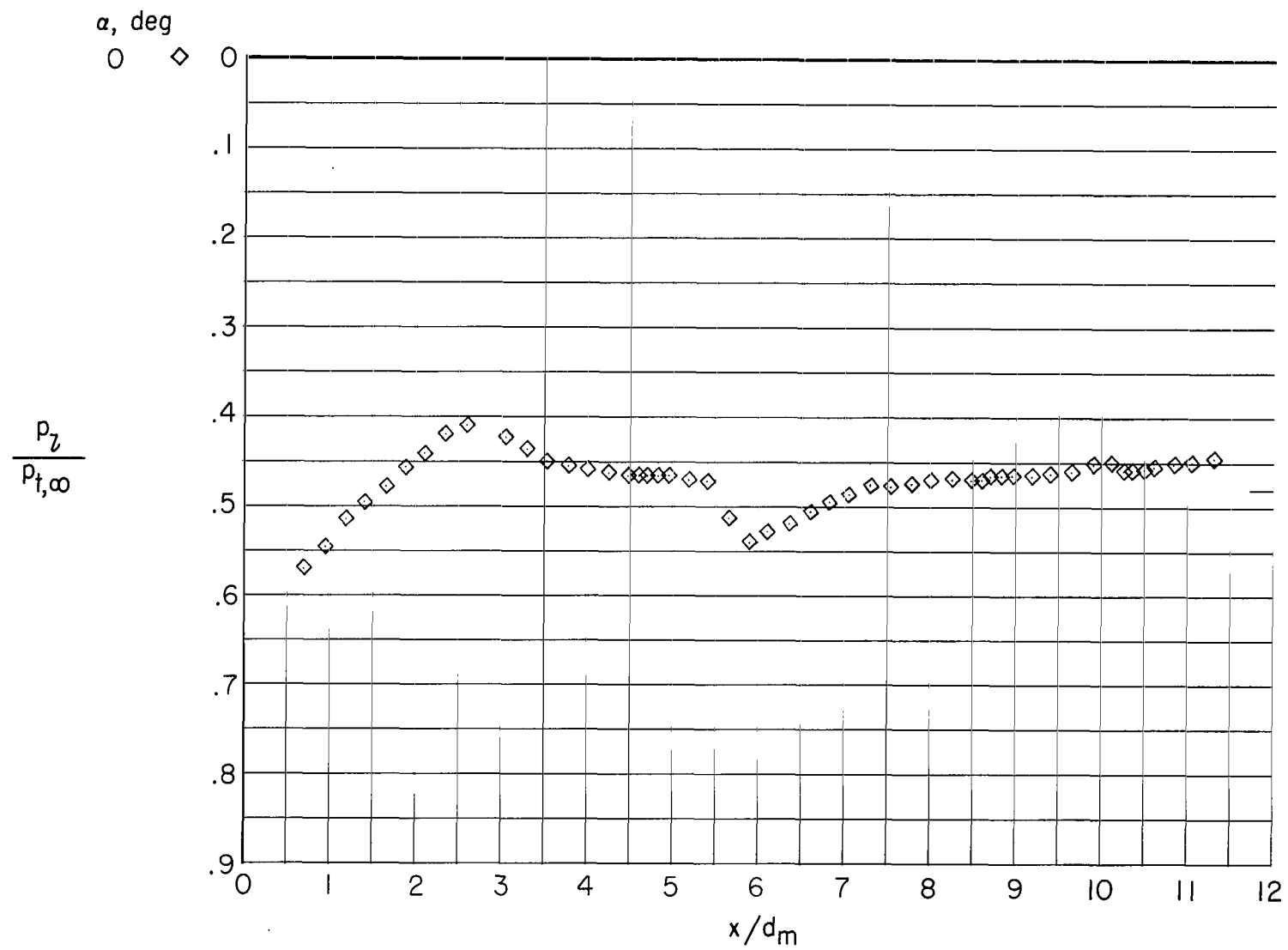
(j) M = 1.08.

Figure 5.- Continued.

52
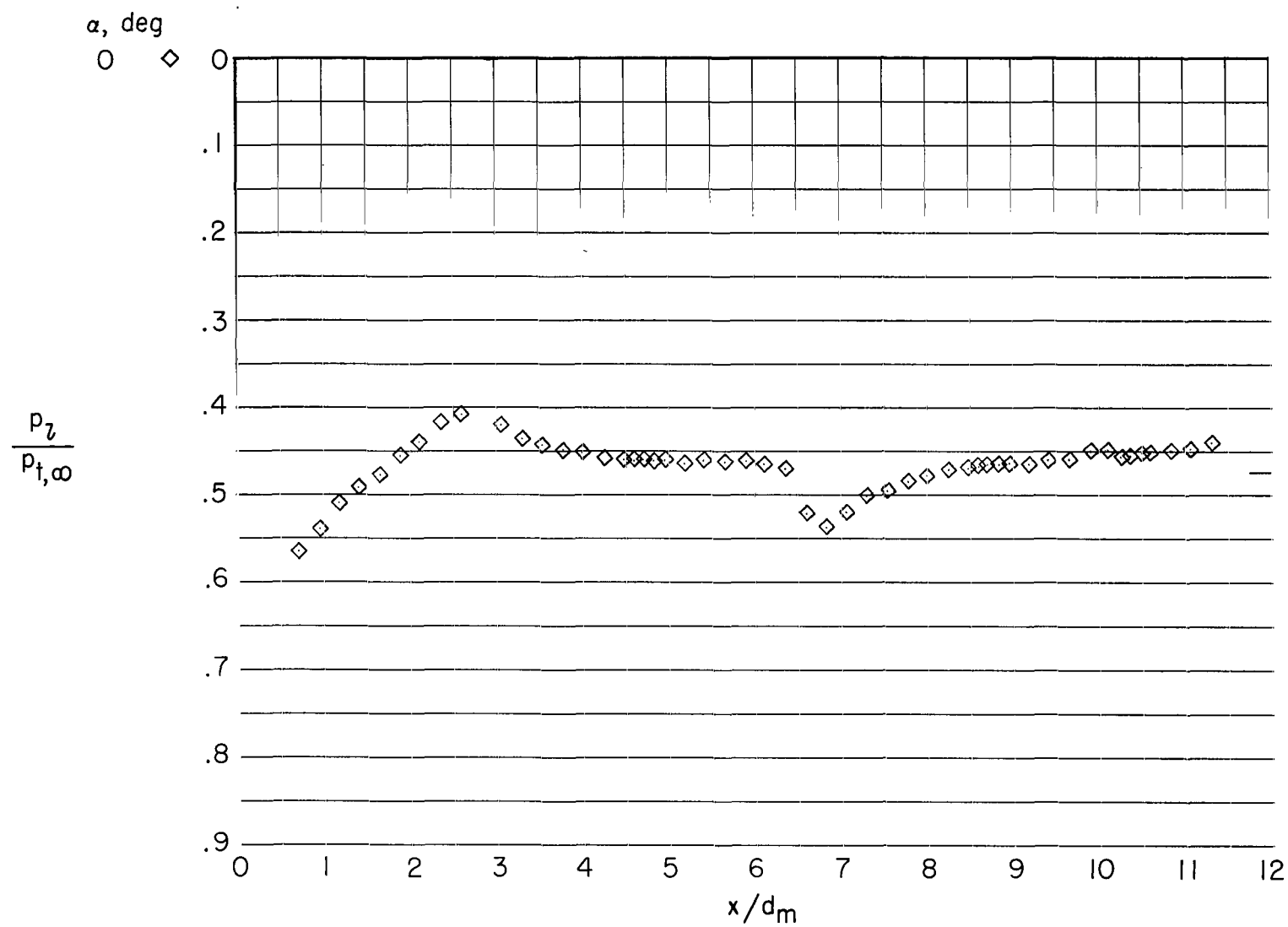
(k) M = 1.09.

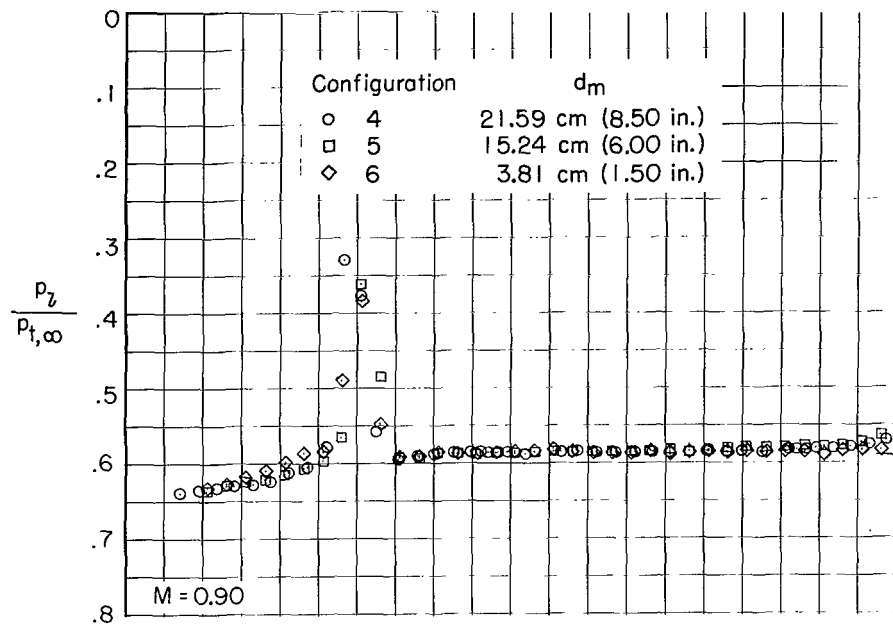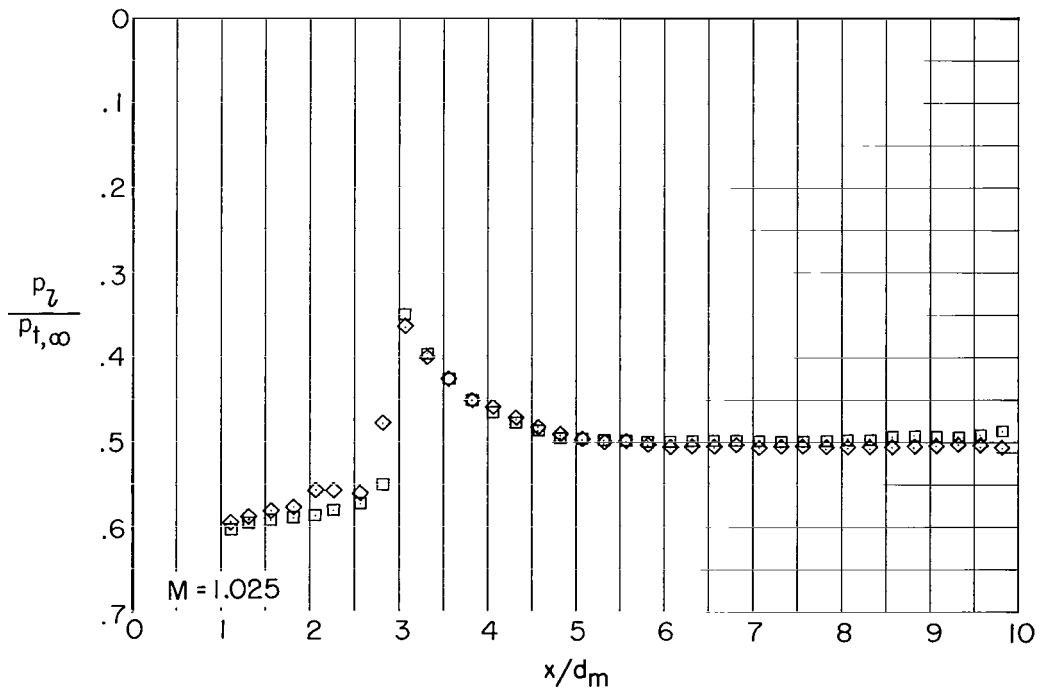Figure 5.- Continued.
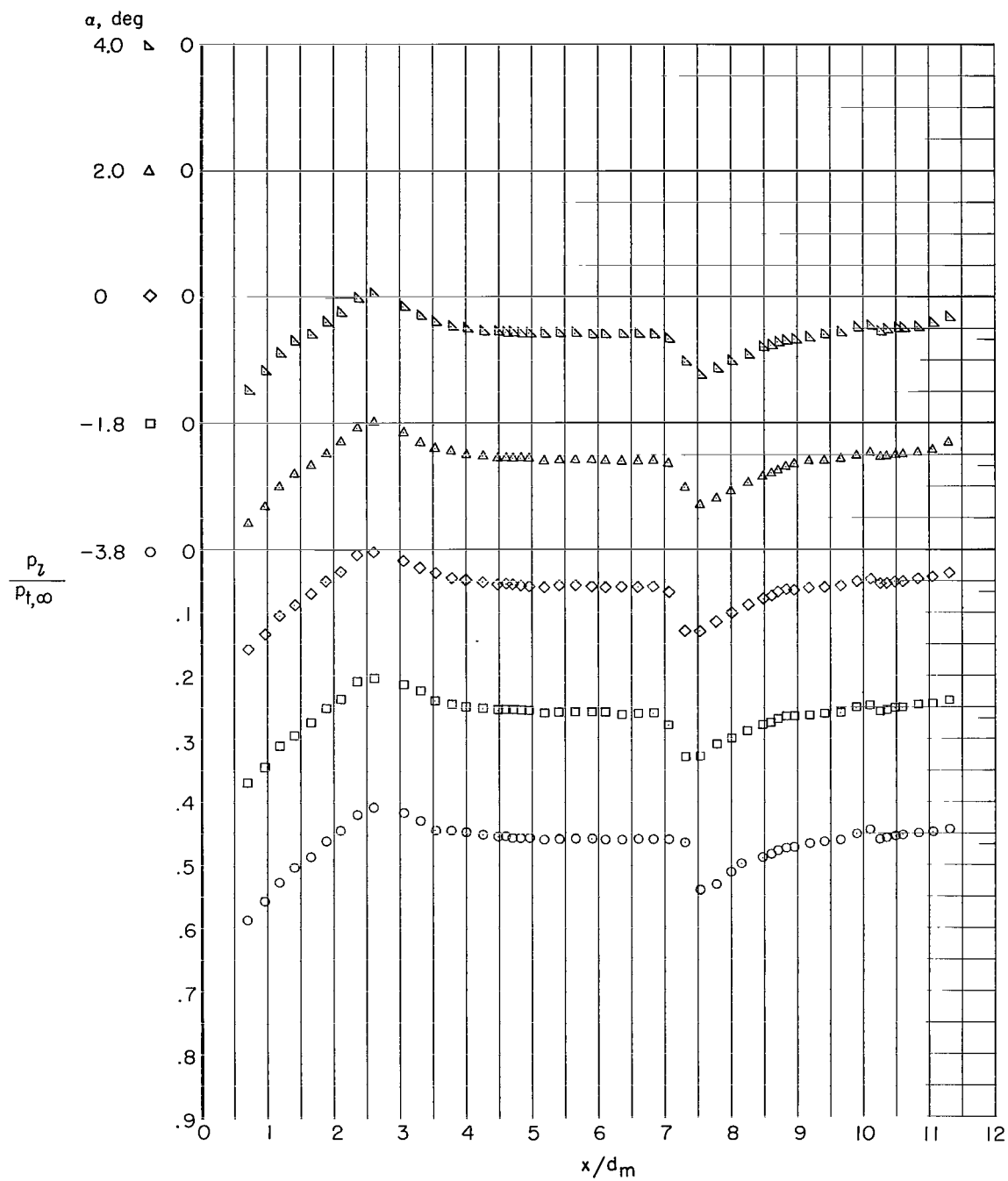
(l) M = 1.10.

Figure 5.- Continued.
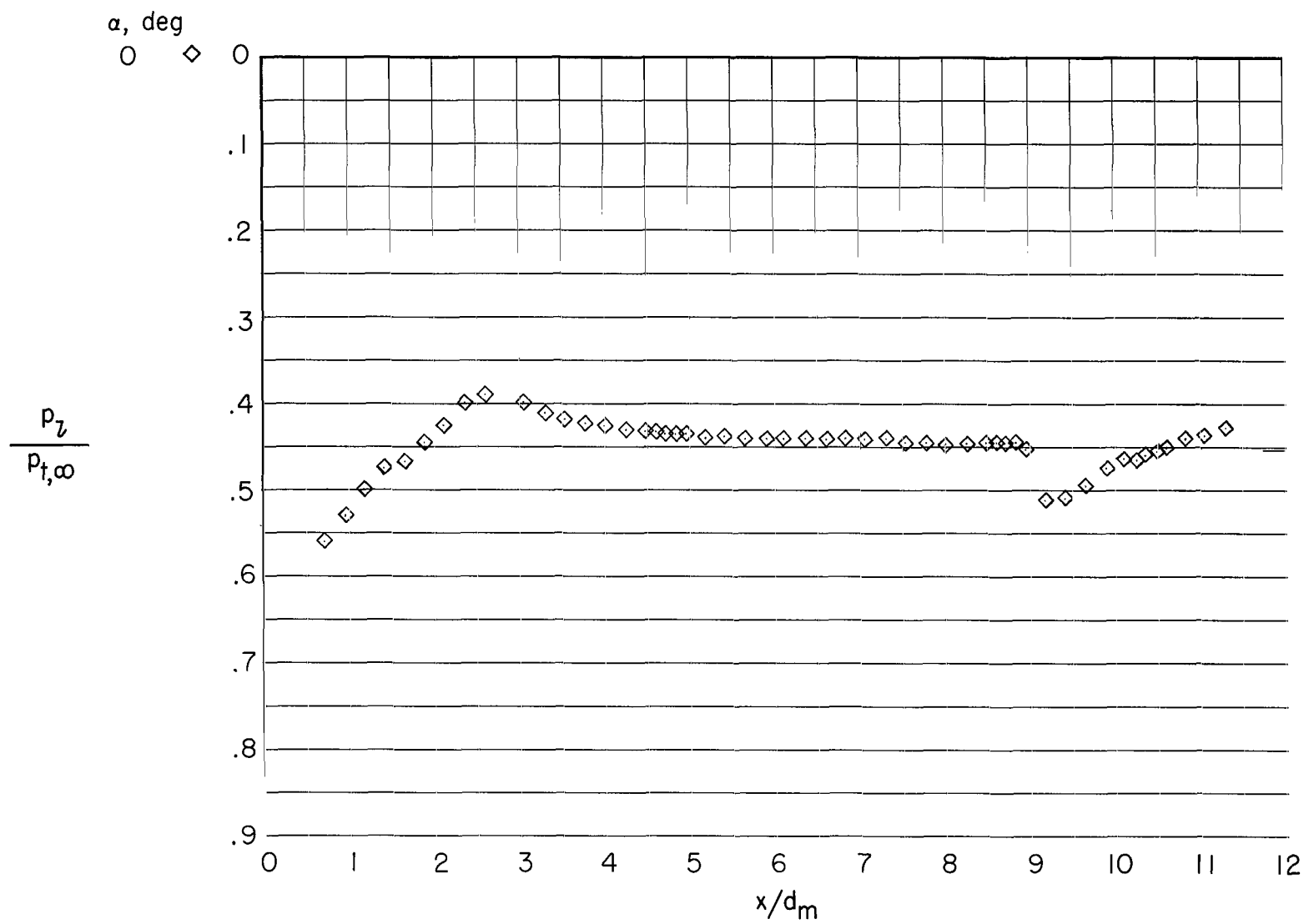
(m) M = 1.125.

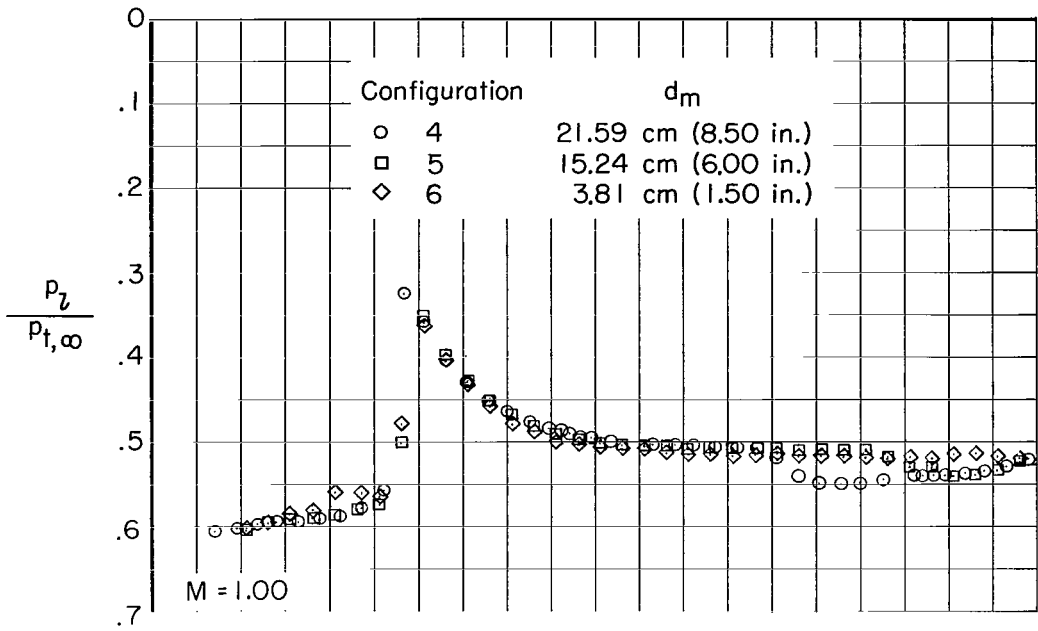Figure 5.- Continued.

(n) M = 1.15.

Figure 5.- Continued.

(o) M = 1.175.

Figure 5.- Continued.

α, deg

0   ◇   0

$\dfrac{p_l}{p_{t,\infty}}$

.1

.2

.3

.4

.5

.6

.7

.8

.9

0   1   2   3   4   5   6   7   8   9   10   11   12

x/d_m

(p) M = 1.185.

Figure 5.- Continued.

57

(q) M = 1.20.

Figure 5.- Continued.

(r) M = 1.25.

Figure 5.- Continued.
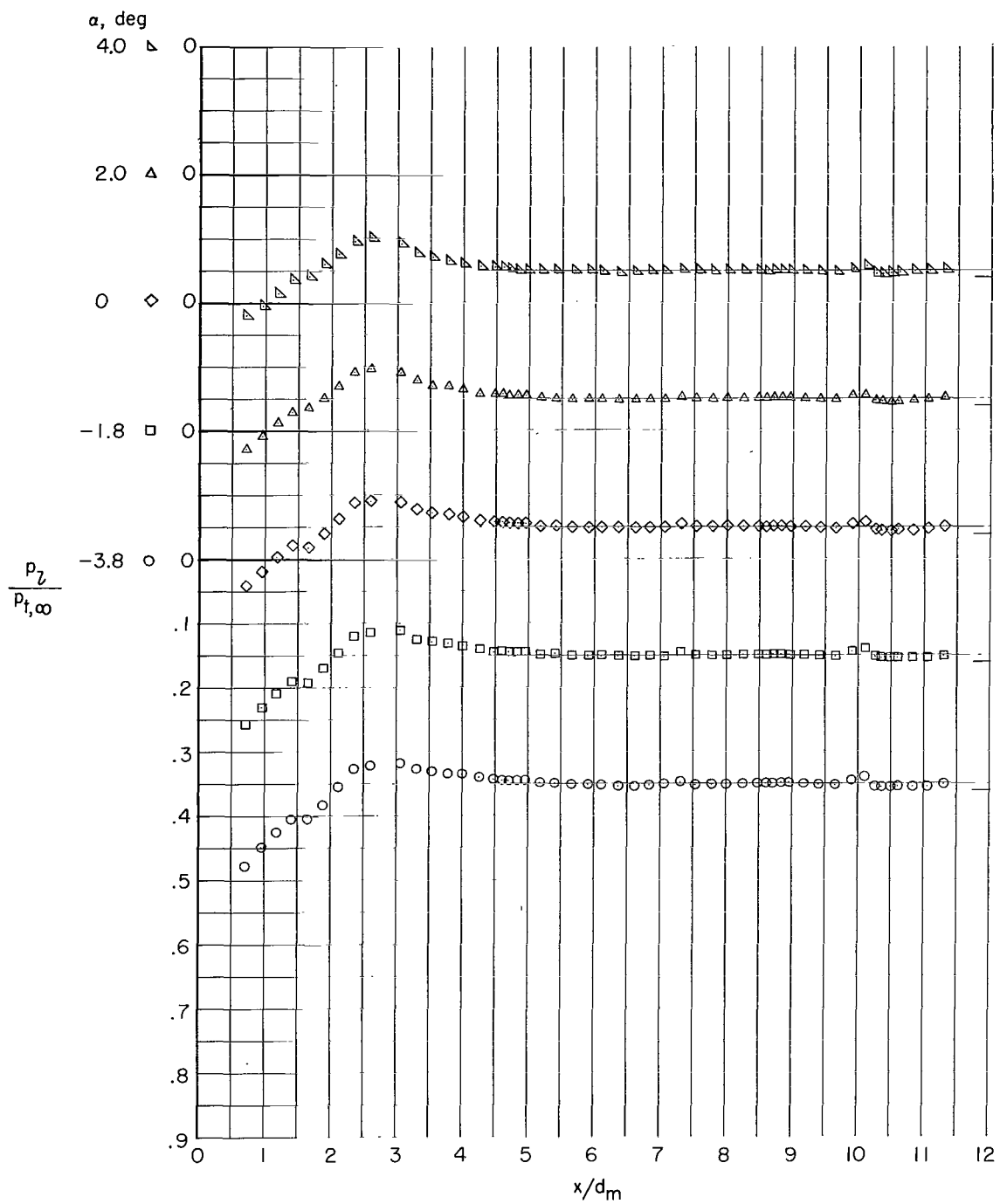
(s) M = 1.30.

Figure 5.- Concluded.

(a) M = 0.70 and 0.80.

Figure 6.- Comparison of pressure distributions for the configurations with a fineness ratio of 10.00. $\theta = 10^0$ at $\alpha = 0^0$.
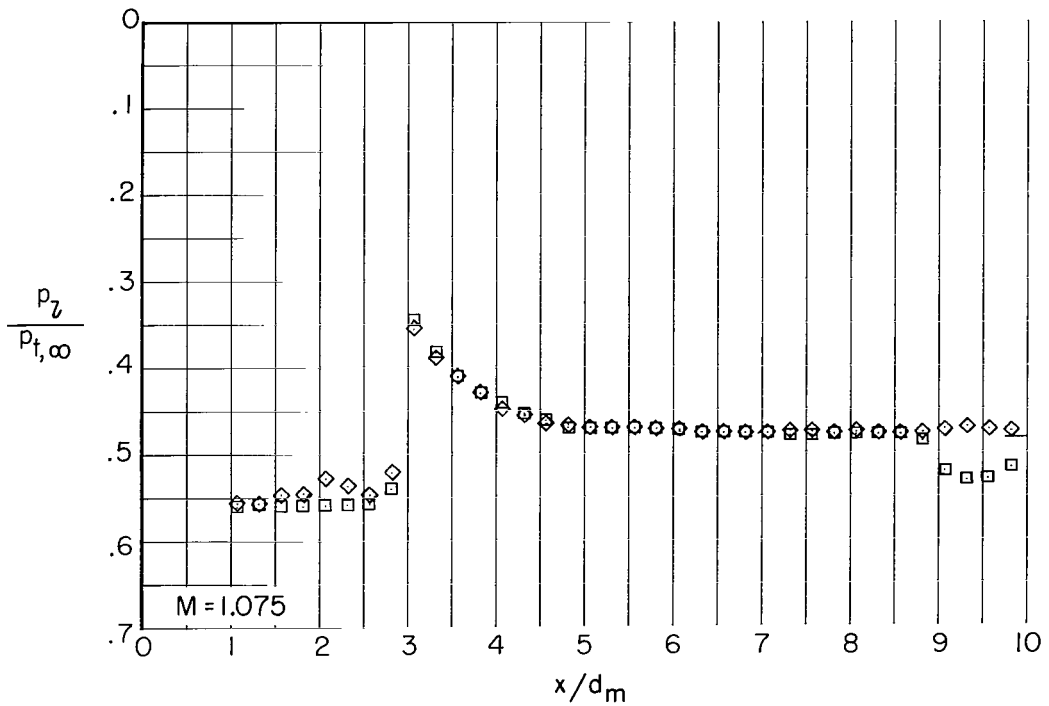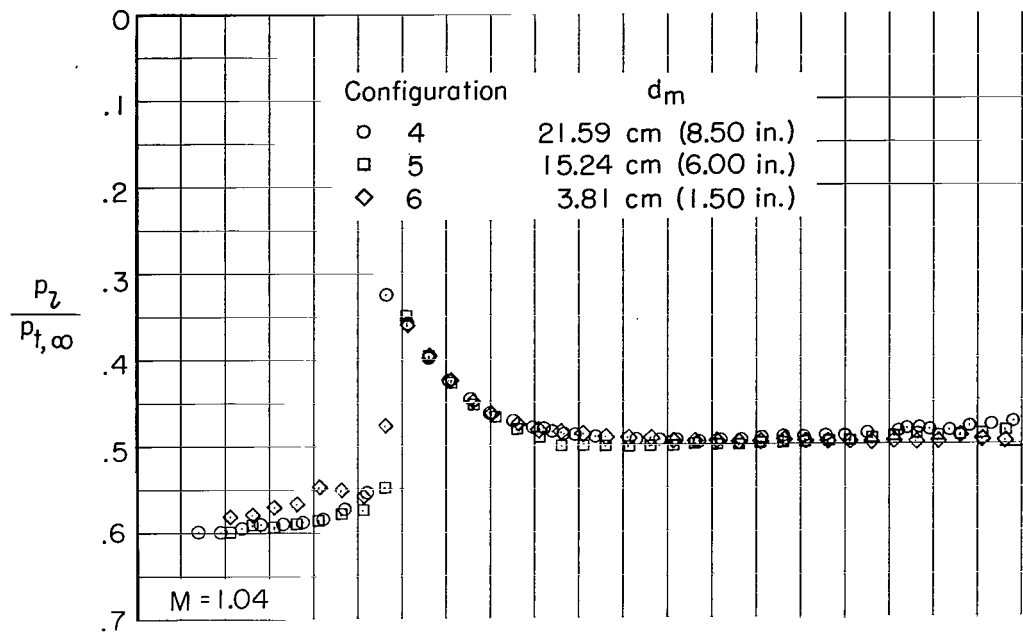Ticks indicate free-stream pressure ratio.

Configuration d_m
○   4   21.59 cm (8.50 in.)
□   5   15.24 cm (6.00 in.)
◇   6   3.81 cm (1.50 in.)

$\dfrac{p_l}{p_{t,\infty}}$

M = 0.90

$\dfrac{p_l}{p_{t,\infty}}$

M = 0.95
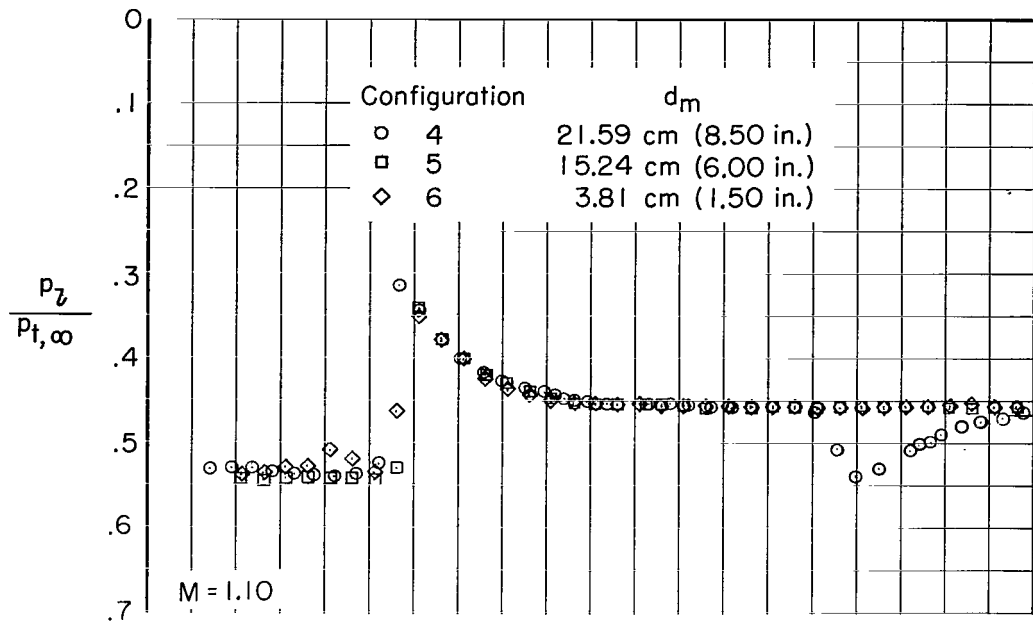
x/d_m
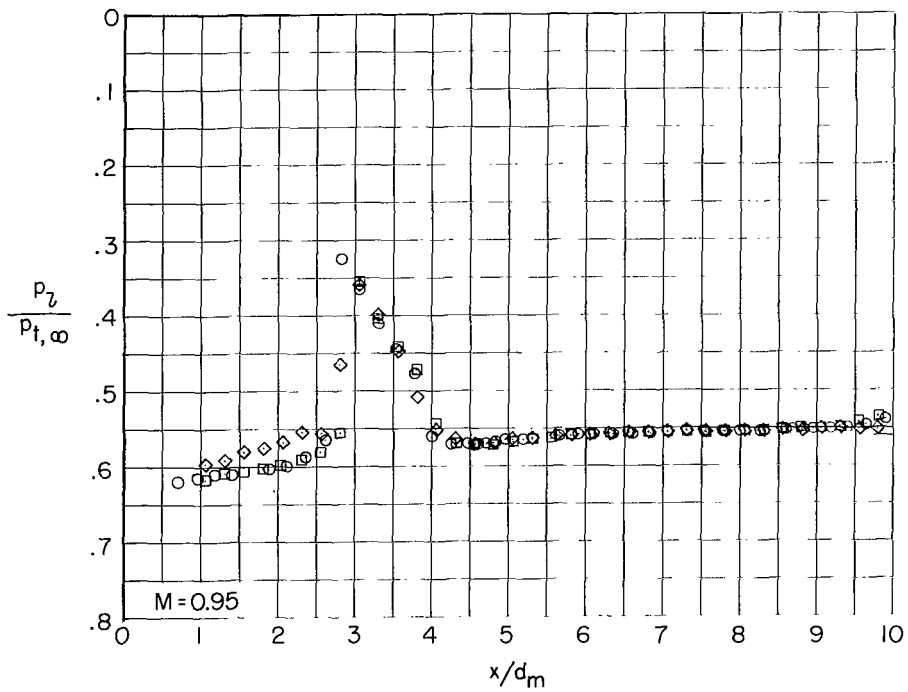
(b) M = 0.90 and 0.95.

Figure 6.- Continued.

(c) M = 1.00 and 1.025.

Figure 6.- Continued.
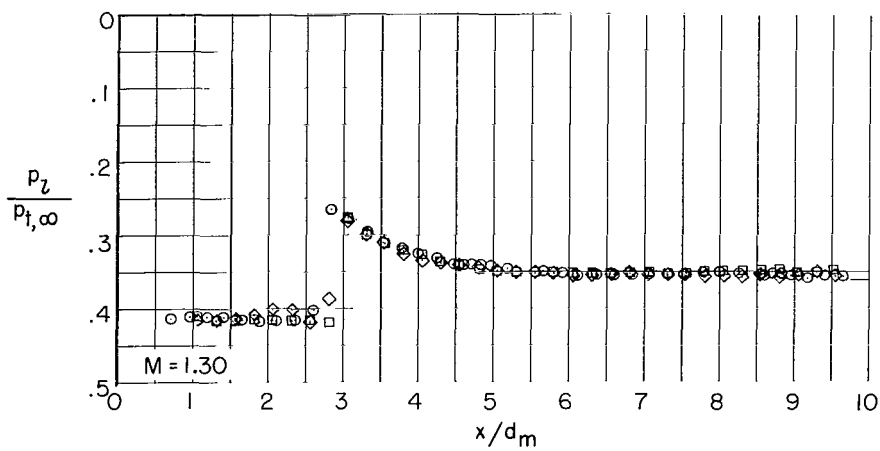
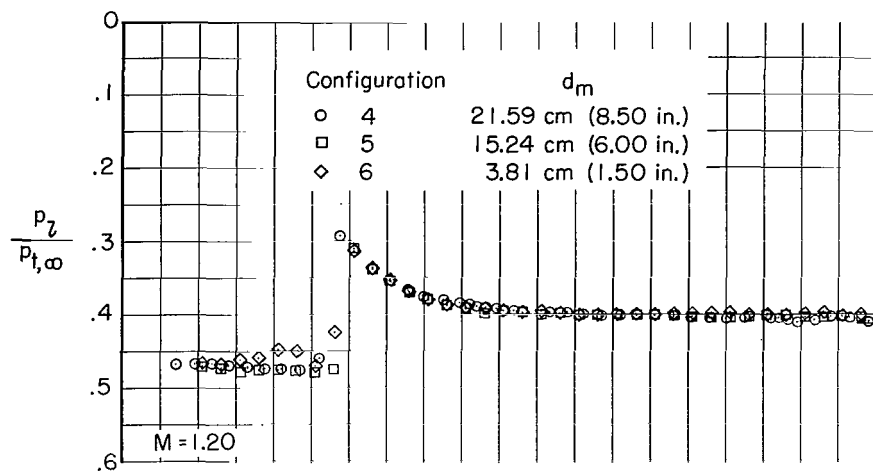(d) M = 1.04 and 1.075.

Figure 6.- Continued.
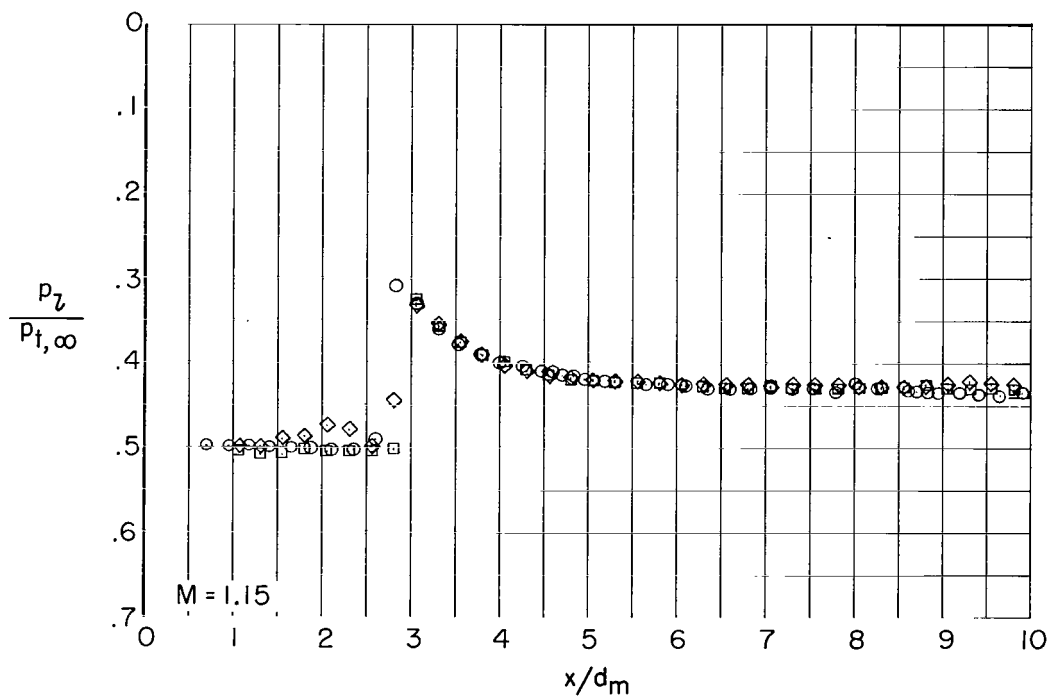
(e) M = 1.10 and 1.15.

Figure 6.- Continued.

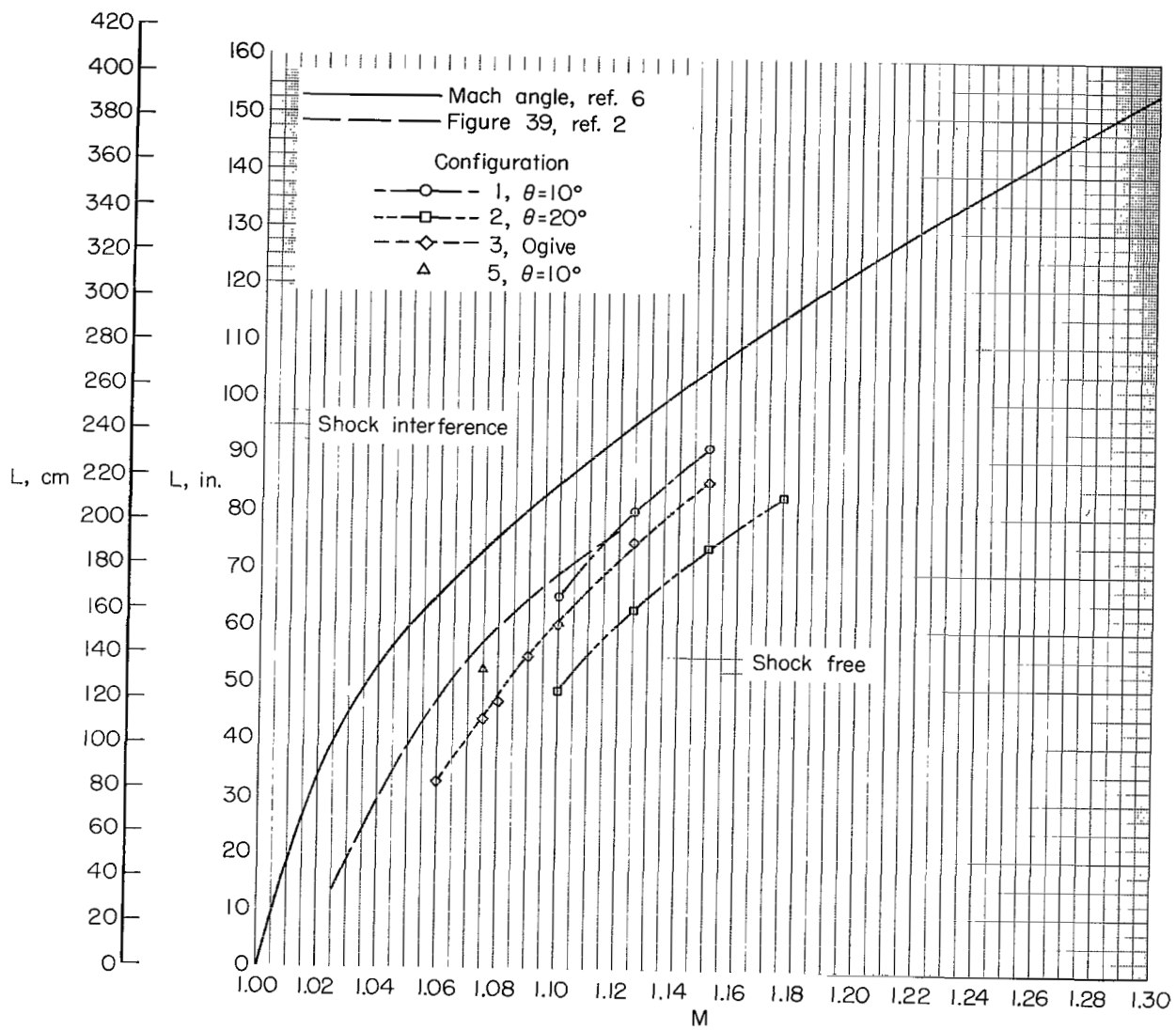(f) M = 1.20, 1.25, and 1.30.

Figure 6.- Concluded.

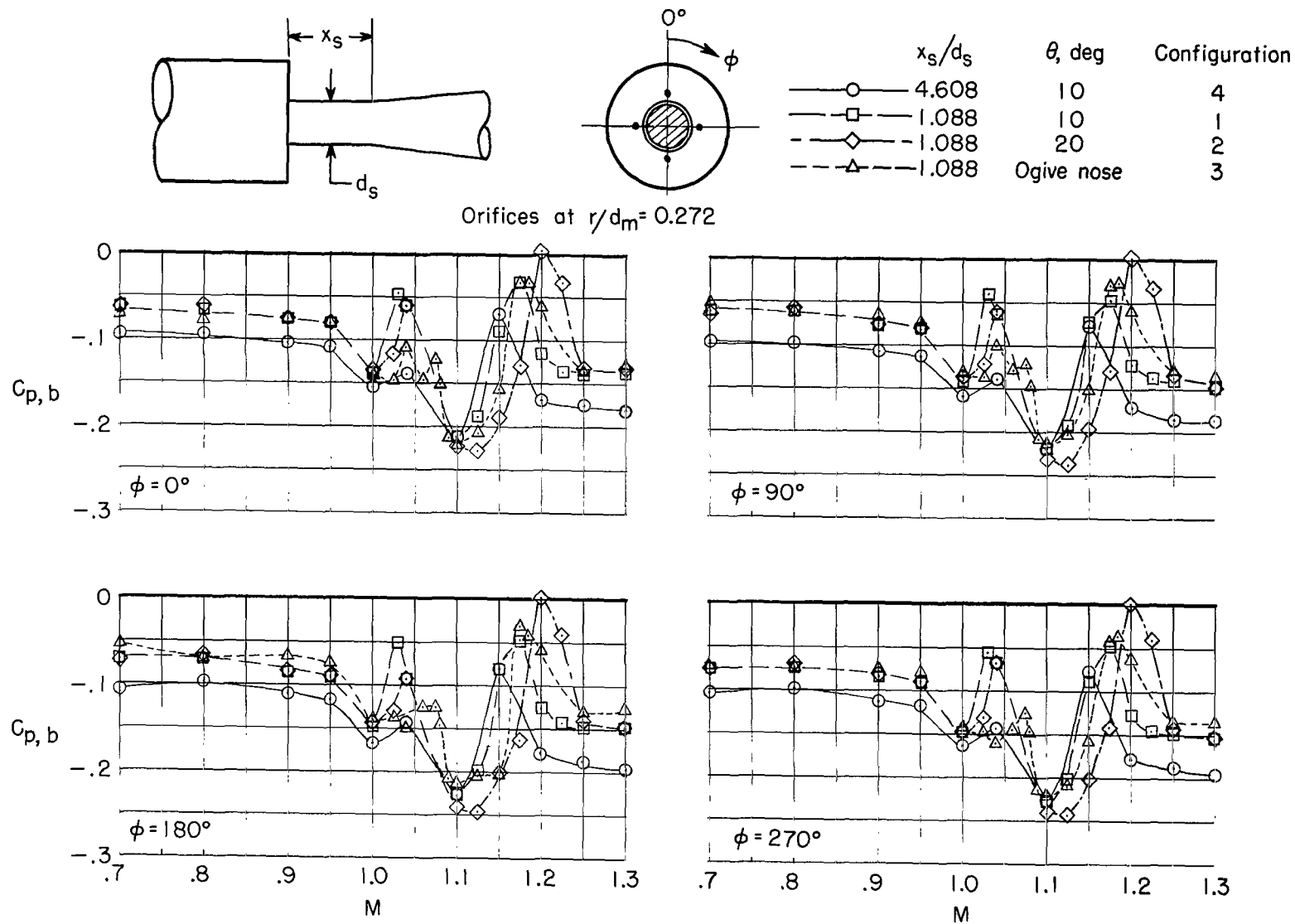Figure 7.- Summary of boundary-reflected-disturbance lengths for the Langley 16-foot transonic tunnel.

Figure 8.- Comparison of base pressure coefficients for configurations 1, 2, 3, and 4.

NASA SCIENTIFIC AND TECHNICAL PUBLICATIONS

TECHNICAL REPORTS: Scientific and technical information considered important, complete, and a lasting contribution to existing knowledge.

TECHNICAL NOTES: Information less broad in scope but nevertheless of importance as a contribution to existing knowledge.

TECHNICAL MEMORANDUMS: Information receiving limited distribution because of preliminary data, security classification, or other reasons.

CONTRACTOR REPORTS: Scientific and technical information generated under a NASA contract or grant and considered an important contribution to existing knowledge.

TECHNICAL TRANSLATIONS: Information published in a foreign language considered to merit NASA distribution in English.

SPECIAL PUBLICATIONS: Information derived from or of value to NASA activities. Publications include conference proceedings, monographs, data compilations, handbooks, sourcebooks, and special bibliographies.

TECHNOLOGY UTILIZATION PUBLICATIONS: Information on technology used by NASA that may be of particular interest in commercial and other non-aerospace applications. Publications include Tech Briefs, Technology Utilization Reports and Notes, and Technology Surveys.

Details on the availability of these publications may be obtained from:

SCIENTIFIC AND TECHNICAL INFORMATION DIVISION
NATIONAL AERONAUTICS AND SPACE ADMINISTRATION
Washington, D.C. 20546